AMERICAN COLLEGE OF VETERINARY RADIOLOGY

2009 Annual Scientific Conference

October 20-24, 2009

PEABODY HOTEL
MEMPHIS, TENNESSEE

PROGRAM COMMITTEE

Andra Voges, Program Chair
Liz Watson, Program Co-Chair (Forum Focus)
Mary Kay Klein, Program Co-Chair (Radiation Oncology)
Stephanie Nykamp, Program Co-Chair (Image Interpretation Session)
Lorrie Gaschen, President Ultrasound Society
Federica Morandi, President Society of Veterinary Nuclear Medicine
Russ Tucker, President CT/MRI Society
Jessica Winger, ACVR Meeting Manager
Susie Wilson, ACVR Administrator

ACVR ADMINISTRATION

Jon Shiroma, President
Marti Larson, President-Elect
Rob McLear, Treasurer
Tom Nyland, Webmaster/Secretary
Bill Brawner, President, Radiation Oncology
Robert D. Pechman, Executive Director
Darryl N. Biery, Assistant Executive Director

Table of Contents

Mezzanine Level Floor Plan

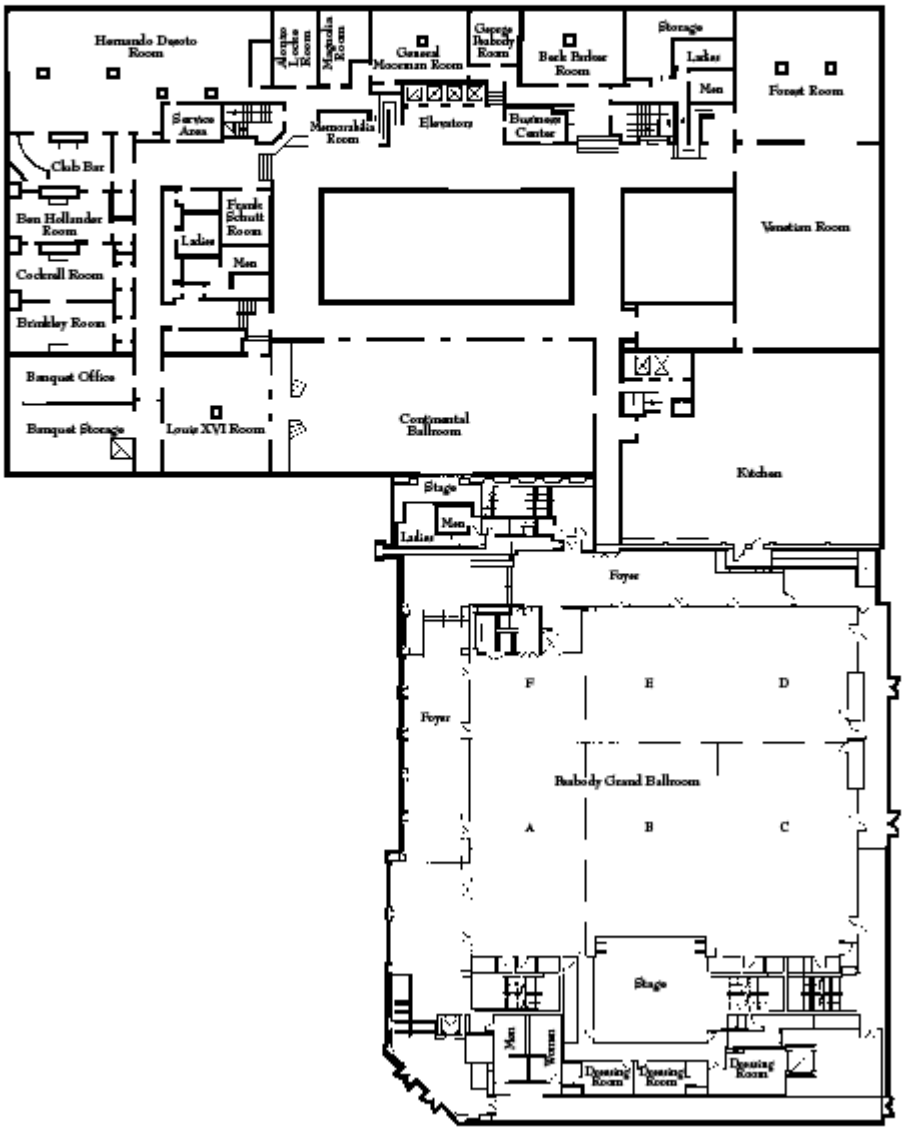

The Peabody Grand Ballroom

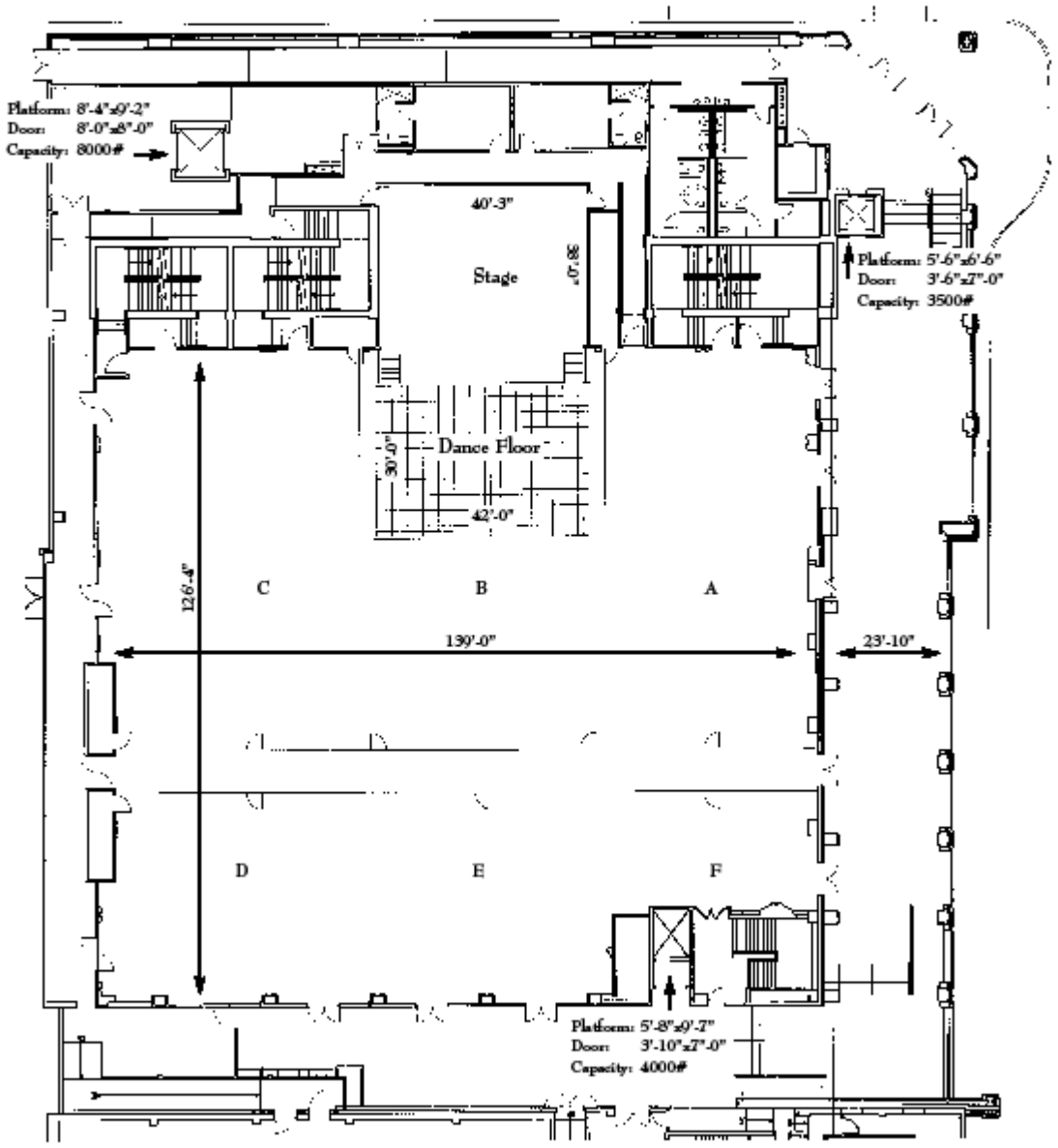

Peabody Executive Conference Center-Third Floor

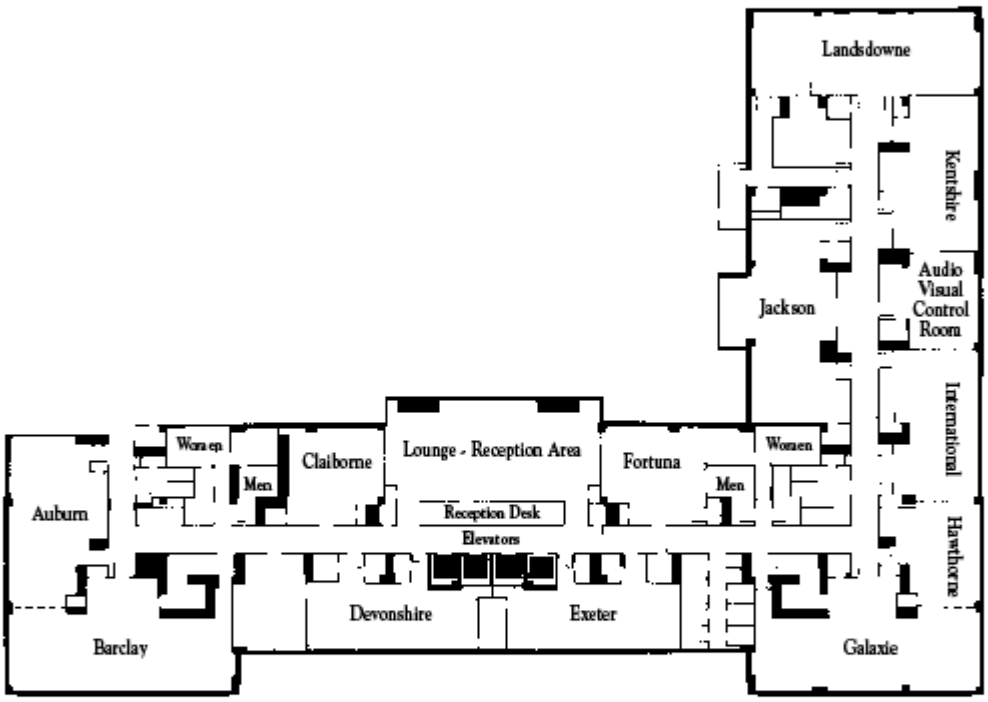

Skyway and Planatation Roof

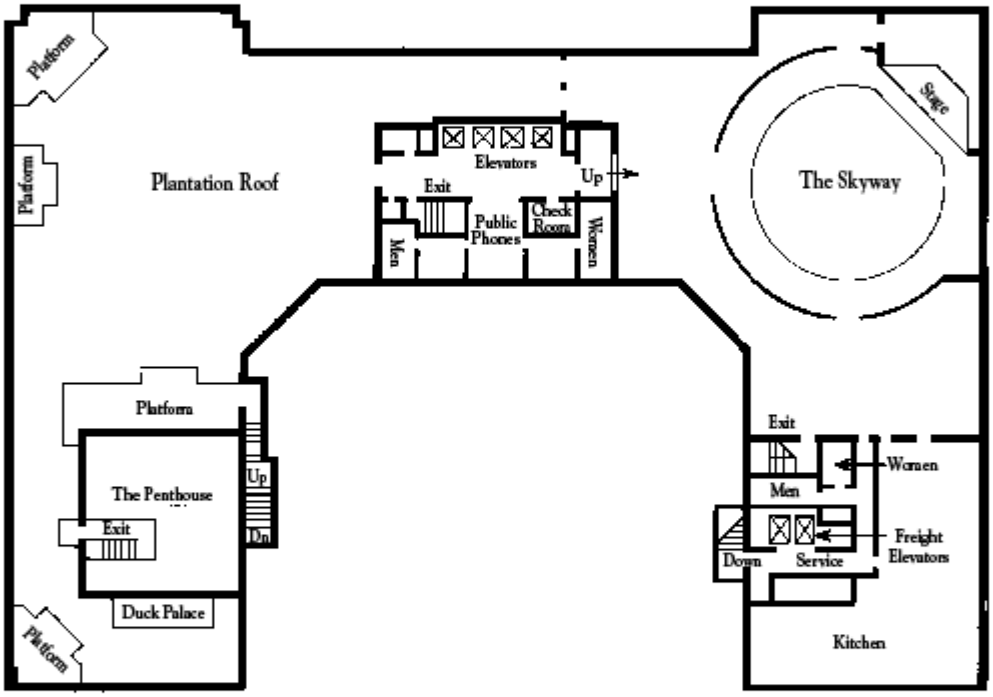

The Tennessee Exhibit Hall

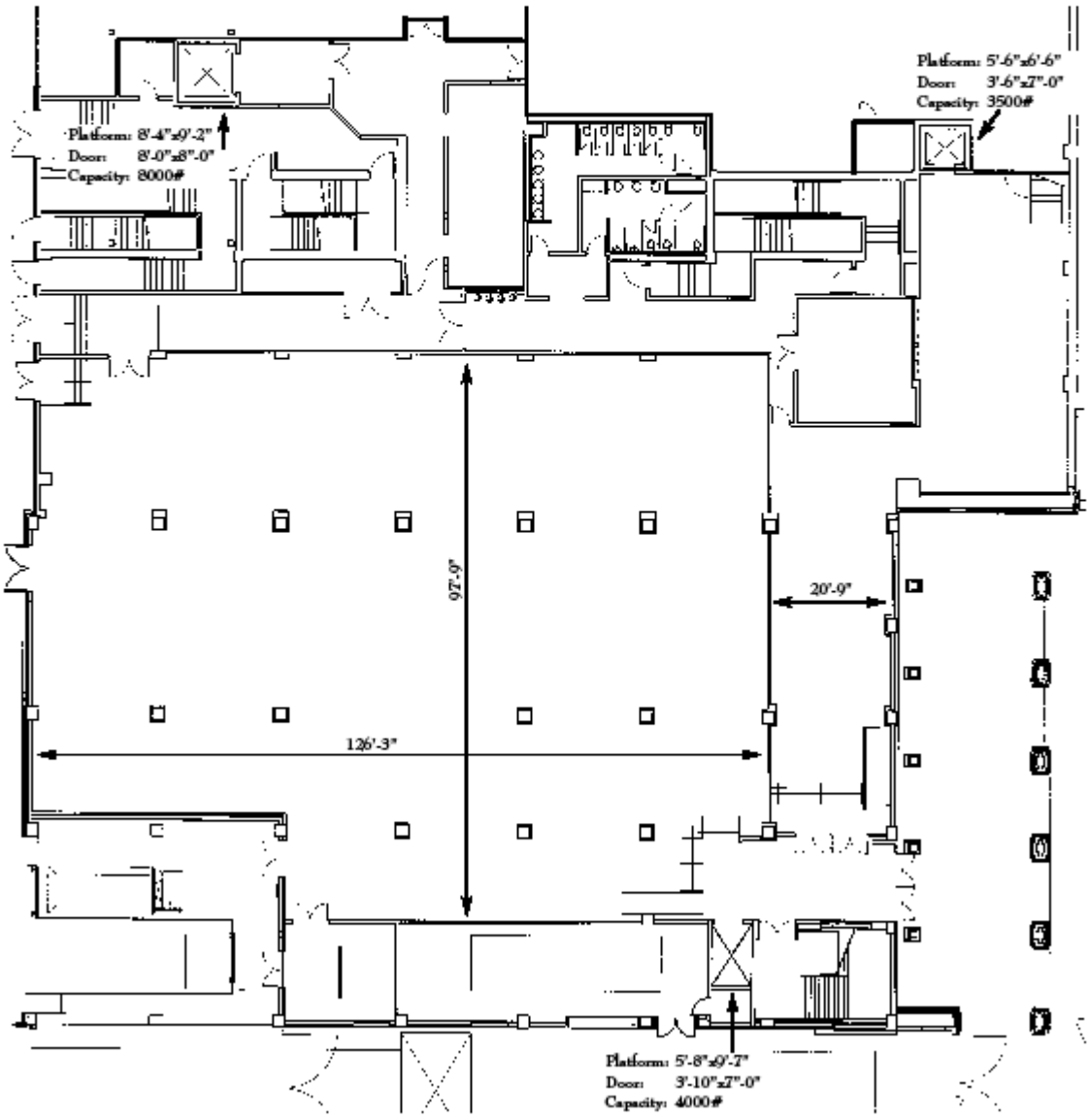

THE AMERICAN COLLEGE OF VETERINARY RADIOLOGY GRATEFULLY ACKNOWLEDGES THE SUPPORT OF THE FOLLOWING COMPANIES AND WISHES TO THANK THEM FOR THEIR CONTRIBUTIONS

ALOKA ULTRASOUND

10 Fairfield Blvd
Wallingford, CT 06492
Phone: 203-269- 5088
Toll Free: 800-872-5652
Fax: 203-269-6075
Email: inquiry@aloka.com
Website: www.alokavet.com

ALOKA has a full range of ultrasound systems for most veterinary applications. The super premium Alpha 7 and premium Alpha 5 offer superb image quality for the most challenging cases. We also offer cost effective solutions in the Prosound-6, SSD-3500, and SSD-4000. Our two portables, the SSD-500 and SSD-900 are reliable, rugged systems that are ideal for large animal reproduction, equine tendons and, with the 500, food animal live carcass evaluation. With the addition of the Sonosite family of battery operated lightweight systems, Aloka can now provide a system so portable you can carry it in a briefcase.

ASTERIS, INC.

P.O. Box 285
Stephentown, NY 12168
Phone: 877-727-8374
Fax: 877-488-6746
Email: sales@asteris.biz
Website: www.asteris.biz

ASTERIS is an innovative, progressive firm focusing on technology solutions for the veterinary practitioner. Founded in 2004, ASTERIS delivers inimitable PACS (Picture Archiving and Communications Systems) solutions and a groundbreaking veterinary information communication platform. A revolutionary concept, ASTERIS Veterinary Communication Network (VCN) enables veterinary practices, practitioners, and clients to access and share the full breadth of patient medical data at any time, from anywhere in the world.

ECLIPSE MEDICAL IMAGING

845 Cotting Ct.
Vacaville, CA 95688
Website: http:\\www.emimaging.com

Eclipse Medical Imaging (EMI) is a world leader in providing professionally refurbished, high-end CT scanners dedicated for veterinary use. From their 25,000 square foot factory, all equipment is refurbished in their state of the art facility by certified EMI professionals. Veterinary Solutions include full site planning, architectural plans, shipping, professional installation, on-site clinical applications training specific for veterinary use, and full service warranty. EMI has worked closely with the veterinary community over the past decade to develop and perfect the highly specialized techniques and protocols to ensure the highest quality images while simplifying scanning procedures. At Eclipse Medical Imaging, you will be sure to receive the highest quality equipment that is truly tailored for veterinarians along with world class service at a cost effective price.

ELSEVIER

P.O. Box 360446
Birmingham, Al 35236
205-542-7755
Email: s.lowry@elsevier.com
Website: www.stevenlowry.com

SAUNDERS, MOSBY, CHURCHILL LIVINGSTONE, BUTTERWORTH HEINEMANN AND HANLEY BELFUS, a combined premier worldwide health science publishing company, now under the umbrella of ELSEVIER, INC., proudly presents our latest titles. Come visit us at our booth and browse through our complete selection of publications including books, periodicals and software. ELSEVIER, INC., building insights, breaking boundaries.

FOVEA DR

P.O. Box 1908
1233 N. Ashley
Nixa, MO 65714
Toll Free: 888-368-3201
Website: www.FoveaDR.com

Fovea Direct Digital Radiography has reset the bar in veterinary x-ray. The entire line of Fovea systems has been designed and built from the ground up to be truly digital. Fovea offers the highest resolution and the fastest DR, with the lowest dose available. Cutting-edge technology, top-of-the-line equipment, and the ability to look ahead and anticipate the demands of veterinarians and their practices have helped cement Fovea's position as the industry leader. Fovea DR provides factory direct pricing, installation and a friendly support staff from our facility in America's heartland.

FUJIFILM Medical Systems USA, Inc.

419 West Avenue
Stamford, CT 06902-6300
Phone: 203-602-3625
Website: www.fujiprivatepractice.com

FUJIFILM Medical Systems, the inventor and world leader in digital x-ray, is excited to launch FCR Prima™, a new digital x-ray system enabling veterinary practices to make the transition from film to digital. This cost-effective system was designed to deliver Fujifilm's renowned image quality and intuitive functionality designed to address the needs of your practice. Fujifilm's portfolio also includes the FCR XL-2 and FCR XC-2 systems which provide Fujifilm's high image quality, proven image optimization tools, and throughputs of up to 94 images per hour. Systems for viewing, archiving and storing digital x-rays are also available. For more information: www.fujiprivatepractice.com.

IDEXX DIGITAL IMAGING

One Idexx Drive
Westbrook, ME 04092
Phone: 207-556-3300
Mobile: 207-239-9055
Email: Melissa-hubbard@idexx.com

IDEXX Digital Imaging- to meet the diverse needs of any veterinary practice, IDEXX offers a full range of digital imaging solutions that were developed in conjunction with independent, board certified veterinary radiologists specifically for veterinary use. The IDEXX-DR™ 1417 and IDEXX-CR™ 1417 Digital Imaging systems can help your practice increase revenue, eliminate film associated expenses and improve productivity by streamlining workflow, in addition to increasing your diagnostic capabilities. Both systems offer complete integration through IDEXX SmartLink™ Digital Imaging with IDEXX Cornerstone® so you can get information where you need it, when you need it.

KINGSBRIDGE VETERINARIAN EQUIPMENT TECHNOLOGY SOLUTIONS, LLC.

150 N. Field Dr.
Suite 193
Lake Forest, IL 60045
Phone: 800-278-1149
Website: www.kingsbridgevets.com

KingsBridge/VETS is the premier provider of refurbished CT, MRI, Ultrasound and other high technology imaging equipment serving the veterinary market. Our meticulous refurbishment process insures that every product meets the highest standards of performance and quality. Each product carries a full one year warranty and is guaranteed to meet original performance specifications. KingsBridge/VETS also offers creative financing and rental programs that allow any veterinary practice to have high quality, high technology diagnostic equipment at its clinic.

ONCONCEPTS, LLC

24 Revella St.
Rochester, NY 14609
Toll Free: 585-317-2546
Email: Michelle@onconcepts.net

Onconcepts was founded with the primary goal of improving cancer care through efficient, high quality products that meet the needs of the Radiation Oncology environment. The three founders have 40 years of combined clinical, technical and service expertise. One of our premium products is the Kodak 2000RT, the only simulation/portal CR system to offer Oncology-specific software and a Beam Dosimetry Imaging Package. The future of Onconcepts includes new and innovative Radiation Oncology Imaging and QA products. For information contact Michelle Donowsky.

ORTHOPEDIC FOUNDATION FOR ANIMALS

2300 E. Nifong Blvd.
Columbia, MO 65201-3806
573-442-0418
Email: ofa@offa.org
Website: www.offa.org

Established as a 501c(3) not-for-profit organization in 1966, the OFA has funded over two million dollars towards animal wellness. The OFA has evolved from solely a hip registry into genetic counseling for hip and elbow dysplasia, congenital cardiac disease, autoimmune thyroiditis, patella luxation, and other inherited canine diseases.

SOUND - EKLIN

5817 Dryden Place, Suite 101
Carlsbad, CA 92008
Phone: 760-448-4842
Toll Free: 800-268-5354
Email: sales@soundvet.com

Sound - Eklin is the veterinary industry's largest and most trusted imaging partner. For Digital Radiography, Ultrasound, Distributed Imaging, or Education, Sound-Eklin can provide you with the most powerful and cost effective solution. Sound-Eklin will deliver solutions that simplify and enhance diagnostic imaging to help your practice thrive.

UNIVERSAL MEDICAL SYSTEMS

29500 Aurora Rd, Unit 16
Solon, OH 44139
Phone: 440-349-3210
Fax: 440-498-2188
Email: sales@universal-systems.com
Website: www.veterinary-imaging.com

Universal Medical Systems, Inc. of Ohio is the only authorized distributor serving the veterinary market selling CT and MRI scanners directly from Toshiba Medical Systems and Esaote designed specifically to meet your needs. New or certified systems are available with a variety of financing and service options. Visit us today and see for yourself how we scan every animal in less than 30 seconds.

UNIVERSAL ULTRASOUND

299 Adams St.
Bedford Hills, NY 10507
Toll Free: 800-842-0607
Fax: 914-666-2454
Email: Sales@UniveralUltrasound.com
Website: www.universalultrasound.com

Universal Ultrasound has partnered with over 10,000 veterinarians to bring veterinary imaging into their practices confidently and affordably. Universal offers a variety of packages for both beginning and advanced users, featuring all digital technology, portability, veterinary specific applications, complete with connectivity and comprehensive training.

VETERINARY INFORMATION NETWORK

Toll Free: 800-700-4636
Fax: 530-756-6035
Email: vingram@vin.com
Website: http://www.vin.com

Company description: The Veterinary Information Network (VIN) is the premier online community, continuing education, and information resource for veterinarians. Founded in 1991, VIN reaches over 42,000 veterinarians, veterinary students, and industry partners worldwide. VIN is the leader in unlimited access to medical, product and practice management information. For a FREE one-month trial membership, join us at www.VIN.com, phone 800-700-4636, or email VINGRAM@vin.com. Let us show you why VIN is the BEST online resource for veterinarians. VIN will provide a free cyber café at ACVR, so please stop by to check your Email, surf the web, and try VIN!

VET RAY TECHNOLOGY BY SEDECAL

2920 N. Arlington Hts. Rd.
Arlington Heights, IL 60004
Website: www.vetray.com

Vet Ray Digital Vet DX offers the industry's only "One Touch" Touch Screen Display for 6 sec. image display and Generator Controls, largest image size: 17 x 17, 500mA High Frequency, 40kW Generator, 4-way float top, hands free collimator light control, the "easiest to use" Digital system on the market today.

VETEL DIAGNOSTICS

4850 Davenport Creek Rd
San Luis Obispo, CA 93401
Phone: 805-781-7691
Toll Free: 800-458-8890
Email: info@veteldiagnostics.com
Website: www.veteldiagnostics.com

VETEL Diagnostics offers veterinarians advanced diagnostic technologies including Envision, Explorer and Empower Digital Radiography Systems. Vetel's digital radiography systems were developed specifically for veterinarians with a focus on intuitive, user-friendly software and excellent image quality. System models include multiple companion animal configurations with a variety of panel sizes, available installed in a table or in a rugged portable case. Vetel's DR systems have the widest dynamic range available and are complete imaging systems with multiple image algorithms per view, image enhancement tools, accurate measurement tools and easy report generation. FLIR thermal imaging systems are revolutionizing veterinary medicine helping to diagnose difficult cases. Thermography applications include lameness diagnostics, pre-purchase exams, saddle fit evaluation and back pain detection.

WEBSTER VETERINARY

86 Leominster Rd.
Sterling, MA 01564
Phone: 800-453-6879

Since 1946, Webster Veterinary Supply has supplied veterinarians with an unsurpassed range of products and services from the leading names in veterinary medicine, backed by a knowledgeable and trained sales and service staff. We are a proud partner of Milburn Equine, Intravet and DIA, and together we have 14 US locations to serve your needs. Please stop by our booth where we will be displaying the latest in pharmaceuticals, biological, equipment and digital X-ray systems.

American College of Veterinary Radiology

Special Thanks to the Following Corporate Partners:

2009 Conference Bag Sponsor
CoActiv PACS 4 Vets

Cyber Café
Veterinary Information Network (VIN)

ACVR Reception Sponsors
Orthopedic Foundation for Animals
Universal Medical Systems, Inc.

Program Overview

2009 ACVR Scientific Conference
October 20-24, 2009
Peabody Hotel
Memphis, Tennessee

Tuesday, October 20, 2009 — Focus on MRI Forum — Peabody Grand Ballroom AB

7:00 am	Registration Opens- Peabody Grand Ballroom Foyer West- Mezzanine Level	
7:50 - 8:00 am	**Focus on MRI Forum** –Introductory Comments Liz Watson, Program Co-Chair (Forum Focus)	
8:00 - 8:50 am	Basics of MR Image Formation/Physics	Shannon Holmes
8:55 - 9:45 am	Understanding Pulse Sequences in MR Imaging	Amy Tidwell
9:45 – 9:55 am	*Break*	
9:55 – 10:45am	MR Artifacts and Compensation	Amy Tidwell
10:50 – 11:40 am	Intracranial MR Imaging	Eric Wisner
11:40 – 12:40 pm	*Lunch*	
12:40 – 1:30 pm	MR Spinal Imaging	Eric Wisner
1:35 – 2:25 pm	MR Musculoskeletal Imaging	Pat Gavin
2:25 – 2:35 pm	*Break*	
2:35 – 3:25 pm	Equine MR Imaging	Russ Tucker
3:30 – 4:20 pm	Thoracic and Abdominal MR imaging, including MRA	Sue Kraft
4:20 – 4:30 pm	*Break*	
4:30 – 5:20 pm	MR Equipment and Safety, including contrast	Sue Kraft
5:20 pm	Adjourn for the day	

Wednesday, October 21, 2009 **Peabody Grand Ballroom AB**

7:00 am *Ultrasound Society Meeting*

8:00 am Conference Welcome – Dr. Andra Voges, 2009 Program Chair

8:05 am ACVR Presidential Address – Dr. Jon Shiroma

8:30 am ACVR Keynote Address
Carlos Restrepo, MD
Assistant Professor, University of Texas Health Science Center
"CARDIAC IMAGING: PAST, PRESENT AND FUTURE"

10:00 am *Break with exhibitors*

10:30 am Ultrasound Society Keynote Address
Norman Rantanen, DVM, MS, DACVR
"THORACIC AND MUSCULOSKELETAL ULTRASOUND"

12:30 pm *Lunch- Continental Ballroom*

1:30 pm **Scientific Session 1: Diagnostic Ultrasound**

3:30 pm *Break with exhibitors*

4:00 pm **Scientific Session 2: Diagnostic Ultrasound**

5:00 pm Opportunity to Meet the Resident Coordinators

6:30 pm *ACVR Welcome Reception- The Skyway*

Thursday, October 22, 2009 **Peabody Grand Ballroom AB**

7:00 am	*Society of Veterinary Nuclear Medicine Meeting*
8:00 am	Nuclear Medicine Keynote Speaker Michael Ross, DVM, DACVS Professor of Surgery, Directory of Nuclear Medicine, New Bolton Center **"EQUINE MUSCULOSKELETAL IMAGING"**
9:30 am	**Scientific Session 3: Nuclear Medicine**
10:06 am	*Break with exhibitors*
10:30 am	**Scientific Session 4: Nuclear Medicine/General Radiology**
12:10 pm	Resident Authored Paper and Grant Awards
12:30 pm	*Lunch- Continental Ballroom*
1:30 pm	ACVR Image Interpretation Session
3:00 pm	*Break with exhibitors*
3:30 pm	Dr. Mary Lunz, Psychometrician, regarding the ACVR Examination
4:30 pm	Welcome new Diplomates, ACVR Business Meeting (Diplomates only)
6:00 pm	Adjourn for the day

Friday, October 23, 2009 **Peabody Grand Ballroom AB**

7:00 am *CT/MRI Society Meeting*

8:00 am CT/MRI Keynote Address
Patrick R Gavin, DVM, PhD, DACVR
"VETERINARY MRI - WHAT I HAVE LEARNED IN THE LAST 20 YEARS"

9:30 am **Scientific Session 5: Poster Session**

10:00 am *Break with exhibitors*

10:30 am **Scientific Session 6: CT/MRI**

12:06 pm *Lunch- Forest and Venetian Rooms*

CT/MRI Afternoon Session **Peabody Grand Ballroom AB**

1:30 pm **Scientific Session 7: CT/MRI**

3:00 pm *Break with exhibitors*

3:30 pm **Scientific Session 8: CT/MRI**

5:00 pm Large Animal Diagnostic Imaging Society Organizational Meeting

RO Afternoon Session **Continental Ballroom**

1:30 pm **Scientific Session 9: RO**

3:30 pm *Break with exhibitors*

4:00 pm **Scientific Session 10: RO**

5:45 pm Adjourn for the day

Saturday, October 24, 2009 **Venetian Room**

8:00 am *VRTOG Meeting*

9:00 am RO Keynote Address
James W. Welsh, MD
"INCREASING THE THERAPEUTIC RATIO, FROM BRAGG PEAKS TO BIOLOGICS AND BEYOND"

10:30 am *Break*

11:00 am **Scientific Session 11: RO**

12:30 pm *RO Business Meeting and lunch*

2:00 pm **Scientific Session 12: RO Forum Discussion** on IMRT, IGRT, Tomotherapy, Cyberknife and Proton Therapy

5:00 pm Adjourn for the day

Tuesday, October 20, 2009 **Focus on MRI Forum** **Peabody Grand Ballroom AB**

7:00 am	Registration Opens	
7:50 - 8:00 am	**Focus on MRI Forum** –Introductory Comments Liz Watson, Program Co-Chair (Forum Focus)	
8:00 - 8:50 am	Basics of MR Image Formation/Physics	Shannon Holmes
8:55 - 9:45 am	Understanding Pulse Sequences in MR Imaging	Amy Tidwell
9:45 – 9:55 am	*Break*	
9:55 – 10:45 am	MR Artifacts and Compensation	Amy Tidwell
10:50 – 11:40 am	Intracranial MR Imaging	Eric Wisner
11:40 – 12:40 pm	*Lunch*	
12:40 – 1:30 pm	MR Spinal Imaging	Eric Wisner
1:35 – 2:25 pm	MR Musculoskeletal Imaging	Pat Gavin
2:25 – 2:35 pm	*Break*	
2:35 – 3:25 pm	Equine MR Imaging	Russ Tucker
3:30 – 4:20 pm	Thoracic and Abdominal MR imaging, including MRA	Sue Kraft
4:20 – 4:30 pm	*Break*	
4:30 – 5:20 pm	MR Equipment and Safety, including contrast	Sue Kraft
5:20 pm	Adjourn for the day	

Wednesday, October 21, 2009 **Peabody Grand Ballroom AB**

7:00 am *Ultrasound Society Meeting*

8:00 am Conference Welcome – Dr. Andra Voges, 2009 Program Chair

8:05 am ACVR Presidential Address – Dr. Jon Shiroma

8:30 am ACVR Keynote Address
Carlos Restrepo, MD
Assistant Professor, University of Texas Health Science Center
"**CARDIAC IMAGING: PAST, PRESENT AND FUTURE**"

10:00 am *Break with exhibitors*

10:30 am Ultrasound Society Keynote Address
Norman Rantanen, DVM, MS, DACVR
"**THORACIC AND MUSCULOSKELETAL ULTRASOUND"**

12:30 pm *Lunch*

1:30 pm **Scientific Session 1: Diagnostic Ultrasound** (Moderator: Lorrie Gaschen)

1:30 pm **ULTRASOUND AND PERICARDIOCENTESIS FINDINGS IN 138 DOGS WITH PERICARDIAL EFFUSION AND CARDIAC TAMPONADE.** Dryden E.S., Siems J.J., Ramirez S., Sande R.S., Inland Empire Veterinary Imaging, Spokane, WA 99202

1:42 pm **ULTRASONOGRAPHIC CORRELATION OF ADRENAL THICKNESS AND LUMBAR VERTEBRAL LENGTH IN NORMAL DOGS**. M.K. Nelson, B.A. Selcer, J. Williams., UGA College of Veterinary Medicine, Athens, GA 30602

1:54 pm **IS ULTRASONOGRAPHIC ADRENAL MEASUREMENT BETTER ON LONG VS. SHORT AXIS VIEW? A RETROSPECTIVE STUDY.** A. Toshima, T. Miyabayashi, A. Sato, D. Sakamaki, Y. Fujiyoshi. The Institute of Veterinary Education & Advanced Technology, Osaka 562-0035, JAPAN

2:06 pm **COMPARISON OF RADIOGRAPHY AND ULTRASONOGRAPHY FOR DIAGNOSING SMALL-INTESTINAL MECHANICAL OBSTRUCTION IN VOMITING DOGS.** A. Sharma, M. S. Thompson, P. V. Scrivani, N. L. Dykes, A. E. Yeager, S. R. Freer, H. N. Erb. Cornell University Hospital for Animals, Ithaca, NY 14853-6401.

2:18 pm **ULTRASONOGRAPHY OF INTESTINAL MAST CELL TUMORS IN THE CAT.** M. Laurenson, A. Zwingenberger. University of California, Davis, CA, 95616.

2:30 pm **GALLBLADDER SLUDGE IN CATS: PREVALENCE AND ASSOCIATION WITH ELEVATED SERUM LIVER PARAMETERS.** Harran N., d'Anjou M.A., Dunn M., Department of clinical sciences, Faculty of Veterinary Medicine, Université de Montréal, St-Hyacinthe, Quebec, Canada J2S 7C6.

2:42 pm **NEW INSIGHTS IN CONTRAST-ENHANCED ULTRASONOGRAPHY (CEUS) OF SPLENIC NODULES.** O. Taeymans, D. Penninck. Department of Clinical Sciences, Foster Small Animal Hospital, Cummings School of Veterinary Medicine, Tufts University, MA, 01536.

2:54 pm **USE OF COLOR DOPPLER ULTRASOUND TO PREDICT MALIGNANCY OF SPLENIC MASSES IN DOGS.** Gall D, Gibbons D, Marolf A, Webb C, Kraft S, Park R. Colorado State University, Fort Collins, Colorado 80525.

3:06 pm **THE EFFECT OF SEVOFLURANE ANESTHESIA AND BLOOD DONATION ON THE ULTRASONOGRAPHIC APPEARANCE OF THE FELINE SPLEEN.** S.L. McMahon, L.J. Zekas, M.C. Iazbik, C.G. Couto, The Ohio State University Veterinary Teaching Hospital, Ohio, 43210

3:18 pm **EVALUATION OF DOGS WITH PORTOSYSTEMIC SHUNTS USING A TRANS-SPLENIC MICROBUBBLE TECHNIQUE AND A RIGHT ATRIAL WINDOW: PRELIMINARY RESULTS**. C.R. Berry, H.W. Maisenbacher, M.D. Winter, A.R. Coomer, R.F. Giglio, and D.J. Reese. College of Veterinary Medicine, University of Florida, Gainesville, FL.

3:30 pm *Break with exhibitors*

4:00 pm **Scientific Session 2: Diagnostic Ultrasound** (Moderator: Anthony Pease)

4:00 pm **SENSITIVITY AND SPECIFICITY OF VARIOUS ULTRASONOGRAPHIC CHANGES OF THE FELINE PANCREAS COMPARED TO FELINE PANCREATIC LIPASE IMMUNOREACTIVITY**. J.M. Williams[1], M.M. Larson[2], D.L. Panciera[2]. [1]Affiliated Veterinary Specialists, Maitland, FL 32751. [2]Virginia-Maryland Regional College of Veterinary Medicine, Blacksburg, VA 24061.

4:12 pm **ULTRASONOGRAPHIC OBSERVATION OF SECRETIN-INDUCED PANCREATIC DUCT DILATION IN HEALTHY CATS**. M.L. Baron, S. Hecht, A.R. Matthews, J.E. Stokes. University of Tennessee College of Veterinary Medicine, Knoxville, TN 37996

4:24 pm **CAN SPECIFIC SONOGRAPHIC FEATURES HELP TO DIFFERENTIATE NON-NEOPLASTIC FROM NEOPLASTIC DEEP LYMPH NODES IN DOGS?** M. de Swarte, K. Alexander, M.A. D'Anjou, B. Rannou, G. Beauchamp. Département de sciences cliniques, Faculté de médecine vétérinaire, Université de Montréal, St-Hyacinthe, Québec, Canada

4:36 pm **CONTRAST-ENHANCED ULTRASOUND IMAGING AND BIOPSY OF SENTINEL LYMPH NODES: FEASIBILITY STUDY IN DOGS.** H.R. Gelb, L.J. Freeman, J.R. Rohleder, P.W. Snyder. Department of Veterinary Clinical Sciences, School of Veterinary Medicine, Purdue University, West Lafayette, Indiana 47907.

5:00 pm Opportunity to Meet the Resident Coordinators

6:30 pm *ACVR Welcome Reception*

ULTRASOUND AND PERICARDIOCENTESIS FINDINGS IN 138 DOGS WITH PERICARDIAL EFFUSION AND CARDIAC TAMPONADE. Dryden E.S., Siems J.J., Ramirez S., Sande R.S., Inland Empire Veterinary Imaging, Spokane, WA 99202

Introduction/Purpose: Echocardiography is commonly used in diagnosing, assessing and guiding treatment in patients with pericardial effusion and cardiac tamponade. Pet owners oftentimes have questions regarding the etiology of pericardial effusion and prognosis. The aim of this study is to describe the ultrasound findings and pericardiocentesis results in 138 dogs; as well as provide information regarding long term survival.

Methods: Medical records of one hundred thirty eight dogs that underwent echocardiography and pericardiocentesis were reviewed. Patients were included in the study if pericardiocentesis was performed at the time of initial echocardiogram. Medical records were evaluated for pericardial effusion and visualization of a right atrial or heart base neoplasm. The character of the pericardial effusion was also recorded.

Results: The mean age at clinical presentation was 9.7 years. Males represented 62.3% (86/138) and females 37.7% (52/138) of the cases. A tumor was visualized in 60.9% (84/138) of the presenting cases. 89 patients were eventually found to have tumors within the pericardial sac (64.5%). 55.1% (49/89) of the tumors were associated with the right atrium, and 44.9% (40/89) were located at the heart base. The effusion was hemorrhagic in 88.4% (122/138) and non-hemorrhagic in 11.6% (16/138) of the cases. A tumor was evident in 68.7% (11/16) of cases with non-hemorrhagic effusion, of these 91% (10/11) were associated with the heart base. Follow-up echocardiograms were performed in 41 cases (range 2-13 exams), of these 53.7% (22/41) had tumors. Heart base tumors were most common at 72.3% (16/22). In cases with heart base tumors the average time between the initial and the last echocardiogram was 239.5 days (range 15-700 days). The average time between the initial and last echocardiogram in cases with a right atrial mass was 48.1 days (range 5-117 days).

Discussion/Conclusion: The number one cause of pericardial effusion in our study was neoplasia. A tumor was visualized approximately 60% of the time at initial presentation. Pericardial effusion was most often hemorrhagic. In cases with non-hemorrhagic effusion the most common location of a visualized tumor was the heart base. Dogs with tumors located at the heart base live longer.

ULTRASONOGRAPHIC CORRELATION OF ADRENAL THICKNESS AND LUMBAR VERTEBRAL LENGTH IN NORMAL DOGS. M.K. Nelson, B.A. Selcer, J. Williams

Introduction/Purpose: With advancements in ultrasound technology, adrenal gland identification and parenchymal assessment has become routine during abdominal ultrasonography. Numerous publications have attempted to quantify adrenal gland size. Most studies have produced ranges for normal adrenal gland size. Evaluating adrenal gland size in very small or large dogs or adrenal glands at the limits of the normal range is therefore subjective and can be difficult. The purpose of this study was to compare the adrenal gland thickness to an internal marker to determine a ratio for objective assessment, similar to those used for radiographic estimations such as renal size in small animals.

Methods: Adrenal ultrasonography was performed using a 5-8 MHz transducer (Phillips HDI). Measurements were obtained from 29 client-owned animals with no clinical signs or indices of suspicion for adrenal disease. All animals were scheduled for routine abdominal ultrasonography for reasons other than adrenal disorders. Body weight ranged from 5.2 kg to 40 kg. Sagittal images of both the left and right adrenal glands were obtained. All adrenal glands were measured in the ventrodorsal dimension at the thickest portion of the gland. Aortic diameter was measured during systole. The sixth and seventh lumbar vertebral lengths were determined via ultrasound by measuring from the most ventral cranial projection to the most ventral caudal projection. This measurement was also performed on radiographs obtained prior to ultrasound. A Pearson analysis was done to determine correlation between adrenal gland thickness and vertebral body length (both ultrasonographic and radiographic), aortic diameter, and body weight.

Results: There were significant moderate correlations between the aorta ($p=0.0222$, $r=0.44$), the length of L7 measured ultrasonographically ($p=0.0272$, $r=0.42$) and radiographically, ($p=0.0374$, $r=0.40$), and body wt ($p=0.0251$, $r=0.43$) and the right adrenal gland thickness. There was a significant moderate correlation between the length of L7 measured ultrasonographically ($p=0.0261$, $r=0.42$) and the left adrenal gland thickness. There was a significant correlation between ultrasonographic and radiographic measurements of L6 length ($p<0.0001$, $r=0.92$) and L7 length ($p<0.0001$, $r=0.78$). The ratio of left adrenal gland thickness to L7 length ranged from 0.17 to 0.60. The ratio of right adrenal gland thickness to L7 length ranged from 0.17 to 0.53.

Discussion/Conclusion: These data in a relatively small number of normal dogs suggest that the length of the 7^{th} lumbar vertebra can be correlated with both left and right adrenal gland thickness and may possibly be used to estimate adrenal gland thickness in dogs of various sizes.

IS ULTRASONOGRAPHIC ADRENAL MEASUREMENT BETTER ON LONG VS. SHORT AXIS VIEW? A RETROSPECTIVE STUDY. A. Toshima, T. Miyabayashi, A. Sato, D. Sakamaki, Y. Fujiyoshi. The Institute of Veterinary Education & Advanced Technology, Osaka 562-0035, JAPAN

Introduction/Purpose: A published normal value of the adrenal glands is less than 6 mm (7 mm in large dogs) on a longitudinal plane. However, when we examine adrenal glands, there appear to be a wide range in measuring width on a long axis plane. A purpose of this study is to retrospectively measure adrenal glands on both long and short axis to see if the measurement planes affect results.

Methods: We used clinical cases that visited our imaging center from January 26, 2009 to May 7, 2009. All studies were recorded on a DVD unit. These dogs had variable clinical signs. When we found a nodule or nodules, we did not use the data. We used the data only when we measured both long and short axes. A total of 37 dogs were used for data analysis. We measured thickness of a middle plane of caudal pole of right and left adrenal glands on long and short axis images. When we did not measure it on a still frame during examination, we measured from DVD images. We analyzed them by Paired Students' t-test whether there was significant difference.

Results: The thickness of left adrenal glands was 4.6 ± 0.81 (range 2.5-6.0) mm on long axis and 4.3 ± 1.27 (range 2.3-7.3) mm on short axis. The thickness of right adrenal glands was 4.5 ± 1.10 (range 2.6-7.5) mm on long axis and 4.0 ± 0.82 (range 2.2-5.4) mm on short axis. The difference between long and short axes was statistically significant ($p<0.01$).

***Discussion/Conclusion*:** Routinely, we have been measuring adrenal thickness on a longitudinal plane. In this study, we found that in a longitudinal plane, we tend to record thicker width than in a transverse plane. The published normal range is based on a longitudinal plane. Thus, we recommend that when a measurement value goes beyond a normal value, a transverse plane should be used to confirm the thickness. Since the shape of the adrenal glands is flat, this measurement error is unavoidable. Although a short axis view is subjectively difficult to obtain in a novice operator, it is important to measure on both long and short axis planes in questionable cases.

COMPARISON OF RADIOGRAPHY AND ULTRASONOGRAPHY FOR DIAGNOSING SMALL-INTESTINAL MECHANICAL OBSTRUCTION IN VOMITING DOGS. A. Sharma, M. S. Thompson, P. V. Scrivani, N. L. Dykes, A. E. Yeager, S. R. Freer, H. N. Erb. Cornell University Hospital for Animals, Ithaca, NY 14853-6401.

Introduction/Purpose: The aims of this cross-sectional study were to compare the overall accuracy of radiography and ultrasonography to diagnose small-intestinal mechanical obstruction in vomiting dogs and to investigate several individual radiographic and ultrasonographic signs to identify their contribution to the final diagnosis and our understanding of pathogenesis.

Methods: The sample population consisted of 82 adult dogs with acute vomiting. Small-intestinal obstruction was diagnosed in 27 of 82 (33%) dogs by surgery or necropsy. Groups were compared using receiver-operator characteristic (ROC) curve analysis and descriptive statistics.

Results: The overall accuracy of both 3-view abdominal radiography (area under the curve [AUC], 0.817; SE, 0.054; 95% confidence interval [CI], 0.716 to 0.894) and abdominal ultrasonography (AUC, 0.954; SE, 0.029; CI, 0.883 to 0.987) was very good for diagnosing small-intestinal obstruction. The difference between areas was 0.136 (SE, 0.055; CI 0.029 to 0.244) and was statistically significant (P = 0.013). There was moderate agreement (weighted Kappa, 0.582; SE, 0.074) between 3-view abdominal radiography and abdominal ultrasonography for diagnosing small-intestinal mechanical obstruction. Radiography and ultrasonography produced the exact same result 52 of 82 times. Intermediate results were produced more often during radiography (n = 24) than ultrasonography (2). Confident results were produced less often during radiography (n = 58) than ultrasonography (80).

Discussion/Conclusion: In conclusion, both 3-view abdominal radiography and abdominal ultrasonography are accurate for diagnosing small-intestinal obstruction in vomiting dogs and either examination may be used depending on availability and examiner choice. Ultrasonography has better accuracy and fewer equivocal results.

ULTRASONOGRAPHY OF INTESTINAL MAST CELL TUMORS IN THE CAT. M. Laurenson, A. Zwingenberger. University of California, Davis, CA, 95616.

Introduction/Purpose: Abdominal ultrasonography is a frequently utilized diagnostic imaging modality to evaluate cats with signs of gastrointestinal disease. The purpose of this study was to retrospectively review the ultrasonographic findings in cats with intestinal mast cell tumors.

Methods: Medical records at the Veterinary Medical Teaching Hospital at the University of California at Davis were searched from 1999 to 2009 to identify cats with intestinal mast cell tumors diagnosed by cytology or histopathology, and a concurrent abdominal ultrasound examination. Ultrasound reports and static images were retrospectively reviewed for intestinal abnormalities. Additional changes to the regional lymph nodes, spleen and liver were also noted and compared with pathologic findings.

Results: Fourteen cats met the inclusion criteria with an average age of 13.2 +/- 2.6 years. Three cats had concurrent diffuse mucosal intestinal lymphoma. Nine of the cats had masses within the jejunum or duodenum, 4 cats had masses at the ileocecocolic junction, and 1 had a colonic mass. The masses had a variety of ultrasonographic appearances, but within the small intestine, a common pattern was a non-circumferential, eccentric mass. Five cats had multiple masses. Metastatic disease was not well detected in the liver (1/4 cats), or spleen (0/3 cats) with ultrasound. Nine of the fourteen cats had regional lymphadenopathy identified ultrasonographically.

Discussion/Conclusion: Mast cell tumors of the small intestine are commonly single or multiple non-circumferential, eccentric masses with local lymphadenopathy. Metastatic spread to the liver and spleen should be considered, even without ultrasonographic abnormalities.

GALLBLADDER SLUDGE IN CATS: PREVALENCE AND ASSOCIATION WITH ELEVATED SERUM LIVER PARAMETERS. Harran N., d'Anjou M.A., Dunn M., Department of clinical sciences, Faculty of Veterinary Medicine, Université de Montréal, St-Hyacinthe, Quebec, Canada J2S 7C6.

Introduction/Purpose: GB sludge is routinely identified in cats and dogs during ultrasound examinations. In cats, it has been reported with various liver diseases, particularly those affecting the biliary tract. Moreover, it has been suggested that GB sludge may be associated with hepatobiliary diseases in cats when compared to dogs. The goals of this study were to determine the prevalence of GB sludge in cats, to describe the associated clinical and laboratory findings, and to compare the elevation of serum liver parameters in cats with and without GB sludge detected by ultrasonography.

Methods: Abdominal ultrasound reports and images of feline patients presented with GB sludge between 2004 and 2008 were reviewed. Signalment, clinical signs, serum alanine aminotransferase (ALT), alkaline phosphatase (ALP) and total bilirubin, haematology and urinalysis were collected when available. A control group of 40 cats without GB sludge identified randomly during the same period was documented for ALT, ALP and total bilirubin. In order to compare serum liver values between groups of cats, a ratio was used: R ratio = parameter value/upper interval reference value for each liver parameter. Mean R ratios were compared between groups. For cats that had serum chemistry testing performed at the Faculty of Veterinary Medicine diagnostic laboratory, mean values of ALT, ALP and total bilirubin were compared between groups. An unequal variance t-test was used for comparisons and a logistic regression analysis was used to determine the probability of increased ALT, ALP and total bilirubin values in cats with GB sludge. Significance level was set at $p < 0.05$.

Results: 152 cats (92 males, 60 females) presented GB sludge on ultrasound, with an estimated prevalence of 14% in our hospital population. Cats with GB sludge had a mean (range) age of 10.3 years (0.3–21.1) and body weight of 4.2 kg (2.0–8.2). These cats were presented for decreased appetite/anorexia (62%), lethargy (55%), weight loss (51%), dehydration (50%) and vomiting (43%). Also, ALT (n=143), ALP (n=143), total bilirubin (n=131) and bilirubinuria (n=97) were increased in 46%, 35%, 43% and present in 25% of cats, respectively. Mean values for ALT, ALP and total bilirubin were increased by a factor (range) of 2.1 (0.1–16.6), 2.0 (0.0–42.9) and 3.2 (0.1–30.6), respectively. R ratios and serum values were significantly higher in cats with GB sludge than in control cats for ALT, ALP and total bilirubin ($p \leq 0.0006$). The odds to obtain an increased value were significantly related to the group for ALT ($p = 0.0008$), ALP ($p = 0.003$) and total bilirubin ($p = 0.005$), and were 4.9 (CI: 1.9-12.3), 6.4 (CI: 1.9-21.9) and 4.2 (CI: 1.5-11.5), respectively, in cats with GB sludge in comparison to control cats.

Discussion/Conclusion: Evaluation of serum liver parameters is commonly used to screen for the presence of hepatobiliary disease in cats. Our study showed that cats with gallbladder sludge on ultrasound are more likely to present elevated serum liver parameters. As compared to dogs, GB sludge in cats appears to be a significant sonographic finding that could predict hepatobiliary disease. Further studies are needed to confirm this suspicion and elucidate its clinical significance.

NEW INSIGHTS IN CONTRAST-ENHANCED ULTRASONOGRAPHY (CEUS) OF SPLENIC NODULES. O. Taeymans, D. Penninck. Department of Clinical Sciences, Foster Small Animal Hospital, Cummings School of Veterinary Medicine, Tufts University, MA, 01536.

Introduction/Purpose: Studies with CEUS on focal splenic lesions have shown discrepancies in accuracy for differentiating benign from malignant lesions.[1-3] A speculative explanation for false positives may be the absence of a dual blood supply to the spleen compared to the liver. We therefore hypothesized that the early wash in / early wash out (EWEW), and the hypoechogenicity during all phases are unreliable in differentiating malignant from benign splenic lesions.
Methods: A retrospective study reviewing CEUS studies of 17 splenic lesions (7 malignant, 10 benign), with concurrent cytology, core biopsy and/or excision biopsy was conducted. Sonovue® at a dose of 0.03 mL/kg was used in all dogs. Tortuosity of feeding vessels, presence of EWEW, and hypoechogenicity during all phases were assessed visually and used to characterize the lesions.
Results: There were 4/10 benign, and 4/7 malignant lesions with EWEW. Therefore, sensitivity, specificity, and accuracy for EWEW in differentiating malignant from benign lesions are 57%, 60%, and 59% respectively. There were 3/10 benign, and 3/7 malignant lesions with persistent hypoechogenicity throughout all phases. Therefore, sensitivity, specificity, and accuracy are 43%, 70%, and 59%. There were 0/10 benign, and 5/7 malignant lesions with tortuous and persistently visible feeding vessels. Sensitivity, specificity, and accuracy are 71%, 100%, and 88%. Finally, there were 7/10 benign and 7/7 malignant lesions with a combination of at least one of the above parameters. Sensitivity, specificity, and accuracy are 100%, 30%, and 59%.
Discussion/Conclusion: These preliminary results support our hypothesis that the interpretation of splenic lesions cannot accurately be performed on the basis of EWEW, or persistent hypoechogenicity throughout all phases. Instead, we recommend assessing the presence of tortuous vessels in the periphery of the lesion during the early phase, and the persistence of these hyperechoic tortuous vessels in the late phase. Further studies with larger numbers are necessary to better assess these findings.
Acknowledgement: We would like to thank the generous support of Bracco Research for the delivery of Sonovue®.

1: Ivancić M, Long F, Seiler GS. Contrast harmonic ultrasonography of splenic masses and associated liver nodules in dogs. J Am Vet Med Assoc. 2009;234:88-94.
2: Ohlerth S, Dennler M, Rüefli E, et al. Contrast harmonic imaging characterization of canine splenic lesions. J Vet Intern Med. 2008;22:1095-102.
3: Rossi F, Leone VF, Vignoli M, Laddaga E, Terragni R. Use of contrast-enhanced ultrasound for characterization of focal splenic lesions. Vet Radiol Ultrasound. 2008;49:154-64.

USE OF COLOR DOPPLER ULTRASOUND TO PREDICT MALIGNANCY OF SPLENIC MASSES IN DOGS. Gall D, Gibbons D, Marolf A, Webb C, Kraft S, Park R. Colorado State University, Fort Collins, Colorado 80525.

Introduction/Purpose: Recent literature has described specific vascular patterns for benign and malignant splenic masses using contrast enhanced ultrasound (CEU). The purpose of this study was to determine if similar vascular patterns could be identified using color Doppler ultrasound and if so, whether these could be used to predict malignancy. An attempt was made to correlate other ultrasonographic findings with malignancy.

Methods: This was a retrospective study of 26 canine patients which had been examined by color Doppler ultrasound between 01/01/1996 and 10/01/2007 and had a histopathologic diagnosis obtained via splenectomy or necropsy. The ultrasound examinations were made using a Siemens Antares Acuson ultrasound unit with a multi-frequency linear array transducer. Still images of color Doppler exams were reviewed retrospectively by a radiology resident and two board certified radiologists and the variable was scored via consensus. Vasculature was graded as distorted if it altered its course around a mass lesion or nodule within the spleen, and not distorted if it did not alter its course. Presence of peritoneal effusion, distortion of the splenic capsule by the mass, presence of hypoechoic cavitations within the mass, and presence of vascularity within the mass as detected by color Doppler were all scored on a yes or no basis.

Results: Ten lesions were diagnosed as benign and 16 as malignant. Histopathological diagnoses included hemangiosarcoma (n=14), hematoma (6), extramedullary hematopoiesis (2), hemangioma (1), mast cell tumor (1), metastatic soft tissue sarcoma (1), and adipose metaplasia (1). There was no statistically significant relationship identified between vascular pattern and histopathological diagnosis. However, there was a trend displaying that those with no distortion of the vascularity were more likely to be malignant (sensitivity 81%, specificity 40%). This is the opposite of what was predicted. Similarly there was no statistically significant relationship identified between malignancy and size of the mass, cavitation, presence of peritoneal effusion, distortion of the capsule of the spleen, or how vascular the mass was relative to the adjacent normal spleen.

Discussion/Conclusion: Color Doppler ultrasound is less time consuming and requires less expertise than CEU. For this reason, color Doppler ultrasound may be more practical for most practitioners to perform than CEU. Although this study failed to identify a significant relationship between vascular pattern and histopathology, the retrospective design may be a limiting factor. These findings should be examined further with a prospective design, examining for distortion of the vasculature in a real-time examination rather than still images.

THE EFFECT OF SEVOFLURANE ANESTHESIA AND BLOOD DONATION ON THE ULTRASONOGRAPHIC APPEARANCE OF THE FELINE SPLEEN. S.L. McMahon, L.J. Zekas, M.C. Iazbik, C.G. Couto, The Ohio State University Veterinary Teaching Hospital, Ohio, 43210

Introduction/Purpose: Ultrasonography is useful for evaluating feline splenic pathology. Normal ultrasonographic measurements of the feline spleen are not well characterized. Unlike the dog and Cheetah, the ultrasonographic response of the feline spleen to drugs and hemorrhage has not been established. This study aims to evaluate normal splenic ultrasonographic size and assess the effect of sevoflurane and non-splenic hemorrhage (blood donation for blood product banking) on the ultrasonographic appearance and size of the feline spleen.

Methods: Sixty healthy cats (24 FS and 36 MC) presenting for blood donation were enrolled in the study. The mean blood donation was 8.4 ±1.1 ml/kg. Transverse images of the midbody of the spleen were made with a multifrequency transducer at 13 MHz. Splenic ultrasonographic measurements (height, width and cross sectional area (CSA)), echogenicity relative to the left kidney and echotexture were recorded at four time periods. Ultrasonographic evaluation was performed at baseline prior to anesthesia/blood donation, following anesthesia induction, following completion of blood donation while under anesthesia and 7-10 days after blood donation.
The variables height, width and area were compared across the four treatment periods using separate linear mixed effects models. The models included period as the primary factor, with multiple covariates as predictors. For each model, the presence of significant two-way interactions with treatment period was assessed. Holm's method was applied to adjust for multiplicity and control the overall Type 1 error rate at α=0.05.

Results: In these clinically normal cats, the mean ±SD for transverse splenic size at baseline was: height 8.2 ±1.4 mm, width 26.7 ±4.4 mm, and CSA 1.6 ±0.5 cm^2. The spleen was diffusely homogenous and subjectively isoechoic or mildly hyperechoic relative to the left renal cortex. Height significantly increased from baseline after anesthetic induction, with a subsequent decrease in size at the post-blood donation period. Width was significantly decreased for castrated male cats at recheck compared with post anesthetic and post-blood donation periods; however, width at the recheck period was not significantly different from baseline. CSA was significantly increased for castrated male cats after anesthetic induction and post-blood donation, when compared with baseline. No significant differences in width or CSA were found at any time period for spayed female cats. Splenic size at recheck was not significantly different compared with baseline for any measurements.

Discussion/Conclusion: Normal ultrasonographic splenic measurements for height, width and CSA in cats are reported. While there was a statistically significant change in splenic height, width and CSA after sevoflurane anesthesia and/or blood collection, these changes were minor and likely not clinically relevant. Sevoflurane anesthesia and blood donation do not alter the subjective echogenicity and echotexture.

EVALUATION OF DOGS WITH PORTOSYSTEMIC SHUNTS USING A TRANS-SPLENIC MICROBUBBLE TECHNIQUE AND A RIGHT ATRIAL WINDOW: PRELIMINARY RESULTS. C.R. Berry, H.W. Maisenbacher, M.D. Winter, A.R. Coomer, R.F. Giglio, and D.J. Reese. College of Veterinary Medicine, University of Florida, Gainesville, FL.

***Introduction/Purpose**:* Congenital portosystemic shunts are the most common extra-cardiac developmental vascular anomaly. Imaging of portosystemic shunts has included trans-splenic scintigraphy and CT, bolus tracking CT, MR and ultrasound. Ultrasound imaging depends on the proficiency of the sonographer and the possibility of false negative studies exists for all techniques in patients with microvascular portal dysplasia. The purpose of this study was to develop a relatively simple technique for documenting the presence or absence of a macroscopic portosystemic shunt in dogs and cats using ultrasound.

Methods: Three dogs with surgically confirmed portosystemic shunts were placed in right lateral recumbency. Under US guidance, a 22 ga, 1 and ½ inch needle placed into the splenic parenchyma. A three-way stop cock with two attached syringes was fixed to the needle. One of the two syringes contained ½ to 1 mL of saline that was agitated back and forth between the two syringes just prior to injection. The US probe was placed in a right parasternal position with the main body of the right atrium being visualized in long-axis. The agitated saline was then injected into the spleen in bolus format. All three dogs were under general anesthesia at the time of the study.

Results: Within 3 to 5 seconds of injection, microbubbles from the saline splenic injection were seen within the right atrium. The shunts that were evaluated included acquired multiple extrahepatic portosystemic shunts, a portoazygus shunt and a portocaval shunt. Evaluation of the site of splenic injection after the study failed to document immediate complications.

***Discussion/Conclusion**:* This study presents preliminary results of a technique that can be performed in general practice using ultrasound guidance and documentation of portosystemic shunting without having to identify the portosystemic shunt itself. Some degree of proficiency with fine needle aspirate technique (placement of the needle into the splenic parenchyma) and imaging of the right atrium in a right parasternal long-axis are required. This technique may prove helpful in the identification of complete occlusion of ameroid constrictors over time. The limitations of this preliminary investigation include: limited number of patients, lack of normal controls, requirement of two semi-experienced operators for the ultrasound equipment, lack of long term splenic histology at the site of injection and general anesthesia. Despite these limitations, this technique warrants further investigation for use in general practice for the identification of the presence of portosystemic shunts for referral of appropriate patients for further evaluation within the specialty practice or academic University setting.

SENSITIVITY AND SPECIFICITY OF VARIOUS ULTRASONOGRAPHIC CHANGES OF THE FELINE PANCREAS COMPARED TO FELINE PANCREATIC LIPASE IMMUNOREACTIVITY. J.M. Williams[1], M.M. Larson[2], D.L. Panciera[2]. [1]Affiliated Veterinary Specialists, Maitland, FL 32751. [2]Virginia-Maryland Regional College of Veterinary Medicine, Blacksburg, VA 24061.

Introduction/Purpose: Despite numerous diagnostic methods, feline pancreatitis remains difficult to accurately diagnose. While histopathology, using multiple tissue sections, is considered the gold standard for diagnosis, feline pancreatic lipase immunoreactivity assay (fPLI) reportedly has high specificity and sensitivity, especially with severe disease. Ultrasound imaging of feline pancreatitis appears to have relatively high specificity, but low sensitivity. Using fPLI as the gold standard, this project determined the sensitivity and specificity of several ultrasonographic changes commonly associated with feline pancreatitis

Methods: A retrospective study through records at the VMRCVM Veterinary Teaching Hospital identified cats with a documented fPLI value and a corresponding abdominal ultrasound.. Sonographic images were reviewed and the following measurements and observations were noted: pancreatic thickness (< 1 cm vs. ≥1 cm), margination (linear vs. mildly irregular vs. severely irregular), echogenicity compared to the liver (isoechoic vs. hypoechoic), and echogenicity of the surrounding fat (isoechoic vs. hyperechoic). Cats were divided into 2 groups based on normal or elevated fPLI results.

Results: A total of 40 cats varying in ages from 5 months to 18 years were identified. Sensitivity and specificity measurements for each of the four ultrasonographic changes listed previously were calculated using fPLI as the gold standard. Sensitivity and specificity for pancreatic thickness was 28% and 98%, respectively. Sensitivity and specificity for pancreatic margination was 48% and 96%, respectively. The sensitivity for echogenicity of the pancreas compared to the liver was 38%, while the specificity was calculated at 96%. The sensitivity and specificity for the echogenicity of peripancreatic fat was 45%, and 100%, respectively.

Discussion/Conclusion: Ultrasound was determined to have low sensitivity and high specificity for the diagnosis of feline pancreatitis when comparing characteristic sonographic changes with fPLI. There was no improvement in the sensitivity of ultrasound appearance when compared to ranges previously reported, but its specificity for the disease remained close to 100%.

ULTRASONOGRAPHIC OBSERVATION OF SECRETIN-INDUCED PANCREATIC DUCT DILATION IN HEALTHY CATS. M.L. Baron, S. Hecht, A.R. Matthews, J.E. Stokes. University of Tennessee College of Veterinary Medicine, Knoxville, TN 37996

Introduction/Purpose: Secretin is a polypeptide hormone that stimulates secretion of bicarbonate from the exocrine pancreas and, in healthy human subjects, has been shown to cause transient pancreatic duct dilation observable via abdominal ultrasonography. In humans afflicted with chronic pancreatitis, secretin administration fails to cause pancreatic duct dilation, theoretically due to the restrictive effects of periductal fibrosis. This diagnostic test has been shown to be highly sensitive and specific for the diagnosis of chronic pancreatitis in humans. The purpose of this study was to establish the potential effects of exogenous secretin administration on the width of the pancreatic duct in healthy domestic cats.

Methods: Nine healthy cats were administered a commercially available secretin product (ChiRho Stim^{TM}) while the pancreatic duct was monitored by percutaneous ultrasonography. Maximum pancreatic duct diameter after secretin stimulation was compared to measurements made prior to injection, and a percentage increase over basal width was calculated.

Results: Mean pancreatic duct diameter increased from 0.77 ± 0.33 mm to 1.42 ± 0.40mm after secretin administration, which was statistically significant ($p = .0017$). The mean percent increase in pancreatic duct diameter over basal diameter for all time points one to fifteen minutes post secretin administration was 101.9 ± 58.8%.

Discussion/Conclusion: Exogenously administered secretin causes significant pancreatic duct dilation in healthy cats that can be observed via percutaneous ultrasound. Applicability of this technique in cats with chronic pancreatitis will need to be investigated in future studies.

This research project was funded by a resident research grant from the American College of Veterinary Radiology.

CAN SPECIFIC SONOGRAPHIC FEATURES HELP TO DIFFERENTIATE NON-NEOPLASTIC FROM NEOPLASTIC DEEP LYMPH NODES IN DOGS? M. de Swarte, K. Alexander, M.A. D'Anjou, B. Rannou, G. Beauchamp. Département de sciences cliniques, Faculté de médecine vétérinaire, Université de Montréal, St-Hyacinthe, Québec, Canada

***Introduction/Purpose*:** With technologic progress, deep lymph nodes (LN) have become more easily detectable by ultrasonography (US) and their features have been described for certain diseases. However, the ability of US to differentiate neoplastic from non-neoplastic LN has only been reported retrospectively or in superficial LN. This study prospectively compared specific sonographic features of neoplastic and non-neoplastic deep canine LN.

Methods: Canine patients undergoing US-guided aspiration with cytologic and/or histopathologic analysis of abnormal abdominal or thoracic LN within seventy-two hours following complete abdominal US were included. Specific US and Doppler US features of each LN were recorded by the radiologist immediately prior to aspiration. Lymph nodes were categorized into non-neoplastic (NN: reactive and lymphadenitis) or neoplastic (N: lymphoma and metastasis) groups. The prevalence of each US feature was calculated within each group and compared using a χ^2 test or Student's t-test for unequal variances. Certain features were combined and prevalence of the combined features was also compared.

Results: Twenty-two cases underwent LN aspiration, including 12 mesenteric (6 NN, 6 N), 8 medial iliac (2 NN, 6 N), one hepatic (NN) and one sternal (N). Based on cytology (21) or histopathology (1), six LN were reactive, two were lymphadenitis, six compatible with lymphoma and seven were metastatic. Only mean height (p=0.01; NN 1.15 +/- 0.36 cm; N 3.27 +/- 2.54 cm) and length (p=0.02; NN 3.65 +/- 1.00 cm; N 5.59 +/- 2.49 cm) were significantly different between non-neoplastic and neoplastic LN. All LN were hypoechoic and no significant differences were seen in echotexture, contour regularity, shape, the presence of hilar tissue definition, the presence of cavitations or the LN height/length ratio. Although not significant, the adjacent mesentery seemed to be more often hyperechoic with neoplastic LN (p=0.08; NN 33%; N 77%). Due to excessive respiratory motion, Doppler was possible in only 4 non-neoplastic and 11 neoplastic LN; of these 7 showed no blood flow and there was no significant difference between flow patterns (peripheral, hilar or mixed) between groups in the other LN. There were no significant combinations of US features differentiating non-neoplastic from neoplastic lymph nodes.

Discussion/Conclusion: The greater height and length of neoplastic LN was consistent with previous studies. Most US features were not significantly associated with a specific LN category. A larger study sample size may reveal further significant differences, although a degree of overlap in US features would likely be found. Doppler evaluation of lymph nodes appeared to be of limited clinical usefulness. The deeper location of the studied LN may influence their features relative to superficial LN and may make neoplastic differentiation more difficult. Other US techniques, such as contrast harmonics, may help better differentiate non-neoplastic from neoplastic LN.

CONTRAST-ENHANCED ULTRASOUND IMAGING AND BIOPSY OF SENTINEL LYMPH NODES: FEASIBILITY STUDY IN DOGS. H.R. Gelb, L.J. Freeman, J.R. Rohleder, P.W. Snyder. Department of Veterinary Clinical Sciences, School of Veterinary Medicine, Purdue University, West Lafayette, Indiana 47907.

Introduction/Purpose: Current sentinel node sampling consists of localizing the node(s) with injection of radioactive isotopes, blue dye, or both, followed by open surgical excision. Our goal was to develop a safe and reproducible, minimally invasive technique for biopsy of sentinel lymph nodes that results in the same diagnostic success as the current method. The objectives of this study were to 1) develop a technique for identifying the sentinel lymph nodes of the mammary chain in dogs using contrast-ultrasound imaging and 2) evaluate the feasibility of obtaining representative samples of a sentinel lymph node under ultrasound guidance using a new handheld, vacuum-assisted biopsy device.

Methods*:* Three healthy, anesthetized dogs were used in the study. An ultrasound unit (ACUSON Sequoia™ 512; Siemens) with 8-15 MHz linear array transducer was used to visualize lymph nodes that drain the mammary chain in the groin or axillary region. Next, a 0.2mL dose of an aqueous suspension of a perfluoropropane-filled lipid microsphere contrast agent (Definity®; Lantheus Medical Imaging) was injected subcutaneously around the closest ipsilateral mammary gland. Ultrasound examination was performed with Cadence™ CPS imaging (Siemens) in a split screen mode to identify the sentinel lymph node. With ultrasound guidance, a 12-gauge, vacuum assisted handheld biopsy device (Celero®, Hologic, Inc.) was used to obtain three to four samples. A regional mastectomy including the draining lymphatics was then performed. The biopsy samples and the residual lymphoid tissue were evaluated histologically and compared.

Results: In three dogs, a total of eight sentinel lymph nodes were identified. The lymph nodes ranged from 2 to 4 mm in diameter. Following injection, the contrast agent was successfully visualized moving toward each respective sentinel lymph node. A total of 31 biopsy samples were obtained. For each node, one to three samples contained adequate lymphoid tissue for evaluation. Following excision, multiple biopsy tracts were identified in each excised lymph node, corresponding to the biopsy samples.

Discussion/Conclusion: Contrast-enhanced ultrasound can be successfully used to image and guide minimally invasive biopsy of the normal sentinel lymph nodes draining the mammary glands in healthy dogs. Further work is needed to evaluate whether this technique may be applicable in breast cancer patients. This study was funded by Hologic, Inc.

Thursday, October 22, 2009 **Peabody Grand Ballroom AB**

7:00 am *Society of Veterinary Nuclear Medicine Meeting*

8:00 am Nuclear Medicine Keynote Speaker
Michael Ross, DVM, DACVS
Professor of Surgery, Directory of Nuclear Medicine, New Bolton Center
"**EQUINE MUSCULOSKELETAL IMAGING**"

9:30 am **Scientific Session 3: Nuclear Medicine** (Moderator: Clifford Berry)

9:30 am **FOCAL SKELETAL MUSCLE UPTAKE OF ^{99m}Tc-HDP CAUSED BY PERONEAL NERVE BLOCKS IN HORSES.** J.F. Griffin, B.D. Young, G.T. Fosgate, M.A. Walker, J.P. Watkins. Texas A&M University, College Station, TX 77843-4475.

9:42 am **QUANTITATIVE PERTECHNETATE THYROID SCINTIGRAPHY AND ULTRASONOGRAPHIC APPEARANCE OF THE THYROID GLAND IN EUTHYROID HORSES.** S. Davies, G. Daniel, D. Barber, M. Crisman and M. Larson. Virginia-Maryland Regional College of Veterinary Medicine, Virginia, 24061.

9:54 am **DEPTH-CORRECTED VERSUS NON DEPTH-CORRECTED GFR DETERMINATION BY QUANTITATIVE RENAL SCINTIGRAPHY IN THE DOG.** G.T. Almond, J.A. Hudson, W.R. Brawner, Jr., M. Holland, J.C. Wright. Auburn University, Alabama, 36849.

10:06 am *Break with exhibitors*

10:30 am **Scientific Session 4: NM/General Radiology** (Moderator: Federica Morandi)

10:30 am **MYOCARDIAL KINETICS OF *META*-[I-131]IODOBENZYL-GUANIDINE IN AN ADRIAMYCIN CARDIOMYOPATHY RAT MODEL.** C. R. Berry, G. Vaidyanathan, M.R. Zalutsky, R. E. Coleman and T.R. DeGrado; College of Veterinary Medicine (Berry), University of Florida, Gainesville, FL; PET Facility, Duke University Medical Center, Durham, NC and the Joint Program of Nuclear Medicine, Brigham & Women's Hospital, Harvard University, Boston, MA (DeGrado)

10:42 am **PORTABLE X-RAY MACHINE TUBE LEAKAGE AND SCATTER RADIATION OPERATOR EXPOSURE WITH AN EQUINE CADAVER RADIOLOGY PHANTOM.** R. Tyson, D.C. Smiley, R.S. Pleasant, G.B. Daniel. Virginia-Maryland Regional College of Veterinary Medicine. Blacksburg, VA 24061.

10:54 am **APPLICATION OF THE PROVENTRICULUS-TO-KEEL RATIO AS A PROGNOSTIC INDICATOR AND FACTORS AFFECTING ITS CALCULATION.** S.E. Dennison[1], W.M. Adams[1], B. S. Yandell[2], P. Johnson[3], J.R. Paul-Murphy[1].[1]School of Veterinary Medicine, University of Wisconsin, WI 53706, USA. [2]Departments of Statistics and Biostatistics and Medical Informatics, University of Wisconsin, WI 53706, USA. [3]Great Western Referrals, Wiltshire, SN1 2NT, UK.

11:06 am **HIP DYSPLASIA TREATED BY JUVENILE PUBIC SYMPHYSIODESIS (JPS): RADIOGRAPHIC RESULTS AT 7 YEARS.** W. M. Adams[1], R.T. Dueland[1], P.M. Crump[2], P. Chinudomsub[3]. [1]School of Veterinary Medicine, [2]Department of Computing and Biometry, [3]College of Agriculture and Life Sciences, University of Wisconsin, WI 53706, USA.

11:18 am **EFFECTS OF INITIAL LATERAL RECUMBENCY ON THE POSITION OF THE SMALL INTESTINES ON THE VENTRODORSAL VIEW IN CATS** S.T. Tibbs, L.E. Ziegler, and C.R. Jessen. College of Veterinary Medicine, University of Minnesota, MN, 55108.

11:30 am **RADIOGRAPHIC CHARACTERIZATION OF PRESUMED PLATE-LIKE ATELECTASIS IN 37 DOGS AND 13 CATS**. C.R. Berry, R.F. Giglio, M.D. Winter, D.J. Reese, D.E. Thrall, and J.P. Graham. College of Veterinary Medicine, University of Florida, Gainesville, FL; North Carolina State University (Thrall), Raleigh, NC; and Affiliated Veterinary Specialists (Graham), Maitland, FL.

11:42 am **RADIOGRAPHIC APPEARANCE OF PULMONARY LYMPHOMA IN CATS AND DOGS.** Geyer N[1], Reichle JK[1], Valdez-Martinez A[2], J Williams[3], Goggin JM[4], Leach L, [5] Hanson J, [6] Hill S[7], Axam T[8]. [1]Animal Surgical and Emergency Center, LA CA; [2]Colorado State University Veterinary Teaching Hospital, Fort Collins CO; [3] University of Georgia, Athens GA; [4]Metropolitan Veterinary Radiology, Ltd, Montclair NJ; [5]Moore Animal Hospital, Fort Collins CO; [6] Veterinary Diagnostic Imaging & Cytopathology, PC, Clackamas OR; [7] Veterinary Specialty Hospital, San Diego CA; [8]Saint Francis Animal Care Center, Atlanta GA.

11:54 am **INTEROBSERVER VARIABILITY OF BOARD CERTIFIED AND NON-BOARD CERTIFIED RADIOLOGISTS FOR PULMONARY NODULE DETECTION WITH CANINE THORACIC RADIOGRAPHS USING NEGATIVE (STD) AND POSITIVE (INV) SOFT-COPY DISPLAYED IMAGES.** D.J. Reese[2], E.M. Green[1], L.J. Zekas[1], J.E. Flores[1], L.N. Hill[1], M.D. Winter[2], C.R. Berry[2], N. Ackerman[2]. [1]The Ohio State University, OH, 43210 and [2]University of Florida, FL, 32610

12:10 pm Resident Authored Paper and Grant Awards (Erik Wisner)

12:30 pm *Lunch*

1:30 pm ACVR Image Interpretation Session
Stephanie Nykamp, Program Co-Chair (Image Interpretation Session)

3:00 pm *Break with exhibitors*

3:30 pm Dr. Mary Lunz, Psychometrician, regarding the ACVR examination

4:30 pm Welcome new Diplomates, ACVR Business Meeting (Diplomates only)

6:00 pm Adjourn for the day

FOCAL SKELETAL MUSCLE UPTAKE OF ^{99m}Tc-HDP CAUSED BY PERONEAL NERVE BLOCKS IN HORSES. J.F. Griffin, B.D. Young, G.T. Fosgate, M.A. Walker, J.P. Watkins. Texas A&M University, College Station, TX 77843-4475.

Introduction/Purpose: Diagnostic perineural anesthesia (nerve blocks) and musculoskeletal scintigraphy are important tools in equine lameness evaluation. Focal skeletal muscle uptake following peroneal nerve blocks could potentially mimic a tibial lesion on the lateral view. Although uptake at peroneal nerve block sites has been seen at several institutions, published descriptions are lacking. The purpose of this study was to estimate the proportion of peroneal nerve blocks that result in focal skeletal muscle uptake, to estimate the proportion of peroneal nerve blocks that result in focal skeletal muscle uptake likely to mimic a tibial lesion, to estimate duration of this effect, to estimate inter-rater agreement regarding the presence of focal skeletal muscle uptake, and to evaluate the effect of local anesthetic dose on uptake intensity and frequency of occurrence.

Methods: Forty five bone-phase scintigrams were performed in 12 horses undergoing peroneal nerve blocks. Following baseline scans, additional scans were performed 1, 3, 7 and 14 days post-block. The superficial and deep branches of the peroneal nerve were blocked by injecting 10 mL of 2% mepivacaine in one limb and 20 mL in the other. Scintigraphically normal horses on day 3 or 7 post-block did not undergo additional imaging. Images were randomized and evaluated by 2 blinded evaluators. An image was independently evaluated for focal uptake at the block site. On lateral views, evaluators were asked whether or not uptake was limited to the plane of the tibia. Studies were classified as “likely to mimic a tibial lesion” if uptake on the lateral view was limited to the plane of the tibia and uptake was not identified on the caudal view. Regions of interest were placed over the block site and distal tibia. Count density ratios were used to estimate quantitative change over time (uptake intensity).

Results: The overall proportion affected was 0.52 (95% CI, 0.36-0.68; $P < 0.001$) day 1 post-block and 0.24 (95% CI, 0.13-0.40; $P = 0.005$) day 3 post-block. The overall proportion likely to mimic a bone lesion was 0.19 (95% CI, 0.09-0.33; $P < 0.001$) day 1 post-block and 0.21 (95% CI, 0.09-0.40; $P = 0.005$) day 3 post-block. Focal skeletal muscle uptake was seen in only 1 horse day 7 post-block. The overall inter-rater agreement as measured by the kappa statistic was 0.50 (95% CI, 0.36-0.65; $P < 0.001$). The kappa statistic for lateral images was 0.65 (95% CI, 0.45-0.86; $P < 0.001$). The kappa statistic for caudal images was 0.26 (95% CI, 0.06-0.47; $P = 0.005$). Increased uptake intensity was associated with the 20 mL dose ($P = 0.042$).

Discussion/Conclusion: Peroneal nerve blocks cause focal skeletal muscle uptake of ^{99m}Tc-HDP on bone phase scintigraphy. This occurs ~50% of blocked limbs and can mimic a tibial lesion on the lateral view in ~20% of blocked limbs. Uptake of ^{99m}Tc-HDP generally lasts < 7 days. Inter-rater agreement for presence of uptake at the block site is higher on lateral views than caudal views. Higher local anesthetic dose is associated with increased uptake intensity as estimated with count density ratios.

QUANTITATIVE PERTECHNETATE THYROID SCINTIGRAPHY AND ULTRASONOGRAPHIC APPEARANCE OF THE THYROID GLAND IN EUTHYROID HORSES. S. Davies, G. Daniel, D. Barber, M. Crisman and M. Larson. Virginia-Maryland Regional College of Veterinary Medicine, Virginia, 24061.

Introduction/Purpose: Pertechnetate thyroid scintigraphy and B mode ultrasonography have been used to evaluate thyroid gland structure and function in dogs and cats with thyroid disease. The purpose of this study was to document these features of the thyroid gland in a group of normal horses.

Methods: Thyroid to salivary (TS) ratio and percent dose uptake (% uptake) of pertechnetate by the thyroid gland were calculated and compared between horses in two age groups. Group A consisted of 8 horses 10 years of age or less, and Group B included 7 horses greater than 11 years of age. Inclusion criterion included normal physical exam, normal hematology and serum biochemistry, and normal total thyroxine (Tt_4). Ultrasound was used to determine gland volume (calculated from length, depth and height) and document the presence of nodules. Scintigraphic images were acquired following injection of 30mCi of $Na^{99m}TcO_4$. Ventral images of the head and neck were acquired at 10, 20, 40 and 60 minutes post injection and were corrected for motion. Regions of interest were drawn around the thyroid and salivary glands in order to calculate TS ratio and % uptake of pertechnetate.

Results: Mean ± STDev * denotes significant difference at $p < 0.05$

Gp	Tt_4 µg/dl *	Thy Vol cm^3(US)	# of Nodules	Gross T:S @ 60 min	Net T:S @ 60 min	% Uptake @ 60 min
A	2.97 ± 0.36	66.82 ± 15.89	3	5.28 ± 2.23	6.47 ± 3.13	2.51 ± 0.54
B	2.34 ± 0.47	83.99 ± 24.54	3	5.82 ± 3.00	7.58 ± 4.57	3.06 ± 1.54

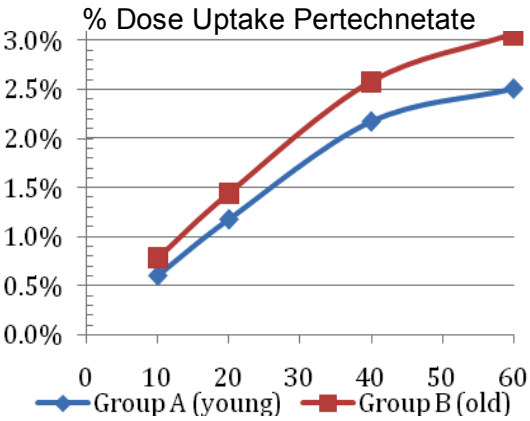

Discussion/Conclusion:
Older horses (Gp B) had lower Tt_4 concentrations. There was no difference in thyroid gland volume, number of nodules or TS ratios between the two groups. There was a trend for increased thyroid % uptake in older horses but the difference was not significant. There was greater variation in Tt_4 concentrations, thyroid size and thyroid % uptake in older horses.

Thyroid % uptake in horses appears to be more variable than in dogs and cats. The greatest variation was seen in the older group of horses. Additional horses need to be studied to determine if there is an age relationship with thyroid % uptake and if increased uptake in older horses is a normal finding or represents early disease.

DEPTH-CORRECTED VERSUS NON DEPTH-CORRECTED GFR DETERMINATION BY QUANTITATIVE RENAL SCINTIGRAPHY IN THE DOG. G.T. Almond, J.A. Hudson, W.R. Brawner, Jr., M. Holland, J.C. Wright. Auburn University, Alabama, 36849.

Introduction/Purpose: The purposes of this study were to determine if the additional step of depth correction for tissue attenuation is necessary in ^{99m}Tc-DTPA scintigraphy studies for determination of GFR in both large and small dogs and to determine if the current depth correction procedure accurately assesses depth.

Methods: Using established methodology, 99mTc-DTPA quantitative renal scintigraphy was performed on 22 healthy sedated dogs to measure glomerular filtration rate (GFR). Using each dog as its own control, GFR values were calculated with and without correction for photon attenuation due to kidney depth. The renal depth measurement was made from a right lateral scintigraphic image. Simultaneously, plasma clearance (PC) of 99mTc-DTPA was determined using a two-sample, one-compartment pharmacologic model with samples at 20 and 180 minutes. One to three days later, the dogs were sedated and computed tomographic (CT) images were obtained of both kidneys with the dogs positioned as during scintigraphy. Measurements of renal depth were made from the center of the kidney to a line perpendicular to the skin at the dorsal midline. The dogs were manually lifted and positioned again and a second CT scan was performed to evaluate repeatability of these measurements.

Results: For all dogs, depth-corrected (DC) and non depth-corrected (nDC) GFR measurements were not different ($p=0.3926$). For small dogs (<13.6 kg), DC and nDC GFR measurements were not different ($p=0.2332$); correlations between scintigraphy and CT depth measurements were poor for the left kidney and modest for the right kidney. For large dogs (>22.7 kg), DC and nDC GFR measurements were different ($p=0.0263$); correlations between scintigraphy and CT depth measurements for the left kidney were modest. DC and nDC GFR measurements were significantly different from PC when considering all dogs together ($p<0.0001$ and $p=0.0003$ respectively) and when considering small dogs alone ($p<0.0001$ for both). In large dogs, PC was also found to significantly differ from DC ($p=0.0016$). Only when comparing PC to nDC GFR in large dogs were the values significantly similar ($p=0.5179$).

Discussion/Conclusion: Scintigraphic measurement of kidney depth was shown to be unreliable when compared to CT. In dogs <13.6 kg DC and nDC are not significantly different, so depth correction does not appear necessary. In dogs > 22.7 kg DC and nDC are significantly different; however, it is not certain from this study whether DC or nDC is more accurate. Before recommendations are made to abandon depth correction in large dogs it would be necessary to repeat the study with the gold standard of inulin clearance. Separate linear regression formulas for small and large dogs may improve the accuracy of GFR measurements by scintigraphy. Because numerous other studies have indicated good agreement between scintigraphy and plasma clearance, the plasma clearance measurements obtained in this study are questionable.

MYOCARDIAL KINETICS OF *META*-[I-131]IODOBENZYLGUANIDINE IN AN ADRIAMYCIN CARDIOMYOPATHY RAT MODEL. C. R. Berry, G. Vaidyanathan, M.R. Zalutsky, R. E. Coleman and T.R. DeGrado; College of Veterinary Medicine (Berry), University of Florida, Gainesville, FL; PET Facility, Duke University Medical Center, Durham, NC and the Joint Program of Nuclear Medicine, Brigham & Women's Hospital, Harvard University, Boston, MA (DeGrado)

***Introduction/Purpose**:* The myocardial kinetics of the catecholamine uptake radiotracer, *meta*-[I-131] Iodobenzylguanidine (MIBG), was studied in the isolated rat heart using an adriamycin induced cardiomyopathy model.

***Methods**:* Experimental conditioning for all rats included the administration of adriamycin (2 mg/kg, IP) or saline sham for six weeks. Hearts were excised and perfused by the Langendorf method. MIBG was administered as a 4 min pulse, followed by an 86 min washout period. Pharmacologic blocking agents were used to effect, including Uptake-1 (neuronal specific), Uptake-2 (myocyte specific), Uptake-1 + Uptake-2, and Uptake-2 + vesicular kinetic mechanisms (n=5 each). External scintillation probes were used to monitor myocardial uptake and retention of MIBG. The uptake rate (K_i, ml/min/gm), mono-exponential clearance rate (k_0, min^{-1}) were calculated and compared using ANOVA analysis and a p value of < 0.05 was considered significant.

***Results**:* In the absence of uptake inhibitors, adriamycin treatment did not significantly alter the uptake (3.9±1.0 vs. 4.5±0.4, p=0.2) or clearance rate (0.0063±0.001 vs. 0.0063±0.001, p=0.7) when compared with saline control. However, a significant decrease in the neuronal specific uptake (2.4±0.4 mL/min/gm vs. 3.6±0.2, p=0.001) and clearance (0.0053±0.0004 min^{-1} vs.0.008±0.002, p=0.03) rates were seen with adriamycin when compared to the saline controls respectively. The myocyte specific kinetics was not altered in the adriamycin treated studies.

Discussion/Conclusion: These results suggest that acute adriamycin toxicity is initially associated with impaired neuronal catecholamine uptake and retention while myocyte catecholamine uptake and retention is unaltered.

PORTABLE X-RAY MACHINE TUBE LEAKAGE AND SCATTER RADIATION OPERATOR EXPOSURE WITH AN EQUINE CADAVER RADIOLOGY PHANTOM. R. Tyson, D.C. Smiley, R.S. Pleasant, G.B. Daniel. Virginia-Maryland Regional College of Veterinary Medicine. Blacksburg, VA 24061.

Introduction/Purpose: Most regulations prohibit or discourage hand holding of portable X-ray units when imaging equine patients however; this is common in ambulatory practices. The purpose of this project is to simulate common radiographic procedures with an equine cadaver phantom and to quantify the exposure risk to the hand and collar region to better determine overall occupational exposure to personnel holding portable X-ray machines.

Methods: Each radiographic exposure was taken with a MinXray HF80 (MinXray, Inc., Northbrook, IL) at the following technique: 80 kVp; 15 mA; 0.5 msec; constant FFD for view. A Model 1015C Radiation Monitor with a Model 10X5-180 Pancake Ion Chamber (Radcal Corporation, Monrovia, CA) was used to measure tube leakage and scatter radiation at various locations immediately around the MinXray machine. Each measurement was repeated for ten exposures. The Radiation Monitor and Ionization Chamber were calibrated immediately before the study with an accuracy of ±4%. The MinXray unit had been recently inspected and passed by a certified medical physicist. An equine cadaver limb was used to generate scatter radiation associated with commonly performed radiographic views including a lateral carpus, lateral foot, palmaroproximal-palmarodistal and dorsal 60° proximal-palmarodistal obliques of the navicular. For each simulated view, radiation measurements were obtained at the handle, to simulate finger dose, and at estimated collar level for a person holding the portable X-ray machine. Measurements at the handle and collar were repeated for the foot views with several variables (concrete/grass/without limb/with steel shoe). Exposure was also recorded within the primary beam at 40" FFD and behind a lead 0.5mm equivalent apron and glove.

Results: All data expressed in mR (mean ± Stdev) per exposure @ 80 kVp and 7.5 mAs

	Lateral Carpus	**Lateral Foot**	**PaPr-PaDi Navicular**	**D60Pr-PaDi Navicular**
Handle (concrete)	0.311 ± 0.001	0.394 ± 0.005	0.619 ± 0.008	0.558 ± 0.004
Grass		0.389 ± 0.010	0.687 ± 0.016	0.566 ± 0.005
Collar (concrete)	0.167 ± 0.004	0.335 ± 0.005	0.430 ± 0.005	0.377 ± 0.005
Grass			0.506 ± 0.088	0.421 ± 0.026
Collar (w/out leg)	0.081 ± 0.001	0.290 ± 0.002	0.399 ± 0.089	0.357 ± 0.004

	Primary	**Behind Apron**	**In Glove**
Exposure	51.5 ± 0.471	1.590 ± 0.020	0.411 ± 0.007

Discussion/Conclusion: This data will allow an estimate of hand and body exposure associated with hand holding portable X-ray equipment.

APPLICATION OF THE PROVENTRICULUS-TO-KEEL RATIO AS A PROGNOSTIC INDICATOR AND FACTORS AFFECTING ITS CALCULATION. S.E. Dennison[1], W.M. Adams[1], B. S. Yandell[2], P. Johnson[3], J.R. Paul-Murphy[1].[1]School of Veterinary Medicine, University of Wisconsin, WI 53706, USA. [2]Departments of Statistics and Biostatistics and Medical Informatics, University of Wisconsin, WI 53706, USA. [3]Great Western Referrals, Wiltshire, SN1 2NT, UK.

Introduction/Purpose: Various etiologies result in psittacines proventricular enlargement through dilatation or hypertrophy, the most notorious being Neuropathic Gastric Dilatation (NGD). The proventriculus:keel ratio (PV:K) was recently developed to differentiate between normal and abnormal proventricular size, but association between PV:K magnitude and prognosis, and factors that might directly affect PV:K have not been investigated.

Methods: Right lateral radiographs of 41 parrots with confirmed proventricular disease were retrospectively evaluated and the PV:K calculated. Data were divided into broad disease categories and into survival and terminal disease groups for statistical analysis. Twenty clinically healthy, research colony Hispaniolan parrots (*Amazona ventralis*) were prospectively radiographed on three occasions in right lateral recumbency: 1) immediately following voluntary feeding then hourly for a 7 hour period of fasting; 2) and 3) awake and under anesthesia 3 weeks apart with additional Rt latero 5/10/15 degree ventral – Le laterodorsal oblique radiographic projections under anesthesia. Radiographs were anonymized and proventriculus:keel ratios calculated by two independent observers.

Results: Retrospective study: PV:K could not differentiate between parrot survival and terminal disease ($P=0.9$). There was complete overlap in ratios between disease categories.
Prospective study: No statistically significant difference was identified between PV:Ks for fed and fasted studies, between repeated hourly measurements, between awake and anesthetized studies ($P>0.2$). Proventricular margin identification became difficult with increasing degrees of rotation, preventing calculation of the ratio in some parrots. Fluctuations in an individual's PV:Ks between occasions were significantly different ($P<0.01$) but remained within the normal range. Interobserver agreement was strong for both retrospective and prospective data ($P<0.001$).

Discussion/Conclusion: Right lateral radiographs taken under anesthesia allow consistent proventricular measurements. PV:K magnitude does not determine prognosis or permit specific disease characterization. Fluctuations in an individual's PV:K will occur and does not indicate proventricular abnormality unless ratio exceeds 0.48.

HIP DYSPLASIA TREATED BY JUVENILE PUBIC SYMPHYSIODESIS (JPS): RADIOGRAPHIC RESULTS AT 7 YEARS. W. M. Adams[1], R.T. Dueland[1], P.M. Crump[2], P. Chinudomsub[3]. [1]School of Veterinary Medicine, [2]Department of Computing and Biometry, [3]College of Agriculture and Life Sciences, University of Wisconsin, WI 53706, USA.

Introduction/Purpose: Treatment of canine hip dysplasia ranges from diet, exercise and weight management to major surgery. Immature dogs (12 – 24 weeks) at risk for developing hip osteoarthritis (OA) may undergo a minor surgical cauterization of the pubic symphysis (JPS), to prematurely close that symphysis and cause ventrolateral rotational gain of the dorsal acetabular margins, bilaterally. Although intent is to improve dorsal acetabular coverage of the femoral head as with triple pelvic osteotomy, no study has been reported regarding long term effect of JPS on the hip joints, or whether severity of laxity pre-operatively would affect late outcome.

Methods: Extended ventrodorsal hip (OFA view) and PennHip distraction radiographs were taken on 35 large breed client-owned puppies aged 15 to 23 weeks. All were at risk for developing OA secondary to hip laxity (DI range was 0.46 – 1.26). Immediately after radiography, 31 puppies underwent JPS and 4 had sham surgery. Twenty–seven had repeat radiographs at 2 years of age and all 35 dogs had late follow up radiographs at 5 – 11 years (median 7.6 years). Radiographs were anonymized for hip change scoring: 0) no femoral head or acetabular changes; 1) a single femoral head patchy metaphyseal, linear metaphyseal or linear femoral neck new bone finding; 2) two or three of the findings listed in level 1 scoring; 3) remodeling of acetabular margin, with or without femoral head / neck new bone; 4) advanced remodeling of the femoral head, neck and acetabulum.

Results: Median pre-operative DI for 31 JPS and 4 control puppies was 0.71 and 0.65, respectively. At 2 years of age, DI for 23 JPS and 4 control dogs was 0.42 and 0.65, respectively. Weight range was 14 – 55 Kg with a median weight of 28.6 Kg. Hip changes were present pre-operatively (score 1 – 3) in 61 of 70 hips (87%) evaluated. Median pre-operative hip score for 31 JPS and 4 control puppies was 1.6 and 1.0, respectively. At 7 years, median hip score for 31 JPS and 4 control dogs was 2.13 (33% increase) and 2.25 (125% increase), respectively. Of the 15 JPS dogs that had a pre-operative DI <0.71, median hip score decreased 35%. Of the 16 JPS dogs that had a pre-operative DI >0.70, median hip score increased 76%. Logistic regression analysis on hip change score at 7 years vs. DI and age at time of JPS, showed no advantage of earlier age for time of JPS. Age at time of JPS was not related to 7 year hip score ($P = .37$), but preoperative DI was significantly related to 7 year hip score ($P < 0.0001$).

Discussion/Conclusion: For large breed puppies at risk for developing hip OA secondary to hip dysplasia, when DI is less than 0.71, JPS will likely decrease progression of OA changes at least through mid-life. When DI is greater than 0.70, progressive OA will occur, despite JPS. Though JPS is recommended at 15 – 16 weeks of age, it may be advantageous up to 23 weeks.

EFFECTS OF INITIAL LATERAL RECUMBENCY ON THE POSITION OF THE SMALL INTESTINES ON THE VENTRODORSAL VIEW IN CATS S.T. Tibbs, L.E. Ziegler, and C.R. Jessen. College of Veterinary Medicine, University of Minnesota, MN, 55108.

Introduction/Purpose: Cats with linear foreign bodies are described as having an appearance of small intestine bunching in the right abdomen (as well as plication, eccentric/tapered luminal gas, and other findings). When assessing survey abdominal radiographs of cats, the majority of the small intestines are often located in the right side of the abdomen on the ventrodorsal (VD) view. When a cat presents with clinical signs of intestinal disease, an interpretation error of intestinal bunching could lead to misdiagnosis. The purpose of this study is to evaluate if postural effects of initial lateral recumbency influence the position of the small intestines on the subsequent VD view. If they do, repeating a VD radiograph after the patient has been in left lateral recumbency (to allow for intestinal redistribution) could discriminate pathologic bunching versus postural displacement.

Methods: Clinical patients were prospectively enrolled with client consent to have either an initial right or left laterally recumbent image to be followed with a VD view to complete the abdominal study. Images were evaluated for position of the intestines on each side of midline by a region of interest. The distension of the stomach and bladder were also evaluated, as they may affect the position of the small intestines. Abdominal width was measured at the second lumbar vertebra (generally the widest point of the abdomen) to consider varying body habitus. Cases were excluded if there was insufficient abdominal detail (age, emaciation, or peritoneal effusion), mass/mass effects (including marked bladder or stomach distension), or if previous intestinal surgery had been performed. Any patients with a definitive diagnosis of intestinal disease (including foreign bodies) were also excluded.

Results: Based on an independent T test analysis there is no significant difference between initial recumbency and intestinal position in the 38 cases evaluated. On average, 68% of the small intestines were within the right side of the abdomen in this group of cats.

Discussion/Conclusion: Postural effects are unlikely to influence intestinal position. The finding of intestinal bunching within the right side of the abdomen on the VD view should be interpreted with caution, as it may be a normal finding. It remains unclear what the underlying factors are that lead to the rightward positioning of cat small intestines. This may be related to distribution of intra-peritoneal fat, or possibly an underlying feline specific embryologic/anatomic factor. Further evaluation of cat intestinal position, with and without gastrointestinal signs, is warranted with a larger study group.

RADIOGRAPHIC CHARACTERIZATION OF PRESUMED PLATE-LIKE ATELECTASIS IN 37 DOGS AND 13 CATS. C.R. Berry, R.F. Giglio, M.D. Winter, D.J. Reese, D.E. Thrall, and J.P. Graham. College of Veterinary Medicine, University of Florida, Gainesville, FL; North Carolina State University (Thrall), Raleigh, NC; and Affiliated Veterinary Specialists (Graham), Maitland, FL.

***Introduction/Purpose**:* In humans, plate-like atelectasis (PLA) has been used to describe discoid or linear areas of sub-segmental lung lobe collapse. The purpose of this study was to retrospectively evaluate the anatomic location of similar radiographic changes seen in small animals, evaluate for concurrent thoracic disease(s), and evaluate CT studies, when available, to document the anatomic position of PLA within the affected lung lobe.

***Methods**:* Fifty cases (37 dogs and 13 cats) that ranged from 2 to 15 years of age, (mean ± SD;10.1 ± 3.6 yrs) were selected from hospital records between 2004 and 2009. There were 28 MN and 22 FN patients. The length and location of the PLA were documented and tabulated. Eleven dogs had thoracic CTs within 7 days of their thoracic radiographs. The pre and post intravenous positive contrast medium CT studies were reviewed in transverse, saggital and dorsal plane reconstructed images.

***Results**:* PLA was seen on the left lateral, (n=21), right lateral (n=16) or both laterals (n=13) and the ventrodorsal radiographs in only 14 animals. On the lateral radiographs, PLA was most commonly observed in the cranial thorax at the level of the trachea (2nd to 4th ICS). The length of the PLA averaged 32.7 mm (±17.9 mm, SD), the width of the PLA averaged 3.2 mm (±1.2 mm, SD) and was usually oriented in a dorsocranial to caudoventral direction. PLA also could be horizontal, appearing at a mid thoracic level on the lateral image. Of the 11 dogs with CT studies, 3 dogs had recumbent or hypoventilatory atelectasis that precluded evaluation for PLA; 3 dogs had linear soft tissue densities within the left cranial lung lobe, extending either from a central to middle position or from a mid lung lobe to peripheral position and in the 5 dogs, no abnormality was seen.

Discussion/Conclusion: PLA is a linear soft tissue opacity seen mainly in the cranial lung lobes of dogs and cats that is located in an atypical anatomic position for interlobar fissure lines and does not align anatomically with the pulmonary vasculature or taper as a vascular structure normally would. PLA should be considered a finding of unknown clinical significance at this time, as histopathology of the lesion was not evaluated in this current retrospective study. It is possible that PLA could represent a sentinel sign for more widespread pathology although focal non-diseased areas of hypoventilation, decreased alveolar volume and/or a localized surfactant deficiency could also play a role in the genesis of these pulmonary changes. Future investigations, including correlative histology, will be required to further understand the underlying pathogenesis and possible clinical significance of these radiographic changes.

RADIOGRAPHIC APPEARANCE OF PULMONARY LYMPHOMA IN CATS AND DOGS.

Geyer N[1], Reichle JK[1], Valdez-Martinez A[2], J Williams[3], Goggin JM[4], Leach L, [5] Hanson J, [6] Hill S[7], Axam T[8]. [1]Animal Surgical and Emergency Center, LA CA; [2]Colorado State University Veterinary Teaching Hospital, Fort Collins CO; [3] University of Georgia, Athens GA; [4]Metropolitan Veterinary Radiology, Ltd, Montclair NJ; [5]Moore Animal Hospital, Fort Collins CO; [6] Veterinary Diagnostic Imaging & Cytopathology, PC, Clackamas OR; [7] Veterinary Specialty Hospital, San Diego CA; [8]Saint Francis Animal Care Center, Atlanta GA.

Introduction/Purpose: Lymphoma of the lung is rare in all species. It can be present as the primary disease process or in patients with multicentric lymphoma. To the authors' knowledge, there is no publication in the literature specifically describing the radiographic appearance of cytologically or histologically confirmed pulmonary lymphoma in the cat and dog. We hypothesize that there are variations of the radiographic appearances of pulmonary patterns, including nodules, masses, and infiltrates.

Methods Cases were requested via emailing to American College of Veterinary Radiology members and cases span 1998-2009. Requirements included thoracic radiographs, signalment, history, method of diagnosis, and cytology or histology of the lung.

Results: Twenty-two cases, consisting of 7 cats and 15 dogs, were evaluated. Patients ranged from 4-15 years of age. Breeds consisted of Scottish Fold (1), Domestic Shorthair (3), and Domestic Longhair (3) felines; Labrador retriever (3), Golden retriever (2), and 1 each of 9 other pure dog breeds. Ten patients were castrated males and the remaining 12 were spayed females. All patients presented with a variety of complaints, including decreased appetite (12), lethargy (10), dyspnea (10), coughing (7), vomiting (5), weight loss (5), nasal discharge and/or sneezing (2). All patients had thoracic radiographs within 0-23 days of the definitive diagnosis (mean 4.6 days, median 2 days). Lymphoma was diagnosed in all lung samples cytologically (3, all with ultrasound guidance) or histologically (16 via necropsy, 2 via surgery, and 1 via ultrasound guided biopsy). Radiographic findings varied but ranged from normal (2) to alveolar and/or interstitial infiltrates (11), nodules and/or masses (7), and bronchial infiltrates (4). Additional thoracic radiographic findings included pleural effusion and lymphadenopathy. Various cases will be illustrated radiographically in the presentation.

Discussion/Conclusion: As hypothesized, pulmonary abnormalities varied greatly. Radiographic identification of pulmonary lymphoma is difficult due to its variation, but should be a consideration when pulmonary infiltrates and nodules or masses are seen.

INTEROBSERVER VARIABILITY OF BOARD CERTIFIED AND NON-BOARD CERTIFIED RADIOLOGISTS FOR PULMONARY NODULE DETECTION WITH CANINE THORACIC RADIOGRAPHS USING NEGATIVE (STD) AND POSITIVE (INV) SOFT-COPY DISPLAYED IMAGES. D.J. Reese[2], E.M. Green[1], L.J. Zekas[1], J.E. Flores[1], L.N. Hill[1], M.D. Winter[2], C.R. Berry[2], N. Ackerman[2]. [1]The Ohio State University, OH, 43210 and [2]University of Florida, FL, 32610

Introduction/Purpose: Pulmonary nodule detection poses a challenge in human and veterinary medicine. With the advent of digital radiography, processing images has diversified radiographic interpretation. Specifically, positive image display, or inversion (INV), compared to negative display, or standard (STD), has been anecdotally suggested to aid in detection of pulmonary nodules. The purpose of this study was to assess pulmonary nodule detection comparing INV to STD, between ACVR-Diplomates and general veterinary practitioners.

Methods: Medical records of dogs presented to The Ohio State University (digital radiography) and University of Florida (computed radiography) were reviewed from October 2005 to March 2007 to identify 3-view thoracic radiographs with pulmonary nodules. The radiographs were reviewed in DICOM format. Additional thoracic radiographic exams were obtained on patients of weight and age matched normal controls. All exams were reviewed, utilizing two-panel 3 megapixel (MP) gray-scale diagnostic monitors, during two, blinded, randomized, reading sessions, separated by a minimum of 2 months, by two ACVR Diplomates (EMG, LJZ) and two general veterinary practitioners (JEF, LNH) in either STD or INV image display. The examiners were asked to identify the presence or absence of nodules, lung lobe location, and the certainty was recorded using a five-point confidence rating scale. All exams were reviewed by three observers (DJR, CRB, MDW) for the presence or absence of pulmonary nodules, by consensus. Receiver operating characteristic curve (ROC) analysis was performed for each reviewer and data set. Agreement was calculated between results of INV and STD image display using a kappa statistic. A p-value for all statistical tests of < 0.05 was considered significant. A kappa value of >0.6 was considered good agreement.

Results: One hundred and fourteen sets of thoracic radiographs were obtained: 54 dogs without nodules and 60 dogs with single or multiple nodules. No significant difference in observer performance was identified by ROC analysis. The areas (±SE) under the ROC curves for the radiologists were as follows: STD, 0.92 (±0.025) and 0.91 (±0.029); INV, 0.89 (±0.032) and 0.92 (±0.025). The ROC curves for the general practitioners were as follows: STD, 0.78 (±0.042) and 0.64 (±0.047); INV, 0.69 (±0.049) and 0.58 (±0.048). The kappa values for both radiologists were 0.75 for STD and 0.72 for INV. The kappa values for practitioners were as follows: STD, 0.45 and 0.24; INV, 0.35 and 0.06.

DiscussionConclusion: There appears to be no advantage to viewing thoracic radiographs in either a STD or INV mode for the detection of pulmonary nodules in dogs.

Friday, October 23, 2009 **Peabody Grand Ballroom AB**

7:00 am *CT/MRI Society Meeting*

8:00 am CT/MRI Keynote Address
Patrick R Gavin, DVM, PhD, DACVR
VETERINARY MRI-WHAT I HAVE LEARNED IN THE LAST 20 YEARS

9:30 am **Scientific Session 5: Poster Session**

MAGNETIC RESONANCE IMAGING TO ASSESS THE LIGAMENTOUS STRUCTURES OF THE OCCIPITOATLANTOAXIAL REGION IN THE DOG. G. Middleton, D.J. Hillmann, H.H. Bragulla, D. Rodriguez, J. Trichel, L. Gaschen. Louisiana State University School of Veterinary Medicine, Louisiana, 70803.

***EX VIVO* FAT-SUPPRESSED SPOILED GRADIENT-RECALLED (SPGR) MAGNETIC RESONANCE IMAGING OF EQUINE METACARPOPHALANGEAL ARTICULAR CARTILAGE.** Olive J.[1], d'Anjou M.-A.[2], Girard C.[1], Laverty S.[1], Théoret C.[2]. Departments of [1]Pathology and [2]Clinical Sciences, Faculty of Veterinary Medicine, Université de Montréal, Saint-Hyacinthe, Québec, Canada J2S 7C6

THE "BETTER MOUSETRAP™": A DEVICE FOR COMPUTED TOMOGRAPHY OF DYSPNEIC CATS WITHOUT GENERAL ANESTHESIA. C.R. Oliveira[1], G.J. Pijanowski[1], S.K. Hartman[1], M.A. O'Brien[1], M. McMichael[1], M.W. Chang[2], R.T. O'Brien[1], [1]University of Illinois at Urbana-Champaign, Illinois 61802, [2]Autonomous

FEASIBILITY FOR USING MULTI-SLICE CT, MOTION CAPTURE, AND COMPUTER ANIMATION TO MODEL JOINT MOVEMENTS IN WORKING DOGS. J.C. Jones, J.C. Tan, T.J. Tucker, B.J. Pierce, J.L. Foxworth, D.C. Dinkins, B. Long, C.L. Hatfield, T.A.M. Harper. Virginia Tech, Virginia, 24061-0442; Wake Forest University School of Medicine, North Carolina 27157; and Winston-Salem State University, North Carolina, 27110.

COMPUTED TOMOGRAPHY OF TEMPORAL-BONE FRACTURES IN HORSES. S.L. Pownder, P.V. Scrivani, A. Bezuidenhout, T.J. Divers, N.G. Ducharme. Cornell University Hospital for Animals, Ithaca, NY 14853

COMPUTED TOMOGRAPHY AND CT ARTHROGRAPHY OF THE EQUINE STIFLE: 57 CASES. Sarah M. Puchalski and H. J. (Erik) Bergman, University of California Davis, Davis CA 95616

MAGNETIC RESONANCE IMAGING OF THE EQUINE TEMPOROMANDIBULAR ARTICULATION - A COMPARATIVE MORPHOLOGICAL STUDY. J. Trichel, H.H. Bragulla, D.J. Hillmann, C.T. McCauley, D. Rodriguez, G. Middleton, L. Gaschen. Louisiana State University School of Veterinary Medicine, Louisiana, 70803.

10:00 am *Break with exhibitors*

10:30 am **Scientific Session 6: CT/MRI** (Moderator: Erik Wisner)

10:30 am **DIAGNOSTIC IMAGING FINDINGS OF ZYGOMATIC SIALOADENITIS IN DOGS**. M.S. Cannon, D. Paglia, A.L. Zwingenberger, S.A.E.B. Boroffka, E.R. Wisner. University of California, Davis CA 95616.

10:42 am **MAGNETIC RESONANCE IMAGING OF THE TEMPOROMANDIBULAR JOINT IN NORMAL DOGS**. D.M. Macready, S. Hecht, L.E. Craig, G.A. Conklin. University of Tennessee School of Veterinary Medicine, Tennessee, 37996

10:54 am **COMPARATIVE MAGNETIC RESONANCE IMAGING FINDINGS BETWEEN GLIOMAS & INFARCTS**. V. Cervera, W. Mai, B. Dayrell-Hart*, C. Vite, G. Seiler. From the University of Pennsylvania, Philadelphia, PA 19104 and *SouthPaws Veterinary Specialists, Fairfax, VA 22031

11:06 am **EFFECT OF ACQUISITION TIME ON OBSERVER VARIABILITY AND QUALITATIVE CHARACTERIZATION OF GADOLINIUM-ENHANCING BRAIN LESIONS IN DOGS AND CATS.** Carmel E.N., d'Anjou M.-A., Blond L., Beauchamp G., Parent J. Department of clinical sciences, Faculté de médecine vétérinaire, Université de Montréal, St-Hyacinthe, Quebec, Canada.

11:18 am **DIFFERENTIATION OF BRAIN LESIONS BASED ON CONTRAST-ENHANCEMENT TEMPORAL CHARACTERISTICS WITH QUANTITATIVE MRI IN DOGS AND CATS.** Carmel E.N., d'Anjou M.-A., Blond L., Beauchamp G., Parent J. Department of clinical sciences, Faculté de médecine vétérinaire, Université de Montréal, St-Hyacinthe, Quebec, Canada.

11:30 am **MRI QUALITATIVE AND QUANTITATIVE CHARACTERIZATION OF MENINGEAL ENHANCEMENT IN DOGS AND CATS: EFFECT OF ACQUISITION TIME AND CHEMICAL FAT SUPPRESSION**. d'Anjou M.-A., Carmel E.N., Blond L., Beauchamp G., Parent J. Department of clinical sciences, Faculté de médecine vétérinaire, Université de Montréal, St-Hyacinthe, Quebec, Canada.

11:42 am **UTILITY OF GADOLINIUM BASED CONTRAST MEDIA FOR SPINAL MR IMAGING; SHOULD ITS USE BE THE STANDARD OF CARE?** R. G. King, J. Sutherland-Smith

11:54 am **MAGNETIC RESONANCE IMAGING APPEARANCE OF VERTEBRAL MARROW CHANGES IN DOGS.** A.R. Matthews, S. Hecht and W.B. Thomas. University of Tennessee College of Veterinary Medicine, TN, 37920

12:06 pm *Lunch*

CT/MRI AFTERNOON SESSION **Peabody Grand Ballroom AB**

1:30 pm **Scientific Session 7: CT/MRI** (Moderator: Pat Gavin)

1:30 pm **CONTRAST ENHANCEMENT OF EXTRADURAL COMPRESSIVE MATERIAL ON MAGNETIC RESONANCE IMAGING.** J.N. Suran, A. Durham, W. Mai, G. Seiler. University of Pennsylvania, PA, 19104.

1:42 pm **COMPARISON OF RADIOGRAPHIC AND COMPUTED TOMOGRAPHIC TECHNIQUES FOR SENSITIVE AND TIME-EFFICIENT DIAGNOSIS OF CANINE ACUTE SPINAL CORD COMPRESSION.** S.E. Dennison, R. Drees, H. Rylander, M. Milovancev, R. Pettigrew, T. Schwarz. School of Veterinary Medicine, University of Wisconsin, Madison, WI 53706.

1:54 pm **INTERACTIVE WEB-BASED THREE-DIMENSIONAL ANATOMIC AND MRI ATLAS OF THE CANINE PELVIC LIMB**. S. Sunico, J. Kornegay, E. Smallwood, M. Styner, D. Chen, S. Murugappan, D. Thrall. North Carolina State University, Raleigh, North Carolina, 27606, and University of North Carolina, Chapel Hill, North Carolina, 27599.

2:06 pm **EVALUATION OF COMPUTED TOMOGRAPHY OSTEOABSORPTIOMETRY IN DETECTION OF HIP DYSPLASIA IN LABRADOR RETRIEVERS.** P.J. Grimm[*], R.L. Echandi[*], W. T. Drost[*], K.A. Mann[†], R.D. Park[‡], C.E. Kawcak[‡], L. Wei[*]. [*]The Ohio State University, OH 43210, [†]U.S. Department of Defense Military Working Dog (DODMWD) Veterinary Service, TX, 78236, [‡]Colorado State University, CO 80523.

2:18 pm **COMPARISON OF ABDOMINAL ULTRASOUND AND ABDOMINAL COMPUTED TOMOGRAPHY IN THE SEDATED CANINE.** E.L. Fields, J.C. Brown, I.D. Robertson, J.A. Osborne. North Carolina State University, College of Veterinary Medicine (Fields, Brown, Robertson) and Department of Statistics (Osborne)

2:30 pm **MULTI-ROW COMPUTED TOMOGRAPHY ANGIOGRAPHY TECHNIQUE OF THE CANINE PULMONARY VASCULATURE.** M. Makara[1], T. Glaus[2], M. Dennler[1], R. Bektas[3], A. Kutter[3], R. Dip[4], M. Schnyder[5], P. Deplazes[5], Stephanie Ohlerth[1], [1]Section of Diagnostic Imaging, [2]Division of Cardiology, [3]Section Anesthesiology, [4]Institute of Veterinary Pharmacology and Toxicology, [5]Institute of Parasitology, Vetsuisse Faculty, University of Zurich, Switzerland.

2:42 pm **PULMONARY ANGIOGRAPHY USING 16 SLICE MULTIDECTOR COMPUTED TOMOGRAPHY IN CLINICALLY NORMAL DOGS.** A. Habing, M. Beal, A. Brown, N. Nelson, J. Coehlo, J. Kinns. Michigan State University, MI, 48824-1314.

3:00 pm *Break with exhibitors*

3:30 pm **Scientific Session 8: CT/MRI** (Moderator: Russ Tucker)

3:30 pm **COMPUTED TOMOGRAPHIC EVALUATION OF THE EQUINE PITUITARY GLAND IN HORSES WITH HYPERADRENOCORTICISM COMPARED TO NORMAL HORSES.** A.P. Pease, H.C. Schott. Michigan State University, East Lansing, MI. 48824

3:42 pm **INTRA-ARTERIAL CONTRAST ENHANCED COMPUTED TOMOGRAPHY IN EQUINE FOOT LAMENESS: 151 HORSES**. S. M. Puchalski, R. M. Schultz, R.J.K. Bell, L.D. Galuppo, M.H. MacDonald, J.R. Snyder and E.R. Wisner

3:54 pm **THE MRI FINDINGS IN HORSES WITH SPINAL ATAXIA.** C.W. Mitchell, S. Nykamp, R.A. Foster. Ontario Veterinary College, Ontario, N1G 2W1.

4:06 pm **DETERMINATION OF T1 VALUES OF NORMAL EQUINE TENDONS USING MAGIC ANGLE MR IMAGING.** M. Spriet, E.R. Wisner, L. Anthenill, M.H. Buonocore. University of California, Davis, CA, 95616.

4:18 pm **INFLUENCE OF THE CHEMICAL SHIFT ARTIFACT ON MEASUREMENTS OF COMPACT BONE THICKNESS OF THE EQUINE DISTAL LIMB.** A.N. Dimock, M. Spriet. University of California, Davis, School of Veterinary Medicine, CA 95616

4:30 pm **DETECTION OF OSTEOCHONDRAL DEFECTS IN THE FETLOCK JOINT USING LOW AND HIGH FIELD STRENGTH MR IMAGING ANDTHE EFFECT OF SEQUENCE SELECTION ON LESION CONSPICUITY AND SIZE.** NM Werpy, CP Ho, AP Pease, CE Kawcak, Colorado State University 80523, Michigan State University 48824

5:00 pm Large Animal Diagnostic Imaging Society Organizational Meeting

MAGNETIC RESONANCE IMAGING TO ASSESS THE LIGAMENTOUS STRUCTURES OF THE OCCIPITOATLANTOAXIAL REGION IN THE DOG. G. Middleton, D.J. Hillmann, H.H. Bragulla, D. Rodriguez, J. Trichel, L. Gaschen. Louisiana State University School of Veterinary Medicine, Louisiana, 70803.

Introduction/Purpose: Instability of the atlantoaxial articulation is a common disorder in small chondrodystrophic dog breeds that can cause neurological sequelae or pain. The atlantoaxial articulation is especially prone to instability, producing neurologic deficits. MRI of the region has not been described in dogs. The goal of this study was to establish an MRI technique and optimal sequences to determine the normal appearance of the atlantoaxial ligaments in canine subjects and compare the findings to matched plane anatomical prosections.

***Methods*:** Ten normal small breed (<9kg body weight) canine cadaver heads and necks were examined from animals euthanized for reasons unrelated to the head and neck. Radiographs, CT and anatomic prosections were used to examine the bony structures of the occipitoatlantoaxial region and rule out congenital abnormalities. MRI (1.5T Hitachi Echelon™) was performed following euthanasia and again following perfusion with neutral buffered formalin in the dorsal, axial, and sagittal planes in 2mm slice thicknesses using an 8-channel knee coil and standard weighted sequences. 3D sequences were used to develop oblique dorsal scan planes.

Results: The MRI appearance of the apical and alar ligaments is that of a continuous band-like structure rather than three distinct elements which cannot be distinguished from the adjacent joint capsule. The transverse ligament can be clearly distinguished from the others as it crosses the dens dorsally within the spinal canal. SAG plane T1 was ideal for viewing the apical ligament and its borders as well as the dorsal atlantoaxial ligament which appeared as a hypointense area between the dorsal articulation of C1 and C2. SAG plane T2 provided excellent contrast between the dark signal of the continuous band formed by the apical and alar ligaments separating the bright signal of the cerebrospinal fluid dorsally and synovial fluid ventrally. AX plane best demonstrated the transverse ligament dorsal to the dens. T2* and FatSat weighted sequences provided the best contrast between the hypointense ligaments (isointense to white matter) and surrounding structures. The PD and T1 weighted sequences provided optimal spatial resolution of the ligaments (isointense to cortical bone in PD and hypointense to muscle in T1). AX plane BASG 3D and DOR plane BASG Water Excitation 3D provided superior overall contrast resolution. 3D MPR post-processing showed dorsal oblique scans planned at a 22° angle from the ventral floor of the vertebral canal of C2 in a SAG plane to be optimal for visualization of the apical and alar ligaments.

Discussion/Conclusion: MRI is an excellent imaging modality for assessing the ligamentous structures of the occipitoatlantoaxial region in small breed dogs. The variable extent of soft tissue and bony abnormalities in atlantoaxial disease makes MRI the modality of choice for future studies aimed at understanding the disease process and its role in therapeutic planning.

***EX VIVO* FAT-SUPPRESSED SPOILED GRADIENT-RECALLED (SPGR) MAGNETIC RESONANCE IMAGING OF EQUINE METACARPOPHALANGEAL ARTICULAR CARTILAGE.** Olive J.[1], d'Anjou M.-A.[2], Girard C.[1], Laverty S.[1], Théoret C.[2]. Departments of [1]Pathology and [2]Clinical Sciences, Faculty of Veterinary Medicine, Université de Montréal, Saint-Hyacinthe, Québec, Canada J2S 7C6

Introduction/Purpose: The equine metacarpophalangeal (MCP) joint is a high motion joint frequently afflicted with osteoarthritis. The ability of magnetic resonance (MR) imaging to assess cartilage structural changes and its potential to detect biochemical alterations early on in the process of osteoarthritis have stimulated great interest in this modality as a tool to measure response to novel therapeutic strategies. The goal of this study was to assess the diagnostic value of a dedicated, clinically-applicable spoiled gradient-recalled echo (SPGR) with fat saturation (FS) sequence on equine metacarpophalangeal articular cartilage, in the context of osteoarthritis.

Methods: Sagittal, 3D SPGR-FS 1.5 T MR images (slice thickness 3.0mm, pixel size 0.57mm by 0.69mm, acquisition time 7 minutes) were acquired *ex vivo* on twenty joints. Cartilage structure was graded (0: normal; 1: superficial irregularities without thickness alteration; 2: reduced thickness; and 3: full-thickness cartilage erosion) macroscopically and on MR by two examiners in 14 subregions of the proximal phalanx, third metacarpal and proximal sesamoid bones. Following joint dissection, specific areas on the third metacarpal condyle were sampled for histological cartilage thickness measurement and modified-Mankin scoring. Cartilage thickness was measured and cartilage signal intensity was graded (0: homogeneous high signal; 1 heterogeneous signal with mild decrease in intensity; 2: moderately decreased signal; and 3: low signal intensity) on MR images at these selected metacarpal sites.

Results: There was good precision (mean error 0.11mm) and moderate correlation ($r=0.44$; $p<0.0001$) of cartilage thickness measurements between MR (0.90±0.17mm) and histology (0.79±0.16mm). There was moderate correlation between modified-Mankin histologic score and signal intensity of cartilage ($r=0.36$; $p<0.01$) or MR cartilage structure assessment ($r=0.49$, $p>0.001$). Gross structure of a total of 280 articular subregions was evaluated semi-quantitatively and prevalence of grade 0 to 3 was n=49 (17.5%), n=92 (32.9%), n=92 (32.9%) and n=47 (16.8%), respectively. The sensitivity to detect cartilage surface and thickness alterations of all grades on MR was 68-81%, while the specificity was 55-63%.The sensitivity to detect full thickness erosion was only moderate (51-60%), and such lesions were often underestimated, particularly when linear. However, the specificity to detect such lesions on MR was high (85-99%).

Discussion/Conclusion: Cartilage erosions affecting the equine MCP joint can be detected with moderate sensitivity and moderate to excellent specificity, and cartilage thickness can be quantified accurately with SPGR-FS sequence at 1.5 T. However, the ability to predict cartilage pathology at the histologic level based on signal changes appears limited with this sequence. The anatomical peculiarities of this joint that include a thin cartilage and a complex shape limit the capacity to assess cartilage with MRI.

THE "BETTER MOUSETRAP™": A DEVICE FOR COMPUTED TOMOGRAPHY OF DYSPNEIC CATS WITHOUT GENERAL ANESTHESIA. C.R. Oliveira[1], G.J. Pijanowski[1], S.K. Hartman[1], M.A. O'Brien[1], M. McMichael[1], M.W. Chang[2], R.T. O'Brien[1], [1]University of Illinois at Urbana-Champaign, Illinois 61802, [2]Autonomous

Introduction/Purpose: Computed tomography (CT) in cats has been historically performed using general anesthesia, produced varying degrees of lung lobe atelectasis and was contraindicated in dyspneic patients. The purpose of this study was to design a low attenuating device for cats that allowed CT imaging without general anesthesia in a clinically supportive environment.

***Methods*:** A cylindrical acrylic device was designed for CT imaging and emergency clinical treatment of dyspneic cats. Requirements of the device were; 1) access for oxygen therapy, 2) access for catheter lines, including IV fluid administration, 3) ability to visually observe the patient throughout the imaging, 4) ability to quickly remove the patient from the device in emergency situations, 5) adequate security of the closure without metallic components, 6) low CT attenuation, 7) symmetrical design to avoid edge or hardening artifacts, 8) narrow design to maintain normal orientation of the patient axis and 9) ability to add additional padding for differing sized cats. Varying lengths and diameters of materials were tested for CT attenuation and artifact production. Whole body CT scans were performed in 22 normal and 18 dyspneic nonsedated, nonanesthetized cats using a 16 multi-detector-row helical CT unit (GE Medical Systems Light speed).

***Results*:** The final design was a transparent acrylic tube with a wall thickness of 5 mm, outer diameter of 21 cm, and 40 cm in length. The CT attenuation number of the wall is 70 HU. The construction has no moving parts or hinges and has a secure closure without additional metallic or plastic components. Patients can be visually monitored throughout the imaging and quickly removed, as necessary. Oxygen and catheter line access is simple and not affected by the apparatus being open or closed. All dyspneic patients were stabilized in the emergency service using the device, without adverse effects. CT imaging was successfully performed in all dyspneic cats and oxygen was easily administered throughout setup and imaging. Two out of 22 normal cats did not tolerate the device. Infrequently cats required more than one scan due to motion. The mean total scanning time was 12.7 minutes (range 5 - 28 min.). Lung lobe atelectasis was detected in only one normal cat and judged to be very mild. No artifacts related to the device were seen and motion artifact was absent or mild in most cases. All images were considered of excellent diagnostic quality.

***Discussion/Conclusion*:** The "Better Mousetrap™" met the imaging and clinical needs of dyspneic cats. It has been incorporated into the emergency service and is routinely used for thoracic CT examination of dyspneic cats. The device described herein appears to support emergency care and improve upon imaging in a clinical setting.

FEASIBILITY FOR USING MULTI-SLICE CT, MOTION CAPTURE, AND COMPUTER ANIMATION TO MODEL JOINT MOVEMENTS IN WORKING DOGS. J.C. Jones, J.C. Tan, T.J. Tucker, B.J. Pierce, J.L. Foxworth, D.C. Dinkins, B. Long, C.L. Hatfield, T.A.M. Harper. Virginia Tech, Virginia, 24061-0442; Wake Forest University School of Medicine, North Carolina 27157; and Winston-Salem State University, North Carolina, 27110.

Introduction/Purpose: Working dogs perform vital functions that include explosives detection, drug detection, patrol and sentry, search and rescue, fire accelerant detection, and tracking for missing persons. Early detection and treatment of joint-related disability is critical for minimizing loss of man-hours, financial investment, mission readiness, and muscle mass in these valuable animals. The purpose of this study was to determine the feasibility for using multi-slice CT, motion capture, and computer animation to model joint movements in working dogs.

Methods: For the pilot study, an adult rat was placed under anesthesia and a whole body CT scan was acquired using a 16-slice CT scanner. Ten days after CT scanning, the rat was placed into a Plexiglas cage and images of his exploration movements were acquired using three digital video cameras. Image data from the CT scan and motion capture were merged and analyzed using a 3D visualization workstation and 3D modeling software. Data were then converted to Stereolithography (STL) format and imported into computer animation software to create a rat skeleton that could be rigged with an Inverse Kinematic (IK) skeleton and animated frame by frame using motion capture videos as reference. The final scene was then analyzed using rendering software to generate an animation video clip. After analyses of the rat data were completed, a volunteer dog-handler working team was recruited. The dog was fitted with a lycra body suit and reflective markers were attached to the head, spine, tail, and legs. Motion capture images were recorded using ten, high speed digital cameras and tracking software while the dog was asked to perform movements typically used for patrol and drug-detection tasks. Two hours after motion capture, the dog was sedated and a whole body CT scan was acquired using the same 16-slice CT scanner as that used for the rat. Image data from the dog CT scan and motion capture videos were merged, analyzed, converted to STL format and imported into computer animation software using the above described protocols. Motion data were also imported as FBX files. The IK chain was constrained to the marker points to add movement before rendering the data to a movie clip.

Results: Computer animation videos were successfully created that demonstrated three-dimensional images of joint movements in both the rat and dog.

Discussion/Conclusion: Findings from this study indicate that use of multi-slice CT, motion capture, and computer animation are feasible techniques for visualizing and modeling joint movements in working dogs. This new technique greatly increases the accuracy of joint movement assessments because actual bone structures can be used instead of commercially available models.

COMPUTED TOMOGRAPHY OF TEMPORAL-BONE FRACTURES IN HORSES. S.L. Pownder, P.V. Scrivani, A. Bezuidenhout, T.J. Divers, N.G. Ducharme. Cornell University Hospital for Animals, Ithaca, NY 14853

***Introduction/Purpose**:* The aims of this study were to depict the temporal-region anatomy during computed tomography (CT) and investigate if various classification schemes of temporal-bone fracture were associated with facial-nerve (CN7) deficit, vestibular-nerve (CN8) deficit or temporohyoid osteoarthropathy (THO).

Methods: The sample population consisted of all horses undergoing temporal-region CT at our hospital between July 1998 and May 2008. Data were collected retrospectively, examiners were blinded, and relationships were investigated between temporal-bone fractures, ipsilateral THO, ipsilateral CN7 or CN8 deficits using Chi-Square or Fischer's exact tests.

Results: Seventy-nine horses had CT examinations of the temporal region (totaling 158 temporal bones). A total of 16 temporal-bone fractures were detected in 14 horses. Cranial-nerve deficits were seen with fractures in all parts of the temporal bone (petrosal, squamous and temporal) and, as expected, temporal-bone fractures were associated with CN7 and CN8 deficits and THO.

Discussion/Conclusion: No investigated fracture classification scheme, however, was associated with clinical outcome. A descriptive classification therefore is recommended that includes the location of the fracture within the temporal bone (squamous part, petrosal pyramid, tympanic part or mastoid process) and the orientation of the fracture line (sagittal, dorsal and oblique). Certain anatomic structures were consistently identified; anatomic detail was dependent on image acquisition. Understanding temporal-region anatomy (canals, fissures and sutures) is important so that normal structures are not mistaken for fractures.

COMPUTED TOMOGRAPHY AND CT ARTHROGRAPHY OF THE EQUINE STIFLE: 57 CASES. Sarah M. Puchalski and H. J. (Erik) Bergman

Introduction/Purpose: The stifle, a large and complex joint, is frequently implicated in equine lameness. However, the definitive diagnosis of injuries to the intracapsular soft tissues, remain elusive. Routine diagnostics such as radiography, nuclear scintigraphy, ultrasonography, and diagnostic arthroscopy while useful, have limitations. Magnetic resonance imaging (MRI) is the dominant modality for knee injuries in people but when MRI is unavailable, computed tomography (CT) arthrography has been used. The purpose of this paper is to describe a technique for CT arthrography in the equine stifle and report results from 57 cases.

Methods: Fifty-seven horses with moderate lameness (2-4/5) localized to the stifle joint via clinical examination and diagnostic anesthesia underwent CT arthrography after complete radiographic and ultrasound examinations. Horses were anesthetized and placed in dorsal or dorsolateral recumbency on a custom built CT table. An initial pre-contrast study was performed and the study was repeated after ultrasound-guided injection of diluted contrast media into the femorotibial and femoropatellar joints. Control images were made for comparison from two cadaver limbs confirmed to be normal on post-mortem exam.

Results: Injuries of the meniscotibial ligaments (n=36), menisci (n=20), caudal cruciate ligaments (n=14), cranial cruciate ligaments (n=11), and subchondral bone (n=11) were identified. Other less common abnormalities included lesions of the collateral (n=4) patellar (n=4) and mensicofemoral (n=1) ligaments, the semitendinosis enthesis, tibial tuberosity and tibial cartilage.

Discussion/Conclusion: Equine stifle CT and arthrography are feasible and clinically useful. Future use of the described technique will increase our knowledge of equine stifle disease.

MAGNETIC RESONANCE IMAGING OF THE EQUINE TEMPOROMANDIBULAR ARTICULATION - A COMPARATIVE MORPHOLOGICAL STUDY. J. Trichel, H.H. Bragulla, D.J. Hillmann, C.T. McCauley, D. Rodriguez, G. Middleton, L. Gaschen. Louisiana State University School of Veterinary Medicine, Louisiana, 70803.

***Introduction/Purpose*:** The temporomandibular joint (TMJ) is an essential part of the masticatory system and knowledge of its morphology and function is fundamental to the understanding of its role in equine mouth disorders. The aim of this study was to develop a magnetic resonance imaging (MRI) examination protocol for the equine TMJ, to compare its appearance in the open versus closed mouthed positions, and to investigate the use of MRI-arthrography for the assessment of the disc and ligaments.

Methods: The heads of ten horses that were euthanized for conditions unrelated to the head were examined. All were preserved *via* perfusion with neutral buffered formalin and 7 were scanned with the mouth closed and three open using a 1.5 T magnet (Hitachi Echelon™) with both a torso (4-5 mm slice thickness) and a surface coil (3 mm slice thickness). Three (two open mouth and one closed mouth) were additionally scanned within 7 hours of euthanasia prior to perfusion. CT examinations were also performed as well as matched plane dissections for anatomic comparison purposes and to confirm that the joints were normal. 3D sequences were run to develop unique imaging planes for the 2D sequences.

Results: The surface coils allowed for the highest resolution (0.78mm) of the TMJ and juxtaarticular structures compared with the torso coil (1.18cm). The following structures were identified: the articular disc, articular cartilage, lateral and caudal ligaments, caudal fibrous expansion of the articular disc, intra-articular fat, masseter muscle, and medial and lateral pterygoid muscle,and the bony structures of the joint. The SAG plane T1 FatSat and 3D RSSG Water Excitation sequences best show the articular cartilage of the condyle as a thin, uniform, hyperintense contour in contrast to the low signal subchondral bone. The articular disc and its fibrous expansion are visualized in all sequences as being hypointense on T2 and isointense to the pterygoid muscles on T1. The T1 hypointense lateral ligament is best visualized in the AX plane and less so in the DOR plane and not visible in the SAG plane. T2*, PD, T1, FatSat, and RSSG 3D allow for the best visualization of the ligaments. Using 3D sequences it was determined that an axial oblique scan planned at a -18° from the vertical axis of the ramus of the mandible best shows the ligament and its attachment sites in the same slice. In the open mouthed position, there is a closer proximity between the retroarticular process and caudal aspect of the mandibular condyle. MRI arthrograms showed communication between the dorsal and ventral synovial pouches making them more distinct.

Discussion/Conclusion: MRI allows visualization of all components of the equine TMJ. Live horses are examined in the open mouth position due to the presence of an endotracheal tube which results in a physiological incongruency of the TMJ. Angling the axial oblique scan plane -18° from the vertical axis of the ramus of the mandible is ideal for visualization of the ligamentous components of the TMJ. While surface coils allow improved resolution of the joint, all structures could be adequately identified with a torso coil which also allows both joints to be examined simultaneously.

DIAGNOSTIC IMAGING FINDINGS OF ZYGOMATIC SIALOADENITIS IN DOGS. M.S. Cannon, D. Paglia, A.L. Zwingenberger, S.A.E.B. Boroffka, E.R. Wisner. University of California, Davis CA 95616.

Introduction/Purpose: The purpose of this study was to evaluate MRI, CT, and ultrasound (US) for zygomatic sialoadenitis diagnosis.

Methods: Records of dogs with zygomatic sialoadenitis were reviewed. Inclusion criteria included diagnosis from aspiration or tissue biopsy and orbital MR, CT or US. MRI, CT, and US of 10 dogs without retrobulbar disease were evaluated for comparison. Normal and abnormal glands on MR and CT images were quantitatively analyzed for cross-sectional area and pre- and post-contrast enhancement signal intensity or density, respectively. US appearance of normal and abnormal glands was compared subjectively.

***Results*:** Ten dogs met inclusion criteria and 2 had bilateral disease. Six MRI (8 glands), 3 CT (3 glands) and 8 US examinations (8 glands) were performed. On MRI, abnormal glands were larger, more T1 hypointense, T2 hyperintense, and more contrast-enhancing ($p<0.05$). Five abnormal glands contained mucoceles. On CT, abnormal glands were larger and more hypodense on unenhanced images. One gland was predominately fluid attenuating consistent with mucocele. On US, a ventral retrobulbar mass was identified in 7 dogs and recognized as the zygomatic gland in 3 dogs.

Discussion/Conclusion: MRI and CT are useful for recognizing the zygomatic gland as the source of a retrobulbar disorder and for excluding other causes for retrobulbar masses. Quantitative MR and CT features of zygomatic sialitis are consistent, and MR qualitatively provides excellent internal architectural detail. US was less specific for differentiating zygomatic gland disorders from other retrobulbar disease but was necessary for guiding aspiration or tissue biopsy.

MAGNETIC RESONANCE IMAGING OF THE TEMPOROMANDIBULAR JOINT IN NORMAL DOGS. D.M. Macready, S. Hecht, L.E. Craig, G.A. Conklin. University of Tennessee School of Veterinary Medicine, Tennessee, 37996

Introduction/Purpose: Evaluation of the canine temporomandibular joint (TMJ) is important in the clinical diagnosis of animals presenting with dysphagia, malocclusion and jaw pain. In human medicine, MRI is the imaging modality of choice for evaluation of the TMJ. The objectives of this study were to establish a technical protocol for performing MRI on the TMJ in dogs and describe the MRI anatomy and appearance of the normal canine TMJ.

Methods: Ten dogs (one fresh cadaver and 9 healthy live dogs) were examined by MRI. MR images were compared to pathologic sections in the cadaver. T1-W transverse closed-mouth, T1-W sagittal closed mouth, T1-W sagittal open-mouth and T2-W sagittal open-mouth sequences were obtained.

Results: The condyloid process of the mandible and mandibular fossa of the temporal bone were hyperintense to muscle and isointense to hypointense to fat on T1 weighted images, mildly hyperintense to muscle on T2 weighted images, and were frequently heterogeneous. The articular disc was visible in 14/20 (70%) TMJs on T1-W images and 13/20 (65%) TMJs on T2-W images. The disc was isointense to hyperintense to muscle on T1-W images and varied from hypointense to hyperintense to muscle on T2-W images. The lateral collateral ligament was not identified in any joint.

Discussion/Conclusion: MRI allows evaluation of the bony and certain soft tissue structures of the TMJ in dogs.

COMPARATIVE MAGNETIC RESONANCE IMAGING FINDINGS BETWEEN GLIOMAS & INFARCTS. V. Cervera, W. Mai, B. Dayrell-Hart*, C. Vite, G. Seiler. From the University of Pennsylvania, Philadelphia, PA 19104 and *SouthPaws Veterinary Specialists, Fairfax, VA 22031

***Introduction/Purpose*:** The MRI appearance of intraxial brain lesions such as gliomas and infarcts have been described in the veterinary literature. Infarcts are commonly characterized as non-enhancing lesions without a discernible mass effect, whereas gliomas typically enhance to a variable degree and create a mass effect. In our clinical experience however, there is a fair amount of overlap between the MRI findings of each lesion type. The purpose of this study was to compare the MRI findings in dogs with gliomas and dogs with confirmed or presumed infarcts to determine if MRI features can distinguish between them.

***Methods*:** Dogs with intraaxial lesions and either a definitive histologic diagnosis of infarct or glioma, or improvement of the clinical signs and survival of at least 1 year after MRI were included. MR images were retrospectively reviewed by a board certified radiologist, blinded to the final diagnosis. All MR images were obtained using a 1.5 T MR scanner. The following MR parameters were used to describe the lesions: neuroanatomic location, shape, size, mass effect, margin definition, signal intensity and regularity, contrast enhancement, perilesional edema, mineralization, hemorrhage, presence of cyst and loss of brain volume. Lesion size was compared using an unpaired Student´s t-test.

***Results*:** Forty one dogs were included in the study, 18 with glioma and 23 with infarct. Gliomas were predominantly located in the telencephalon (75.6%) compared to a small number of infarcts (24%). Only 25% of infarcts but none of the gliomas were wedge shaped. Mean size of gliomas was significantly larger (23mm, SD 7.37) compared to infarcts (12mm, SD 6.75) ($P<0.01$). 84% of gliomas had mass effect compared to 33% of infarcts. A similar percentage of both types of lesions enhanced after contrast administration with various enhancement patterns. Perilesional edema was observed in 78% of gliomas, but only in 16% of infarcts. Distribution of other findings was very similar between infarcts and gliomas.

***Discussion/Conclusion*:** Gliomas were more commonly located in the telencephalon compared with infarcts. Although not frequent, when present, a wedge shaped lesion was indicative of infarct. Gliomas were significantly larger in size compared to infarcts and lead more frequently to a mass effect and perilesional edema. Nevertheless, clinicians should be aware that there may be considerable overlap between the MR findings of both lesions if diffusion weighted imaging is not available.

EFFECT OF ACQUISITION TIME ON OBSERVER VARIABILITY AND QUALITATIVE CHARACTERIZATION OF GADOLINIUM-ENHANCING BRAIN LESIONS IN DOGS AND CATS. Carmel E.N., d'Anjou M.-A., Blond L., Beauchamp G., Parent J. Department of clinical sciences, Faculté de médecine vétérinaire, Université de Montréal, St-Hyacinthe, Quebec, Canada.

Introduction/Purpose: Contrast-enhanced T1-weighted (T1w) sequences are routinely performed to characterize and differentiate brain lesions in small animals. However, little is known about the effect of time on the distribution and conspicuity of contrast-enhancing brain lesions. The purpose of this study was to determine whether acquisition time influences inter-observer agreement and qualitative characterization of different types of brain lesions in dogs and cats.

Methods: In addition to standard precontrast sequences, transverse T1w FLAIR images were acquired prior to, and immediately following gadolinium injection (T0), as well as 5 minutes (T5) and 18 minutes (T18) post-injection. Postcontrast image series were scored randomly by two radiologists (MAD, LB) for the presence and distribution of enhancement (focal, multifocal or mixed), with only access to precontrast T1w FLAIR. All cases for which enhancement was recognized with high certitude by at least one observer on at least one postcontrast sequence and for which a diagnosis was available were then further characterized by consensus at T0, T5 and T18: enhancement intensity (0-3) and homogeneity, border definition, and number of lesions. All postcontrast sequences were then compared to determine the relative conspicuity and identify the sequence that allowed diagnosis in the shortest time.

Results: All 3 postcontrast sequences were performed in 171 animals. Overall inter-observer agreement on presence of enhancement was very good (κ=0.87). Agreement on the presence of one lesion was good and similar in time (κ_{T0}=0.80; κ_{T5}=0.72 and κ_{T20}=0.78), while the agreement for multifocal distribution increased over time (κ_{T0}=0.40, κ_{T5}=0.6 and κ_{T20}=0.69). From that population, postcontrast series of 50 dogs and 2 cats (26 intra-axial [IA], 26 extra-axial [EA]) were then assessed by consensus. In cases of multifocal IA lesions, the number of lesions increased in 9/26 cases between T5 and T0, and in 4/26 cases between T5 and T18, while the number of EA lesions was constant over time. EA lesions were more consistently well-defined at all times when compared to IA lesions. Higher enhancement scores were significantly associated with EA lesions at T0 and T5, and intensity score and conspicuity of IA lesions increased progressively over time. T0 was considered the most useful sequence for EA lesions, compared to T18 for IA lesions ($p<0.0001$).

Discussion/Conclusion: Our results indicate that the temporal pattern of contrast-enhancement varies among brain lesions and is significantly related to localization, i.e. EA vs. IA. Immediate postcontrast acquisition allows to consistently identifying EA lesions, whereas the size, number and conspicuity of IA lesions can increase on delayed imaging. While such information may not always be essential, it may contribute in increasing the sensitivity and specificity of contrast-enhanced MRI. The use of sequential acquisitions should be further investigated in the context of differentiating different types of IA and EA lesions.

DIFFERENTIATION OF BRAIN LESIONS BASED ON CONTRAST-ENHANCEMENT TEMPORAL CHARACTERISTICS WITH QUANTITATIVE MRI IN DOGS AND CATS.
Carmel E.N., d'Anjou M.-A., Blond L., Beauchamp G., Parent J. Department of clinical sciences, Faculté de médecine vétérinaire, Université de Montréal, St-Hyacinthe, Quebec, Canada.

***Introduction/Purpose*:** Different mechanisms play a role in the accumulation of gadolinium in brain lesions. While contrast-enhanced T1w sequences are routinely performed in small animals to characterize and differentiate such lesions, the impact of acquisition time has never been studied. The purpose of this study was to determine quantitatively the signal values and surface over time of different types of brain lesions in dogs and cats.

Methods: Transverse post-contrast T1w FLAIR images of dogs and cats that presented enhancing lesion(s) and for which a diagnosis was obtained were used for quantitative measurements. For each animal, transverse T1w FLAIR images were acquired immediately following gadolinium injection (T0), as well as at 5 minutes (T5) and 18 minutes (T18) post-injection. A region of interest (ROI) was drawn around each contrast-enhancing lesion (largest when multifocal) on each postcontrast series. Maximum and mean±SD signal intensity, and surface (mm^2) were recorded. To correct for background noise and contrast variations, a separate 20mm^2 elliptical ROI was drawn in the air just dorsal to the head, on the midline, and a ratio (R=ROI/air) was generated for the signal mean (R_{mean}) and maximum (R_{max}) values. Changes over time and between groups were assessed with a repeated-measures linear model corrected by Bonferroni method using sequence (T0, T5 and T18) as within-subject factors.

Results: Fifty dogs and two cats with 26 intra-axial (IA) and 26 extra-axial (EA) lesions were analyzed. R_{max} and R_{mean} for IA lesions were significantly lower at T0 when compared to T5 and T18 ($p \leq 0.001$), whereas these values did not change over time for EA lesions. All sequences combined, the average R_{max} was significantly higher for EA vs. IA lesions ($p=0.04$). R_{max} was also lower for IA lesions at T0 when compared to T5 and T18 ($p \leq 0.002$). EA lesions were consistently larger at all times ($p \leq 0.001$) and IA lesions increased in size between T0 and T18 (58.7 mm^2 vs. 72.1 mm^2; $p=0.003$). IA lesions signal heterogeneity (expressed as SD) was significantly reduced over time ($p \leq 0.0003$).

Discussion/Conclusion: Contrast enhancement of EA lesions consistently peaked immediately and persisted over time, while both enhancement and size of IA lesions progressively increased over time. These differences are likely explained by the fact that EA lesions are not restricted by the blood-brain barrier (BBB) and therefore enhance as rapidly as other hypervascular extracranial structures, whereas IA progressively enhance as contrast medium traverses the BBB and diffuses into brain parenchyma. These results indicate that clinically-applicable, quantitative MRI on sequential post-contrast acquisitions allows a better differentiation of EA and IA lesions. This method may prove valuable in the absence of other reliable predictors (e.g. dural tail sign). Quantitative MRI should be further investigated in the context of differentiating different types of IA and EA lesions.

MRI QUALITATIVE AND QUANTITATIVE CHARACTERIZATION OF MENINGEAL ENHANCEMENT IN DOGS AND CATS: EFFECT OF ACQUISITION TIME AND CHEMICAL FAT SUPPRESSION. d'Anjou M.-A., Carmel E.N., Blond L., Beauchamp G., Parent J. Department of clinical sciences, Faculté de médecine vétérinaire, Université de Montréal, St-Hyacinthe, Quebec, Canada.

***Introduction/Purpose*:** Meningeal contrast enhancement is usually associated with meningitis or neoplastic infiltration. However, few reports described the characterization of such enhancement in small animals. In humans, the use of fat suppression (FS) and delayed imaging following gadolinium injection has been shown to increase the diagnostic sensitivity of MRI for meningeal diseases. The purpose of this study was to characterize qualitatively and quantitatively meningeal enhancement, over time and using chemical fat suppression, in animals with inflammatory and neoplastic diseases.

***Methods*:** Transverse T1w FLAIR images were acquired prior to, and immediately following gadolinium injection (T0), as well as at 5 minutes (T5) and 17±3 minutes (T17) post-injection, and with FS at 19±6 min. All series were scored randomly by two radiologists (MAD, LB) for the presence of meningeal enhancement (absent, equivocal, or definite). All cases for which enhancement was recognized with high certitude by at least one observer on at least one postcontrast sequence and for which a diagnosis was available were then further characterized by consensus at T0, T5, T17 and FS for type (pachymeningeal [PM] or leptomeningeal [LM]) and distribution (focal, regional or diffuse). For each animal, series were compared to identify the one on which meningeal enhancement was most conspicuous. For each series, maximal meningeal thickness (mm) was measured and a square region of interest (ROI) was drawn at the same level to obtain mean signal intensity (SI). This value was divided by the mean SI of a separate 20mm^2 ROI drawn selecting normal grey matter (normal SI on all pre- and postcontrast sequences) to calculate contrast ratio. Meningeal thickness and contrast ratios when compared between categories of disease, and images series.

***Results*:** Thirty-two patients (31 dogs and one cat; 19 inflammatory, 13 neoplasia) were included. Inter-observer agreement was similar among sequences and was globally moderate (κ=0.60). However, chances to obtain a definite result on individual assessment increased over time and with the use of FS ($p \leq 0.004$). When averaging results of all series, meningeal enhancement was more often diffuse and LM in animals with inflammation vs. neoplasia (50% vs.40%, and 64% vs. 38%, respectively), but there was no significant association between type of meningeal enhancement and disease group. When considering all image series, meningeal thickness and contrast ratio were higher for animals with neoplasia ($p \leq 0.02$). Meningeal contrast ratio did not vary significantly between series for either group. Still, qualitatively, it was considered that FS was most useful in 50% of cases.

***Discussion/Conclusion*:** Type and distribution of meningeal enhancement vary substantially among animals with intracranial inflammatory and neoplastic diseases. Our results show that meningeal enhancement is not consistently interpreted by different observers, but that the use of delayed imaging or fat suppression may help identifying its presence with more confidence.

UTILITY OF GADOLINIUM BASED CONTRAST MEDIA FOR SPINAL MR IMAGING; SHOULD ITS USE BE THE STANDARD OF CARE? R. G. King, J. Sutherland-Smith

Introduction/Purpose: MR sequence selection is often based on a protocol developed by the imaging center, or in collaboration with other imaging centers. This protocol provides standardization and efficiency for what are often lengthy examinations under general anesthesia. In recent years, our spine MR protocol has included T2-w sagittal images, followed by T2-w and T1-w transverse images at selected locations based on evaluation of the sagittal images, and on clinical exam findings (neurolocalization). In addition, the protocol has increasingly included post-contrast T1-w transverse images (at the same locations), as well as dorsal and sagittal plane images. Additional sequences (eg. STIR, T2* etc.) are left to the judgment of the radiologist interpreting the examination. MR contrast media administration may expose the patient to increased risk due to contrast reaction (rare) and increased time under anesthetic (~15-45 minutes). Additionally, there is a financial burden associated with administration of MR contrast media ($140 + anesthesia time at our hospital). The goal of this study is to examine the value of contrast administration by interpreting spinal studies with and without the use of post-contrast images. The null hypothesis is that contrast administration does not change MR diagnosis.

Methods: The Tufts Cummings School of Veterinary Medicine MRI database was searched for cases that had pre and post contrast (Gadolinium) MR examination of the spine. The 100 most recent cases were selected. Pre contrast transverse and sagittal MR images and pre and post contrast transverse and sagittal MR images of the same cases were presented to two ACVR boarded radiologists on two separate occasions. The radiologists recorded location and degree of spinal cord compression, gave a presumptive diagnosis and were asked to state whether contrast was recommended (based on pre images), or helpful (based on post images). Age, breed, and weight of the patient were obtained from the DICOM meta data. Interobserver agreement, as well as change in location, diagnosis or severity were evaluated.

Results: 120 lesions in 100 patients were identified by both observers (240 total lesions). Overall, a change in primary diagnosis (pre vs post contrast) was observed in 5% of lesions and change in severity was observed in 1%. No changes in location were observed. In cases where intervertebral disc disease was the primary pre-contrast differential, no changes in diagnosis were observed. In cases where IVDD was not the primary pre-contrast differential, a change of diagnosis was noted in 11% of lesions. The most common alteration was in order of differentials in lesions in which the diagnosis could not be differentiated on MR findings (eg. gliosis vs ischemic myelopathy).

Discussion/Conclusion: The use of gadolinium based MR contrast has minimal impact on the diagnosis of spinal disease in dogs. Contrast administration is unlikely to alter the diagnosis in cases suspected to have IVDD on pre-contrast images. Contrast administration may alter the diagnosis if the pre-contrast primary differential diagnosis is not IVDD.

MAGNETIC RESONANCE IMAGING APPEARANCE OF VERTEBRAL MARROW CHANGES IN DOGS. A.R. Matthews, S. Hecht and W.B. Thomas. University of Tennessee College of Veterinary Medicine, TN, 37920

Introduction/Purpose: The Modic classification system categorizes vertebral endplate and adjacent marrow changes in humans into five groups (types I, II, II, mixed I/II, mixed II/III) based on magnetic resonance imaging (MRI) characteristics. The objective of this study was to assess the appearance and frequency of vertebral bone marrow changes seen on MRI in dogs.

Methods: Spinal MR images from 54 dogs were retrospectively reviewed. Signal intensity changes in vertebral endplates were classified based on the Modic classification system. Other vertebral marrow signal changes not associated with the endplates were categorized as focal (1 vertebral body affected), multifocal (2-7 vertebral bodies affected) or diffuse (≥ 8 vertebral bodies affected).

Results: Ten dogs (18.5%) had vertebral endplate signal changes. Of these, 60% were type II, 30% were type III, and 10% were mixed type II/III. Modic type I and mixed type I/II changes were not identified. T1 and T2 hyperintense vertebral marrow changes not associated with the endplates were seen in 27/54 dogs, all of which suppressed on post-contrast, fat saturated T1-weighted sequences. These fatty changes were noted diffusely in 14/54 (25.9%), multifocally in 11/54 (20.3%) and focally in 2/54 (3.7%) of dogs.

Discussion/Conclusion: The most common type of vertebral marrow change seen in our population was a diffuse fatty marrow change not associated with the vertebral endplates. Vertebral endplate changes similar to those classified by the Modic system in humans can also be identified in dogs.

CONTRAST ENHANCEMENT OF EXTRADURAL COMPRESSIVE MATERIAL ON MAGNETIC RESONANCE IMAGING. J.N. Suran, A. Durham, W. Mai, G. Seiler. University of Pennsylvania, PA, 19104.

Introduction/Purpose: Compressive myelopathy from intervertebral disc herniation is common among dogs. The onset and clinical signs may be insidious or precipitous. Magnetic resonance imaging (MRI) is widely used to diagnose spinal cord compression in dogs. Gadolinium-enhancement of compressive extradural material with magnetic resonance imaging is occasionally detected, but of unknown clinical significance. In humans, contrast enhancement of peri-discal "scar" material has been associated with neovascularization and granulation tissue, providing information on chronicity and influencing therapeutic options.

***Methods*:** Medical records of dogs with clinical signs of less than 6 months duration and MRI findings consistent with compressive myelopathy were reviewed. Duration of clinical signs and neurologic grade (1-5) were recorded, as well as surgical and/or necropsy findings when available. Corresponding MRI series were retrospectively evaluated for presence or absence of enhancement of the meninges and/or extradural compressive material. Where available, compressive material extracted at surgery was assessed histopathologically for origin, inflammation, fibroplasia, fibrosis, blood, vascularity, and necrosis. Duration and severity of clinical signs were compared between dogs with and without enhancement using a Wilcoxon rank-sum test.

***Results*:** We included 112 dogs in the study with a median age of 7 years (range 2 – 14). Median duration of signs was 6 days (range 1-105) and median neurologic grade was 3 (range 1 to 5). Intervertebral disc herniation was confirmed in 92 cases by surgery (n = 90) and necropsy (n = 2). Of these, histopathology was available for 17. Enhancement was present within the meninges, compressive material, or both in 34.8, 33.9, and 9.8%, respectively. There was no statistically significant difference in neurologic status between dogs with and without meningeal or compressive material enhancement (P=0.39 and 0.20, respectively). Duration of clinical signs was significantly shorter in dogs with meningeal enhancement (P=0.008), but not different in dogs with enhancement of extradural compressive material (P=0.84). Histopathologically, enhancing material was considered subacute or chronic in 50% of cases, whereas non-enhancing material was mainly acute (90%). Neovascularization was only observed in compressive material with enhancement (25%). Hemorrhage was seen in 33% of enhancing material and 11% in non-enhancing material. Fibroplasia and fibrosis was absent in patients without enhancement. Mineralization was present in all intervertebral discs, with the exception of one.

***Discussion/Conclusion*:** Contrast enhancement of extradural compressive material was associated with evidence of hemorrhage and neovascularization. Enhancing disc material was more often considered subacute or chronic than non-enhancing material; however, duration of clinical signs could not be associated with disc enhancement. These results should be interpreted with caution, as the disc herniations may have been acute in the presence of chronic disc disease.

COMPARISON OF RADIOGRAPHIC AND COMPUTED TOMOGRAPHIC TECHNIQUES FOR SENSITIVE AND TIME-EFFICIENT DIAGNOSIS OF CANINE ACUTE SPINAL CORD COMPRESSION. S.E. Dennison, R. Drees, H. Rylander, M. Milovancev, R. Pettigrew, T. Schwarz. School of Veterinary Medicine, University of Wisconsin, Madison, WI 53706.

Introduction/Purpose: Myelography is frequently utilized for diagnosing and localizing spinal cord compression although recent studies have advocated the application of CT studies. Myelography is technically demanding, time-consuming and occasionally challenging to interpret. Our goal was to determine the most time-efficient method for diagnosis of acute spinal cord compression without compromising sensitivity.

Method: Forty-six dogs presenting with signs of either acute C1-T2 (n = 25) or T3-L3 (n = 25) extradural spinal cord compression confirmed at surgery or necropsy were recruited. Survey and angiographic CT, myelography and CT myelography were performed consecutively through the entire region of neurolocalization in axial mode (survey & CT myelography), 1mm slice thickness, gantry tilt parallel with C4/5 or L2/3 disc space or helical mode, pitch of 1.4, 2mm slice thickness (angiographic CT) on a single-slice CT unit. 300mgI/ml iohexol was administered via a lumbar puncture for myelography. Series were pseudonymized prior to independent review by two DACVRs.

Results: CT myelography was the most sensitive technique followed by myelography, survey CT and angiographic CT. However for mineralized disc herniations and neoplasia, CT myelography and survey CT performed similarly. CT myelography performed better than myelography in cases of low-volume disc herniation and was the only technique permitting diagnosis, localization and lateralization of extradural lesions with concurrent spinal cord edema. Non-myelographic studies were significantly faster to perform than myelographic studies and CT myelography image acquisition was faster than myelography.

Discussion/Conclusion: Dachshunds and beagles without loss of motor function may be adequately diagnosed from survey CT due to the frequent occurrence of mineralized intervertebral disc herniation. For other breeds and in dachshunds and beagles with loss of motor function, survey CT combined with CT myelography is most sensitive and time-efficient.

INTERACTIVE WEB-BASED THREE-DIMENSIONAL ANATOMIC AND MRI ATLAS OF THE CANINE PELVIC LIMB

S. Sunico, J. Kornegay, J. E. Smallwood, M. Styner, D. Chen, D. Thrall. North Carolina State University, Raleigh, North Carolina, 27606, and University of North Carolina, Chapel Hill, North Carolina, 27599.

Introduction: Understanding muscle anatomy is important for veterinary students learning the integration of structure and function, and for clinicians in making accurate diagnoses and implementing appropriate therapy. The aim of this project was to address both needs with regard to the canine pelvic limb. The first goal was to create a multiplanar diagnostic atlas for rapid muscular identification in magnetic resonance (MR) images while the second was to provide a three-dimensional (3D) interactive web-based anatomic model of the canine pelvic limb.

Methods: The multiplanar diagnostic atlas is comprised of proton density-weighted MR images of the pelvic limbs of a dog, acquired in transverse, dorsal and sagittal planes on a 1.5 T MR unit. Pelvic limb muscles were segmented using the 3D computer program ITK-SNAP and the images were co-registered in each plane to allow simultaneous identification on all imaging planes. For the 3D anatomic model, a helical computed tomography (CT) dataset of the pelvic limbs was reconstructed into 0.75 mm slices and a volumetric T2-weighted 3D dataset acquired on a 3T MR unit was reconstructed into 1 mm isotropic voxels. The CT and MR data were then fused. Structures visible in the CT and MR images were manually segmented using ITK-SNAP and identified based on anatomic texts and other available atlases.

Results: For the diagnostic atlas, images are displayed using Java-based software that allows simultaneous viewing of all 3 planes. Clicking on any muscle in any plane provides automatic scrolling to that muscle position in the other planes; the muscle's identification, innervation and function are displayed. For the anatomic model, muscles are displayed superimposed on a 3D model of the underlying skeleton. All, or only selected, muscles can be displayed. The ability to display selected components facilitates understanding the translation of structure to function. To increase the utility of the 3D atlas, self-study exercises are provided to reinforce functional muscle groupings. Both atlases are available as an open access resource.

Discussion/Conclusions: The combination of advanced imaging modalities and sophisticated computer modeling will advance the veterinary knowledge base to a new level. Computer models can provide integrative anatomic resources that allow teaching topographic and tomographic anatomy simultaneously, as well as provide a clinically relevant reference outside of the anatomy laboratory. In addition to expanding veterinary didactic resources, tomographic anatomic atlases will facilitate efficient clinical identification and description of musculoskeletal lesions, allowing for more specific therapeutics and more accurate treatment planning.

EVALUATION OF COMPUTED TOMOGRAPHY OSTEOABSORPTIOMETRY IN DETECTION OF HIP DYSPLASIA IN LABRADOR RETRIEVERS. P.J. Grimm[*], R.L. Echandi[*], W. T. Drost[*], K.A. Mann[†], R.D. Park[‡], C.E. Kawcak[‡], L. Wei[*]. [*]The Ohio State University, OH 43210, [†]U.S. Department of Defense Military Working Dog (DODMWD) Veterinary Service, TX, 78236, [‡]Colorado State University, CO 80523.

Introduction/Purpose: Canine hip dysplasia is a chronic, debilitating developmental condition where incongruity of the coxofemoral joint often results in osteoarthrosis. Multiple radiographic methods for assessment of hip dysplasia are available, however can be limited in their capability to reliably diagnose hip dysplasia within juvenile dogs. As a new approach to the understanding of the pathologic processes and potential for earlier diagnosis of canine hip dysplasia, our objective was to determine if acetabular and femoral subchondral bone density (SBD) changes can be detected within normal and dysplastic coxofemoral joints via CT osteoabsorptiometry at 6 months of age.

Methods: 33 Labrador Retrievers from the U.S. DODMWD Breeding Program were diagnosed with normal or dysplastic coxofemoral joints based on computed radiographic pelvic studies by a consensus of 3 board-certified radiologists utilizing the OFA evaluation grades at 6, 12, 18, and/or 24 months of age. Helical pelvic CT studies were made at 6 months of age in dorsolateral subluxation test positioning (3.0 mm slice thickness, bone algorithm). A calibration phantom was in the field of view of every study to convert all Hounsfield Unit values to Calcium Hydroxyapatite Equivalent Density units (CHED, mg/ml). CT data was converted into 3D reconstructions for SBD assessment along the femoral heads and acetabula 2 mm beneath their articular margins. Nine standardized ROI were made within the load-bearing regions of the acetabula (n=3) and femoral heads (n=6). Descriptive statistics and a Repeated Measures ANOVA were computed for CHED values of ROI between normal and dysplastic dogs, considering correlations between left and right joints. Significance was set at $P<0.05$.

Results: 17, 11, and 5 dogs were diagnosed with bilaterally normal, bilaterally dysplastic, or unilaterally dysplastic coxofemoral joints, respectively. Strong correlations were present between all mean CHED values of the ROI within bilaterally normal and dysplastic dogs except for two (caudodorsal aspect of the acetabulum and craniolateral aspect of the femoral heads), which had moderate to weak correlations ($r=0.47$ and 0.56, respectively). Bilaterally dysplastic dogs had a significant decrease ($P<0.01$) in mean CHED ROI values along the caudodorsal aspect of the acetabulum (484.16 mg/ml) and craniolateral aspect of the femoral heads (350.03 mg/ml) when compared with bilaterally normal dogs (533.14 mg/ml and 404.74 mg/ml, respectively).

Discussion/Conclusion: The decrease in mean SBD within the dysplastic joints is likely due to decreased distribution of load-bearing forces through these regions of the incongruent joints in accordance with Wolff's Law. A concurrent increase in mean SBD was not seen in the other ROI as expected, which may be due to severity of disease, study limitations (sample size and volume averaging), or age at time of imaging.

Disclaimer: The views expressed in this abstract are of the authors and do not reflect official policy of the Dept. of the Army, the Dept. of Defense, or the U.S. Government.

COMPARISON OF ABDOMINAL ULTRASOUND AND ABDOMINAL COMPUTED TOMOGRAPHY IN THE SEDATED CANINE. E.L. Fields, J.C. Brown, I.D. Robertson, J.A. Osborne. North Carolina State University, College of Veterinary Medicine (Fields, Brown, Robertson) and Department of Statistics (Osborne)

Introduction/Purpose: Computed tomography in sedated patients is facilitated by multidetector row CT scanners that are capable of scanning patients more quickly, using high pitch values. The greater speed reduces respiratory motion artifacts and decreases the time spent under sedation. In human medicine, abdominal CT has become the standard screening test for abdominal disease, in part because of the speed and ease of examination. Using a 16 slice multidetector CT scanner, we compared abdominal CT scanning to abdominal ultrasound for detection of abdominal abnormalities in sedated dogs.

Methods: Twenty-seven sedated canine clinical patients were examined under the same sedation event, using both CT scanning and standard abdominal sonography. CT scans were performed both before and after intravenous administration of iodinated contrast medium. These 27 patients were divided evenly into 3 weight classes: less than 10 kg, 10-25 kg, and greater than 25 kg. Intraabdominal abnormalities detected by each modality were recorded and compared. Abnormalities were also categorized as clinically relevant, equivocally relevant, or unimportant.

Results: With respect to detection of abdominal lesions, detection rate is significantly higher ($p = .0010$) using sedated abdominal CT than when using US, but only in dogs over 25 kg in body weight. That is to say, there is a significant size by technology interaction ($p = .0047$). For dogs weighing 25 kg or less, there is no significant difference in detection rates between modalities.

Discussion/Conclusion: Multidetector row CT may be the preferred screening method for abdominal disease in sedated dogs weighing greater than 25 kg due to its greater sensitivity in lesion detection in this study. For dogs weighing 25 kg or less, detection of abdominal abnormalities was not statistically different between modalities, and factors such as operator skill, radiation exposure, availability of modalities, and time should be considered in deciding between the two modalities. Advantages of CT scanning include the possibility of detection of extra-abdominal lesions and decreased dependence on operator skill for accuracy of diagnosis. As multidetector CT scanners become more widely available to veterinary practitioners, further exploration of this modality as a screening tool is warranted.

MULTI-ROW COMPUTED TOMOGRAPHY ANGIOGRAPHY TECHNIQUE OF THE CANINE PULMONARY VASCULATURE. M. Makara[1], T. Glaus[2], M. Dennler[1], R. Bektas[3], A. Kutter[3], R. Dip[4], M. Schnyder[5], P. Deplazes[5], Stephanie Ohlerth[1], [1]Section of Diagnostic Imaging, [2]Division of Cardiology, [3]Section Anesthesiology, [4]Institute of Veterinary Pharmacology and Toxicology, [5]Institute of Parasitology, Vetsuisse Faculty, University of Zurich, Switzerland.

Introduction/Purpose: A computed tomography (CT) angiographic technique was developed to image the canine pulmonary vasculature using a nonselective peripheral injection of contrast medium.

Methods: Ten age- and weight-matched Beagle dogs experimentally infected with *Angiostrongylus vasorum* were randomly divided in 2 groups. In group A (6 dogs) CT angiography of the thorax was performed using an empiric protocol with a fixed contrast medium injection rate of 3 ml/s and a fixed post-injection scanning delay of 20 sec. All dogs in this group were scanned 13 weeks post infection but only 4 dogs were scanned 9 weeks post treatment. In group B (4 dogs) the iodine injection rate was adjusted to the scanning time and was calculated as follows: contrast volume / scanning time + 10 seconds. The time of contrast arrival to the region of interest was measured with a bolus triggering technique at the level of the main pulmonary artery with a pre-selected threshold of 150 HU. All dogs in group B were scanned before infection and 4 times post infection at a 2 week interval. Contrast medium dose for both groups was 800mg/Kg of an iodinated high-osmolar contrast medium*. The CT study was performed with a multi-row unit@ using 24 rows, slice collimation of 1.5 cm and pitch of 1.3 for both groups. Measurements of the pulmonary vasculature enhancement were performed by drawing ROI along the z-axis. The distance between measurements was 1 cm. A value of 300 HU has been suggested as adequate for pulmonary artery enhancement[1]. The mean of the pulmonary artery enhancement measurements for both groups was calculated and an unpaired t-test with Welch correction was used to compare group A and B, and healthy and infected dogs in group B. The study was approved by the local ethical committee.

Results: In group B, the time of contrast arrival ranged from 9 to 13 sec and the calculated injection rate varied between 1.5 to 2 ml/s. Mean enhancement in group A and group B was 164.84 HU (SD 53.34) and 467.46 HU (SD 112.27) respectively. Vascular enhancement was 2.8-times higher in dogs from group B compared to dogs in group A ($p<10^{-4}$). There was no statistically significant difference in vascular enhancement between healthy and infected dogs in group B.

Discussion/Conclusion: Adjustment of the iodine injection rate and timing of the contrast medium by bolus triggering clearly exceeded the proposed value of 300 HU for enhancement of the pulmonary vasculature, while the empiric protocol failed to reach this suggested value. Additionally, we speculate that this technique could potentially translate into lower doses of contrast medium.

@ Somatom Sensation Open ,Siemens AG, Medical Solutions, Erlangen, Germany;
* Telebrix® , 350mgI/ml, Guerbert, Zürich, Switzerland
1) Schoellnast H, et al. AJR Am J Roentgenol. 2006;187: 1074-1078.

PULMONARY ANGIOGRAPHY USING 16 SLICE MULTIDECTOR COMPUTED TOMOGRAPHY IN CLINICALLY NORMAL DOGS. A. Habing, M. Beal, A. Brown, N. Nelson, J. Coehlo, J. Kinns. Michigan State University, MI, 48824-1314.

Introduction/Purpose: The purpose of this study was to develop a pulmonary angiographic technique using a 16 slice multidector computed tomography (CT) scanner that would allow consistent evaluation of the pulmonary arterial system. This technique may be valuable in diagnosing pulmonary thromboembolism in future clinical patients.

Methods: Pulmonary angiography was performed using a 16 slice multidetector CT scanner on five healthy, anesthetized beagles. A helical acquisition with pitch of 1.4 was utilized. The time delay for the angiographic study was determined using a bolus tracking program. A dose of 400mg I/kg of nonionic contrast media (Iohexol 300mg/ml) was administered to each dog via a cephalic catheter using an angiographic power injector at a rate of 5ml/sec. In two dogs a second study with doses of 200mg I/kg and 600mg I/kg respectively was performed Arterial enhancement was subjectively classified as excellent, good, or poor on transverse images and images reformatted in multiple planes. Arterial enhancement was also assessed objectively by measuring Hounsfield units at the right main pulmonary artery of each study. Each angiographic study was evaluated by two radiologists to determine the number of sub-segmental arterial branches that could be seen. The first generation artery was considered to be the primary lobar artery with the first branch of this being the 2nd generation artery.

Results: The time attenuation curve obtained by the bolus tracking program showed consistent enhancement of the right main pulmonary artery beginning at 6 seconds and peaking at 8 seconds in 4/5 dogs. In one dog peak arterial enhancement occurred at 10 seconds, however this dog was found to have an anomalous persistent left cranial vena cava. In the first imaged dog, scanning was initiated at the time of arterial peak enhancement, which resulted in incomplete mixing of contrast within the main pulmonary artery. Subsequent scans were initiated 5 sec after the arterial peak and resulted in uniform enhancement. The contrast dose of 400mg I/kg resulted in good to excellent vascular enhancement in the 4 normal dogs. 200mg I/kg resulted in subjectively poor enhancement. The number of branches of small segmental arteries seen varied from 2 to 7, with a median of 5.

Discussion/Conclusion: Pulmonary angiography using multidetector computed tomography and an automated bolus tracking program allows rapid, consistent evaluation of the pulmonary vasculature using a single 400mg I/kg injection of contrast medium.

COMPUTED TOMOGRAPHIC EVALUATION OF THE EQUINE PITUITARY GLAND IN HORSES WITH HYPERADRENOCORTICISM COMPARED TO NORMAL HORSES. A.P. Pease, H.C. Schott. Michigan State University, East Lansing, MI. 48824

Introduction/Purpose: Pituitary pars intermedia dysfunction (PPID) in horses, also known as equine Cushing's disease or equine hyperadrenocorticism, is the most common endocrinologic disorder of older horses. Prolonged treatment is used to control chronic laminitis due to excess cortisol, which contributes to the morbidity and mortality of this disease. In horses, PPID is almost exclusively attributed to hyperplasia or micro- and macro-adenoma formation in the pars intermedia that appears to be due to the loss of hypothalamic innervation. CT has been reported as an accurate measure of the equine pituitary gland in normal horses; however, no description of the CT appearance of PPID pituitary glands is present in the literature. Our goal was to evaluate the size of the pituitary gland in horses that are confirmed positive for PPID, and compare them to the size of the pituitary gland in horses that have normal bloodwork and no evidence of PPID (control group). We hypothesized that the pituitary glands of horses with PPID would be significantly larger than those of normal horses.

Methods: Eleven horses were included in this study; 8 horses which were confirmed positive for PPID and 3 confirmed negative for PPID based on dexamethasone suppression testing. Horses were anesthetized and imaged using a 16 slice GE Lightspeed (GE Medical Solutions, Milwaukie, WI) CT scanner. A survey helical scan of the brain was obtained to determine the approximate location of the pituitary gland based on the sella turica. Contrast medium (150mL MD-76 (Mallinckrodt Inc. St. Louis, MO)) was injected at a rate of 3 mL per second via a power injector into a 14 gauge catheter into the jugular vein. A post contrast medium helical scan was performed four minutes after the initial injection. The pituitary gland was measured using DICOM viewing software (Merge eFilm, Milwaukie, WI) and statistical analysis was performed using Sigma Stat (Systat Software, Chicago, IL). The length measurement was made based on a sagittal reconstruction of the transverse images. A one way repeated measures analysis of variance was performed on the length, width and height measurements with statistical significance set at $p < 0.05$.

Results: The mean size of the pituitary gland in horses with PPID was 2.0 cm x 2.3 cm x 1.6 cm (length x width x height). In the control group the mean size of the pituitary gland was 1.6 cm x 1.5 cm x 0.6 cm. Horses with PPID had significantly larger pituitary glands both in height ($p<0.0001$) as well as width ($p<0.001$) compared to controls. The length was not statistically different between the two groups ($p = 0.07$). The power of this test with alpha set at 0.05 was 1.

Discussion/Conclusion: Pituitary glands in horses with PPID were significantly larger in the dorsoventral and left-right direction, but not in the rostrocaudal direction, compared to normal horses. This finding may be useful in monitoring the response to treatment in horses with PPID.

INTRA-ARTERIAL CONTRAST ENHANCED COMPUTED TOMOGRAPHY IN EQUINE FOOT LAMENESS: 151 HORSES. S. M. Puchalski, R. M. Schultz, R.J.K. Bell, L.D. Galuppo, M.H. MacDonald, J.R. Snyder and E.R. Wisner

***Introduction/Purpose*:** To describe lesions identified using contrast enhanced computed tomography (CECT) in horses with foot lameness.

Methods: Medical records and CECT images from 151 horses (200 limbs) with foot lameness were retrospectively reviewed. Age, breed, lameness grade, use, and results of diagnostic anesthesia were recorded. Imaging lesions were characterized by anatomic structure, location, configuration and extent. Descriptive statistics were used for lesion frequency and location.

Results: Lesions of bone or soft tissue were identified in 151 (76%) limbs. 253 deep digital flexor tendon (DDFT) lesions were present in 116 (77%) limbs. Fifty-seven horses (49%) had DDFT lesions in multiple locations or had DDFT lesions that were continuous through multiple anatomic zones. DDFT lesions were most common at the level of the collateral sesamoidean ligament (CSL) (n=92) and navicular bone (n=51). Core lesions (n=93), dorsal abrasions (n=82), insertional lesions (n=42) and sagittal splits (n=36) were identified. Lesions of the navicular bursa, DIP joint, flexor cortex of the navicular bone, distal navicular border fractures, CSL, distal sesamoidean impar ligament, and collateral ligaments of the distal interphalangeal joint were less common. Warmblood horses were most commonly represented (n=83). Initial lameness grade ranged from 1-4/5 with a median of 3/5. Lameness improved in all horses following palmar digital nerve, distal interphalangeal joint and/or digital tendon sheath anesthesia.

***Discussion/Conclusion*:** Results indicate that CECT is useful for the identification of lesions of bone and soft tissues within the hoof capsule of the horses with clinical lameness localized to the region.

THE MRI FINDINGS IN HORSES WITH SPINAL ATAXIA. C.W. Mitchell, S. Nykamp, R.A. Foster. Ontario Veterinary College, Ontario, N1G 2W1.

Introduction/Purpose: Antemortem diagnosis of cervical stenotic myelopathy (CSM) is currently made by neurological evaluation, exclusion of other diseases and radiographic examination. The information provided by radiographs, either survey or contrast, is often insufficient and can be misleading. The primary goal of this study is to establish the accuracy of MRI for diagnosing CSM by comparison of MRI findings to the gold standard of pathology.

Methods**:** 39 horses with spinal ataxia and 20 controls underwent clinical and neurological examinations and standing survey cervical radiographs. Horses were euthanized and the head and neck were dismembered. MRI of the cervical spine was performed using the following protocol: 3 plane localizer, T2 frFSE (sagittal, transverse, dorsal), T1 FSE (sagittal, transverse, dorsal), GRE T2* (sagittal) and STIR FSE (sagittal). Each horse underwent routine post mortem examination. A final pathological diagnosis was made of normal (control), idiopathic ataxia (no cause for ataxia found on post mortem examination), definitive cause of ataxia identified (other than CSM), CSM or cervical vertebral stenosis (CVS) (obviously stenotic on gross post mortem examination but no histopathological evidence of myelopathy). In the CSM cases, the site of histological evidence of compression was identified. The MR images were assessed by two board certified radiologists for spinal cord intensity changes, spinal cord compression, spinal cord compression direction, shape of spinal cord, and the presence of synovial cysts, joint mice and osteoarthritis. The height, width and area of the spinal cord, dural tube and vertebral canal as well of the height of the vertebral bodies were measured. Qualitative data was analyzed for agreement between observers and chi-square analyses were used to determine correlation to histological groups. Quantitative data was analyzed for agreement between and within observers and ANOVA was used to determine differences in means between histological groups.

Results**:** 24 horses were diagnosed with CSM, 5 with CVS, 7 with idiopathic ataxia and 3 horses with other ataxia. The identification of spinal cord compression on MRI was statistically significant in determining the histological group for both observers. In the CSM group, the identification of spinal cord compression on MRI images had poor to slight agreement with the presence or absence of histological lesions of compression (Wallerian degeneration or malacia). Hyperintensity within the spinal cord was statistically significant in determining histological type for both observers. Horses with CSM or CVS were more likely to have osteoarthritis than control horses or horses with other or idiopathic ataxia. The quantitative assessments were generally not useful in determining histological group.

Discussion/Conclusion**:** MRI examination can differentiate between compressive myelopathy and other causes of spinal ataxia, but would not be able to identify the exact compressive site if surgery was being contemplated.

DETERMINATION OF T1 VALUES OF NORMAL EQUINE TENDONS USING MAGIC ANGLE MR IMAGING. M. Spriet, E.R. Wisner, L. Anthenill, M.H. Buonocore. University of California, Davis, CA, 95616.

Introduction/Purpose: With conventional MR imaging, little information can be obtained about the T1 properties of tendons due to the extremely short T2 values and the resulting signal void. The magic angle effect, responsible for an increase of tendon T2, was initially considered a musculoskeletal MR artifact but recent studies have suggested that this phenomenon could be beneficial for tendon imaging. Using magic angle MR imaging, increased T1 values have been identified in humans with chronic Achilles tendinopathy. The objectives of this study were to validate a method to measure T1 values in equine tendons and to determine the T1 values of the superficial digital flexor tendon (*SDFT*), the deep digital flexor tendon (*DDFT*) and the suspensory ligament (*SL*) in normal horses.

Methods: The metacarpus of 6 isolated equine front limbs was imaged with a 1.5T MR unit using a flexible surface coil. The limbs were positioned with the long axis of the metacarpus at 55° relative to the main magnetic field. Axial images of the tendons were obtained using a spin-echo proton density (SEPD) pulse sequence and two inversion recovery pulse sequences with inversion times of 250 msec and 350 msec (defined “IRSE 250” and “IRSE 350”, respectively). The T1 values of the *SDFT*, *DDFT* and *SL* were calculated in 5 different locations for each specimen using 3 different methods based respectively on ratios of signal intensity between IRSE 350 and SEPD (the “350/PD” method), IRSE 250 and SEPD (the “250/PD” method) and IRSE 250 and IRSE 350 (the “250/350” method).

Results: Minimal variation was obtained for the 5 different measurements for each tendon within each specimen with a coefficient of variation less than 6% for each method. The results obtained with the 350/PD method were on average 5.3% higher than the results obtained with the 250/PD method and 8.9% higher than the 250/350 method. With the 350/PD method, the T1 values for *SDFT, DDFT* and *SL* were respectively 288 (+/- 17), 244 (+/- 14) and 349 (+/- 16) msec. The difference in T1 values between *SDFT*, *DDFT* and *SL* was statistically significant with all 3 methods ($p<0.05$, Wilcoxon sign-rank test).

Discussion/Conclusion: It is possible to measure the T1 values of equine tendons using magic angle imaging with a clinical MR unit. Minor variation in the results occurs depending on the technique used. The normal *SDFT*, *DDFT* and *SL* have different T1 values. The knowledge of the range of T1 values in normal equine tendons may be useful to identify horses with chronic tendinopathy, where based on the human literature, increased T1 values will be expected.

INFLUENCE OF THE CHEMICAL SHIFT ARTIFACT ON MEASUREMENTS OF COMPACT BONE THICKNESS OF THE EQUINE DISTAL LIMB. A.N. Dimock, M. Spriet. University of California, Davis, School of Veterinary Medicine, CA 95616

***Introduction/Purpose*:** On MR images, the subchondral bone plate and cortical bone are well-demarcated regions of hypointense signal bounded by hyperintense cartilage or periosteum on one margin and fat on the other. Measurements of compact bone thickness are easily made, although the accuracy of such measurements may be questioned due to the possible misregistration of the bone/fat interface in the frequency encoding direction resulting from the chemical shift artifact. The objective of this study was to assess the impact of the chemical shift artifact on MR measurements of compact bone thickness in the equine distal limb.

***Methods*:** Six isolated, mature equine distal limbs were imaged using a 1.5 T MR unit with a quadrature head coil. Sagittal T1 weighted spin echo (SE) and 3D spoiled gradient echo (SPGR) images were acquired twice, switching the frequency encoding direction between the two acquisitions. Measurements of compact bone thickness were performed on a single parasagittal image in 10 different locations involving all 3 phalanges and the navicular bone. Radiographic measurements of compact bone thickness were performed on a 3mm thick section of bone from the same location as the selected MR image. The measurements obtained from MR images were compared between the two different frequency encoding directions, as well as with the radiographic measurements. The expected chemical shift was calculated for both SE and SPGR pulse sequences.

***Results*:** Measured compact bone thickness was significantly different when comparing MR images acquired with different frequency encoding directions for both SE and SPGR sequences ($p<0.05$, Wilcoxon signed-rank test). The average differences were 1.42mm and 1.55mm for SE and SPGR sequences respectively. The average differences between MR and radiographic measurements in the frequency encoding direction were higher and significantly different than measurements made in the phase encoding direction, for SE and SPGR sequences ($p<0.05$). The calculated chemical shift was 1.27mm for SE and 1.26mm for SPGR sequences.

.

Discussion/Conclusion: Errors in MR evaluation of compact bone thickness occur when measurements are performed in the frequency encoding direction. These errors are due to misregistration of the bone/fat interface due to the chemical shift artifact. For better accuracy, compact bone measurements should be performed parallel to the phase encoding direction. Alternately, a correction factor based on the calculated chemical shift should be applied to measurements performed in the frequency encoding direction.

DETECTION OF OSTEOCHONDRAL DEFECTS IN THE FETLOCK JOINT USING LOW AND HIGH FIELD STRENGTH MR IMAGING ANDTHE EFFECT OF SEQUENCE SELECTION ON LESION CONSPICUITY AND SIZE. NM Werpy, CP Ho, AP Pease, CE Kawcak, Colorado State University 80523, Michigan State University 48824

Introduction/Purpose: The purpose of this study was to evaluate the effect of field strength and sequence selection on MR images of fetlock joints with subchondral bone and articular cartilage defects that were imaged at three field strengths, 0.27 T, 1.0 T and 1.5 T and assess the potential effect of motion on 0.27 T images.

Methods: Four different lesions were created on each metacarpus and curetted to specific dimensions using 6 cadaver limbs. MR sequences used were individually maximized for clinical imaging on each system. The images were evaluated, the visible lesions were measured, the sequence that best demonstrated the lesion and a confidence score were recorded. Statistical analysis of the results was performed.

Results: The conspicuity of the lesions was the greatest on the 1.5 T images, followed by 1.0 T and then 0.27 T. On the high field images the PD FSE was preferred for lesion detection followed by the PD and T2 FSE, which were equally represented. On the low field images the T1-weighted GRE was most commonly used, however certain lesions were most apparent on the T2 FSE images. When lesions were visible, they appeared smaller and more shallow with less distinct margins on the T1 and T2* gradient echo images when compared to the PD, PD FSE and T2 FSE images on all systems.

Discussion/Conclusion: There is a difference in detection of subchondral bone and articular cartilage defects when comparing high and low field MR systems. Despite the superior spatial resolution of the gradient echo sequences, they did not provide the best lesion conspicuity. The contrast resolution of the turbo and fast spin echo sequences as well as a lack of susceptibility artifact resulting from local tissues provided superior lesion conspicuity. The T1 GRE sequence is the only sequence that appears to allow visualization of the articular cartilage on the low field images. However, in this study the signal intensity in the defects was unchanged or minimally changed with this sequence, falsely representing the presence of articular cartilage

RO AFTERNOON SESSION

1:30 pm **Scientific Session 9: RO** (Moderator: MK Klein)

1:30 pm Rodney Ayl, DVM, DACVR
"**RADIATION THERAPY IN THE TREATMENT OF BENIGN DISEASE"**

2:30pm **STEREOTACTIC RADIATION THERAPY FOR APPENDICULAR BONE TUMORS.** Stewart D. Ryan, Nicole E. Ehrhart, Deanna Worley, Joseph F. Harmon, Jamie Custis, Joanne Tuohy and Susan M. LaRue. Colorado State University Animal Cancer Center, Fort Collins, CO, 80523

2:50 pm **IDENTIFYING FACTORS PREDICTIVE OF OSTEOSARCOMA RELATED PATHOLOGIC FRACTURE FOLLOWING STEREOTACTIC RADIATION THERAPY**. J.T. Custis, S.D. Ryan, A. Valdés-Martínez, J.F. Harmon, S.L. Kraft, S.M. LaRue Colorado State University Animal Cancer Center, Colorado, 80523

3:10 pm **THE ELECTRON BEAM ATTENUATING PROPERTIES OF SUPERFLAB, PLAY-DOH, WET GAUZE, AND PLASTIC WATER.** Koichi Nagata, Jimmy Lattimer. College of Veterinary Medicine, University of Missouri, Columbia, MO.

3:30 pm *Break with exhibitors*

4:00 pm **Scientific Session 10: RO** (Moderator: Bill Brawner)

4:00 pm **ENDOCRINE FUNCTION IN CATS FOLLOWING STEREOTACTIC RADIATION THERAPY FOR TREATMENT OF ACROMEGALY.** SM LaRue, Joseph F. Harmon, James T. Custis and Katherine F. Lunn. College of Veterinary Medicine and Biomedical Sciences, Colorado State University, Fort Collins, CO

4:20 pm **CHARACTERIZATION OF CANINE BLADDER VARIATIONS TO OPTIMIZE FRACTIONATED RADIATION THERAPY PROTOCOL USING CONE-BEAM COMPUTED TOMOGRAPHY.** J.R. Nieset, J.F. Harmon, S.M. LaRue, Department of Radiological Health Sciences, Colorado State University, Fort Collins, Colorado, 80523

4:45 pm Deb Prescott, DVM, DACVR
"**A REVIEW OF THE RADIATION THERAPY PROTOCOLS USED MOST COMMONLY IN VETERINARY RADIATION ONCOLOGY**"

5:45 pm Adjourn for the day

STEREOTACTIC RADIATION THERAPY FOR APPENDICULAR BONE TUMORS. Stewart D. Ryan, Nicole E. Ehrhart, Deanna Worley, Joseph F. Harmon, Jamie Custis, Joanne Tuohy and Susan M. LaRue**.** Colorado State University Animal Cancer Center, Fort Collins, CO*,* 80523

Introduction/Purpose*:** Single fraction stereotactic radiosurgery (SRS) has been described as a treatment option for canine extremity osteosarcoma. The Varian Trilogy™ linear accelerator allows ***fractionated stereotactic delivery of intensity modulated radiation with a high degree of precision. Our hypothesis is that that Stereotactic Radiation Therapy (SRT) may provide a non-surgical limb salvage option in a variety of anatomic sites.

Methods: Twenty-five dogs with appendicular bone tumors were treated with SRT. A bone anchored temporary fixation was used in 16 cases and a non-invasive positioning system was used in 9 cases. A radiation planning CT scan of the affected region was acquired in the indexed positioning frame. The Varian Eclipse Treatment planning system was used to develop a hypofractionated treatment plan with radiation delivered using at least 5-7 static fields in three fractions. Initially 42-45 Gy was prescribed to 95% of the prescribed tumor volume (PTV), with no more than 1% of the skin receiving over 40Gy. After identifying a patient with a grade 3 skin effect, the prescription was modified and intensity modulated treatment was instituted so that no more than 0.5% of skin received more than 35Gy. The dose to 95% of the PTV in these dogs averaged 39 Gy. At treatment, orthogonal view kVp images from the on board imaging system were matched to bony landmarks from the planning CT. Carboplatin was administered intravenously before the first or second fraction and chemotherapy was continued with either Carboplatin or Carboplatin/Adriamycin every three weeks for 4-6 treatments. Intravenous pamidronate was administered. Patients had regular lesion and thoracic radiology following treatment.

***Results*:** Tumor locations included 9 radii, 2 ulnas, 10 humeri, 2 tibia and 2 femurs. Nineteen dogs are alive (median follow-up 133 days). Five dogs were euthanized or died due to disease and one dog died of a GDV. Clinical outcome has been good to excellent based on radiographic follow up and assessment of limb use and durable pain palliation. Post treatment complications included moderate to severe acute radiation effects to the skin in the first three cases. Patients who received skin doses not exceeding 35 Gy had mild grade I or no skin effects. Nine fractures have occurred and will be discussed in another abstract. Documented metastases have occurred in 7 cases to either lungs or bone. In 5 limbs that have been assessed histologically after death or amputation, 100% tumor necrosis was observed.

Discussion/Conclusion: Although the frame positioning system should have provided rigid immobilization and repeatable positioning, pins often bent or loosened between fractions. The non-invasive positioning system provided repeatable patient positioning with less patient morbidity and client expense. Acute radiation side effects were mild and focal when 0.5 ml skin radiation dose did not exceed 35Gy. Local tumor control is excellent to date. Long-term follow up is required to evaluate tumor control, survival and late effects.

IDENTIFYING FACTORS PREDICTIVE OF OSTEOSARCOMA RELATED PATHOLOGIC FRACTURE FOLLOWING STEREOTACTIC RADIATION THERAPY. J.T. Custis, S.D. Ryan, A. Valdés-Martínez, J.F. Harmon, S.L. Kraft, S.M. LaRue
Colorado State University Animal Cancer Center, Colorado, 80523

Introduction/Purpose: Stereotactic radiation therapy (SRT), a non-surgical limb salvage procedure, is effective at achieving local control for appendicular osteosarcoma. Pathologic fracture remains the most frequent and severe complication associated with SRT. The purpose of this study was to determine if patients with increased risk of early fracture can be identified prior to treatment.

Methods: Retrospective analysis of 25 dogs with bone tumors treated with SRT was performed. The most recent orthogonal radiographic projections of the lesion obtained prior to the administration of the first fraction of SRT were evaluated and scored with regard to anatomic site, nature of the lesion (blastic, mixed, or lytic), pattern of lysis if present (ie geographic, moth-eaten, or permeative), whether the lesion was expansile, size of the lesion relative to the diameter of the bone (<1/3, 1/3-2/3, or >2/3), and number of cortices impacted by the lesion. The medical record was reviewed to determine age, bone biopsy prior to SRT, timing of pamidronate administration, and the level of lameness present upon initial presentation to the CSU ACC. The Varian Eclipse treatment plan was reviewed to determine the planned target volume (PTV), the bone volume irradiated, and the 95% dose to the PTV. Voxar 3D reconstruction software was utilized to convert all radiation planning images (CT) into transverse images along the long axis of the bone of interest. The individual slice with the greatest degree of cortical lysis (25%, 50%, 75%, or 100%), as determined by dividing each transverse image into four equal quadrants, was evaluated. We utilized logistic regression to determine the set of variables that best predict fracture within 3 months after radiation. Variable selection was based on predictive values and the area under the ROC curve.

Results: Twenty-five patients (10 humerus, 9 radius, 2 ulna, 2 femur, and 2 tibia) were treated with SRT. Eight patients (3 humerus, 4 radius, and 1 femur) developed a pathologic fracture following the completion of SRT. Pathologic fractures occurred only in predominately lytic or mixed radiographic lesions. Seven of the eight patients that would eventually develop a pathologic fracture following SRT possessed an initial lesion involving greater than 2/3 the diameter of the bone, and all eight of those patients demonstrated an initial lesion involving two or more cortices. Evaluation of the reconstructed CTs revealed that all eight fracture patients had at least one CT slice with 50% complete or partial cortical lysis at the time of radiation planning.

Discussion/Conclusion: Pathologic fracture is common after SRT. Identifying the patients with an increased risk for the development of a pathologic fracture prior to radiation therapy should improve case selection as well as improve the ability of the clinician to determine if and when prophylactic surgical fixation is indicated.

THE ELECTRON BEAM ATTENUATING PROPERTIES OF SUPERFLAB, PLAY-DOH, WET GAUZE, AND PLASTIC WATER. Koichi Nagata, Jimmy Lattimer. College of Veterinary Medicine, University of Missouri, Columbia, MO.

Introduction/Purpose: Electron beams are commonly used to treat the veterinary patients in veterinary hospitals with linear accelerators. Bolus materials are materials which have an electron density closer to tissue, and they are used in order to shift the isodose curves closer to the patient's surface. Several types of bolus materials are commonly used in practice, which includes Superflab (commercially available material), Play-Doh, and wet gauze. To our knowledge, the properties of these materials in terms of electron beam attenuation have not been documented. The purpose of this study is to compare the electron beam attenuating properties of these three kinds of materials to that of plastic water, and evaluate their usefulness as bolus materials when electron beam therapy is conducted.

Methods: Electron beams of 5, 6, 7, 8, 10, and 12 MeV were evaluated. Play-Doh, wet gauze, and Superflab were evaluated as bolus materials and compared to plastic water which was used as the reference material. The thickness of each bolus material was made to equal the Dmax for each electron energy. A 15cm x 15cm field was used, and the distance of the source to the parallel-plate ionization chamber was fixed at 100 cm. Multiple dose measurements for each material were made using a parallel plate ionization chamber coupled with an electrometer.

Results: Superflab had electron attenuation/buildup similar to plastic water with less than 3% difference except for 12 MeV, when Superflab showed more attenuation and/or less buildup of the electron beam (5.9%) than plastic water. Play-Doh showed more attenuation and/or less dose buildup compared with plastic water, especially at lower energies. The difference was as high as 24.7% with a beam energy of 5 MeV and as low as 5.5% with a beam energy of 12 MeV. Wet gauze resulted in more dose buildup and/or less attenuation compared to plastic water (up to 8%) at a beam energy of 5 MeV.

Discussion/Conclusions: Play-Doh should not be used as a bolus material when lower-energy electron beams are used to avoid underdosing. Use of wet gauze can lead to overdosage due to buildup without attenuation. There did not seem to be a clear correlation between this phenomenon and the electron beam energy used.

ENDOCRINE FUNCTION IN CATS FOLLOWING STEREOTACTIC RADIATION THERAPY FOR TREATMENT OF ACROMEGALY. SM LaRue, Joseph F. Harmon, James T. Custis and Katherine F. Lunn. College of Veterinary Medicine and Biomedical Sciences, Colorado State University, Fort Collins, CO.

Introduction/Purpose: Seven cats received stereotactic radiation therapy (SRT) for treatment of acromegaly, and endocrine testing was performed before and after SRT. All cats had clinical signs of acromegaly, including diabetes mellitus with insulin resistance. Improvement in endocrine status has been noted in cats with pituitary tumors following treatment with fractionated radiation therapy, but the durability and mechanism of the improvement has not been thoroughly examined. SRT of human patients with pituitary tumors has been associated with a quicker and more durable improvement in endocrine status compared with patients treated with fractionated radiation therapy, although neurological responses were equivalent. The purpose of this study was to evaluate pituitary function in acromegalic cats treated with SRT.

Methods: To be admitted to the study, cats had to have typical clinical manifestations of acromegally. Growth hormone(GH), Insulin-like growth factor I (IGF-I), endogenous ACTH, thyroid hormones and cortisol levels before and after ACTH stimulation test were performed prior to treatment and at weeks 2, 6, 12, 26, 39 and 52. Cats were placed in a customized bite block type immobilization device and a planning CT of the head was acquired using 2 mm slices. The Varian Eclipse Treatment planning system was used to develop a hypofractionated treatment plan. SRT was administered in 2-4 fractions over 4 days using a Varian Trilogy™ linear accelerator. Dose (28-36 Gy) was based on normal tissue constraints including brain and optic chiasm. In the first 2 cats, 7 static fields were used. In the remaining 5 cats sliding leaf technology and inverse treatment planning for intensity modulation was employed.

Results: All cats had a substantial decrease (over 50%) in insulin requirements. One cat was taken off insulin at 14 weeks post treatment and remains off at 28 weeks. GH levels are pending. All cats had elevated IGF-1 levels prior to SRT. IGF-1 levels fell in some cats, but not as rapidly as decrease in insulin resistance. At all time points evaluated, thyroid panels were unremarkable, and ACTH stimulation tests showed elevated pre- and post-ACTH cortisol values in all cats, however there were no clinical signs of hyperadrenocorticism. Endogenous ACTH levels varied, but did not indicate pituitary hypofunction. There was no evidence of diabetes insipidus and electrolyte values remained normal in all cases. One cat was mentally dull immediately after SRT, but responded to s short course of prednisolone. No other adverse effects of SRS were noted in any patient. Intensity modulation produced treatment plans that provided better sparing of critical normal tissue structures compared to static field plans.

Discussion/Conclusion: SRS is well-tolerated in cats with acromegaly, and may lead to improved clinical signs within 6 months. Pituitary function remains normal at least for 26 weeks post-SRS, but IGF-1 levels may improve within this time. These patients should be monitored beyond 26 weeks, as continued endocrine changes are likely. Long term tumor control and survival need to be assessed as data matures.

CHARACTERIZATION OF CANINE BLADDER VARIATIONS TO OPTIMIZE FRACTIONATED RADIATION THERAPY PROTOCOL USING CONE-BEAM COMPUTED TOMOGRAPHY. J.R. Nieset, J.F. Harmon, S.M. LaRue, Department of Radiological Health Sciences, Colorado State University, Fort Collins, Colorado, 80523

Introduction: Canine bladder cancer proves to be difficult to treat with fractionated radiation therapy (RT) due to daily changes in size, shape and position of the bladder and surrounding soft-tissue structures. Despite advances in RT treatment, very little is known about the motion characteristics of the bladder in veterinary or human patients. This uncertainty can lead to side effects from accidental irradiation of neighboring critical structures. Tumor control can also be compromised if the dose is decreased to avoid these effects.

Purpose: This study aims to quantify the size, shape and volume changes of the bladder that occur daily in each of three positions (dorsal, sternal and lateral) to determine which provides the best possible treatment scenario. The secondary aim of the study will use this information to determine the optimal planning target volume (PTV) expansion that ensures inclusion of the bladder in the treatment field each day and minimizes irradiation of nearby healthy tissues.

Methods: Data from ten dogs receiving fractionated RT for bladder or prostate cancer at CSU since May 2008 were included in the study. Images from patients undergoing treatment for either disease can be used because the organs of interest (bladder and rectum/colon) are visible in the images in either case. Both aims are accomplished by using retrospective cone beam CT (CBCT) data that is obtained daily for positioning of patients undergoing standard-of-care fractionated RT and will not alter patient treatment. The CBCT images are acquired with the Varian Trilogy On-Board Imaging kV X-ray source on the gantry of the linear accelerator. Organs of interest are contoured on each CBCT data set and the images, along with the contours, are registered to the original planning CT. All measurements are made with reference to the planning CT and dosimetric data for the organs of interest is determined using a dose volume histogram (DVH).

Results: Of the 10 dogs in the study, 3 were treated in lateral recumbency, 3 in dorsal recumbency and 4 in sternal recumbency. We acquired a total of 30 lateral CBCT image sets, 56 dorsal CBCT image sets and 37 sternal CBCT image sets. Preliminary results show a wide range of bladder volumes and also characterize bladder deviations in six directions. Additional data is currently being evaluated and will be described.

Discussion/Conclusion:These findings will allow for the development of a treatment protocol for patients with bladder cancer that will allow for more accurate coverage of the tumor volume while reducing side effects. This information also makes the options of image-guided RT (IGRT) and adaptive RT (ART) possibilities in the curative-intent treatment of bladder cancer.

Saturday, October 24, 2009 **Venetian Room**

8:00 am *VRTOG Meeting*

9:00 am RO Keynote address
James W. Welsh, MD
Assistant Professor, Dept of Radiation Oncology,
University of Texas MD Anderson Cancer Center, Houston TX
"**INCREASING THE THERAPEUTIC RATIO, FROM BRAGG PEAKS TO BIOLOGICS AND BEYOND"**

10:30 am *Break*

11:00 am **Scientific Session 11: RO**
Wendell Lutz, PhD
"**INCREASING THE THERAPEUTIC RATIO FROM THE PHYSICS PERSPECTIVE: A BRIEF REVIEW OF IMRT, IGRT, TOMOTHERAPY, THE CYBERKNIFE AND PROTON THERAPY"**

12:30 pm *RO Business Meeting and lunch*

2:00 pm **Scientific Session 12: RO Forum Discussion** with Representatives from:

IMRT - Margy McEntee
IGRT - Sue LaRue
Tomotherapy - Lisa Forrest
The Cyberknife - Sarah Charney
Proton Therapy - Barbara Kaser-Hotz

5:00 pm Adjourn for the day

American College of Veterinary Radiology

ACVR 2009 Conference Special Activities

Wednesday, October 21

Skyway
Reception supported by
Orthopedic Foundation for Animals
and
Universal Medical Systems, Inc.
6:30 – 7:30 p.m.

Special dedication to the memory of Dr. Myron “Mike” Bernstein

IDENTIFICATION OF REGISTRANTS

Blue name badges

ACVR Diplomates

Gray name badges

ACVR Residents in Training

Green name badges

Post Trainees
ACVR Society Members
Veterinarians

Yellow name badges

Exhibitors/Sponsors